SILICON BASED MULTILAYER PHOTOELECTRODES FOR PHOTOELECTROLYSIS OF WATER TO PRODUCE HYDROGEN FROM THE SUN

by

Faisal Faruque

A thesis submitted to the faculty of
The University of Utah
in partial fulfillment of the requirements for the degree of

Master of Science

Department of Electrical and Computer Engineering

The University of Utah

May 2011

The University of Utah Graduate School

STATEMENT OF THESIS APPROVAL

The thesis of **Faisal Faruque**

has been approved by the following supervisory committee members:

Massood Tabib-Azar	, Chair	**01/28/2011**
		Date Approved
Faisal Khan	, Member	**01/31/2011**
		Date Approved
Hanseup Kim	, Member	**01/31/2011**
		Date Approved

and by **Gianluca Lazzi** , Chair of

the Department of **Electrical and Computer Engineering**

and by Charles A. Wight, Dean of The Graduate School.

ABSTRACT

The main objective of this work is to study different materials for the direct photosynthesis of hydrogen from water. A variety of photocatalysts such as titanium dioxide, titanium oxy-nitride, silicon carbide, and gallium nitride are being investigated by others for the clean production of hydrogen for fuel cells and hydrogen economy. Our approach was to deposit suitable metallic regions on photocatalyst nanoparticles to direct the efficient synthesis of hydrogen to a particular site for convenient collection. We studied different electrode metals such as gold, platinum, titanium, palladium, and tungsten. We also studied different solar cell materials such as silicon (p- and n-types), silicon carbide and titanium dioxide semiconductors in order to efficiently generate electrons under illumination. We introduced a novel silicon-based multilayer photosynthesis device to take advantage of suitable properties of silicon and tungsten to efficiently produce hydrogen. The device consisted of a silicon (0.5mm) substrate, a deposited atomic layer of Al_2O_3 (1nm), a doped polysilicon (0.1µm), and finally a tungsten nanoporous (5-10nm) layer acting as an interface electrode with water. The Al_2O_3 layer was introduced to reduce leakage current and to prevent the spreading of the diffused p-n junction layer between the silicon and doped polysilicon layers. The surface of the photoelectrode was coated with nanotextured tungsten nanopores (TNP), which increased the surface area of the electrodes to the electrolyte, assisting in electron-hole mobility, and acting as a photocatalyst. The reported device exhibited a fill factor (%FF)

of 27.22% and solar-to-hydrogen conversion efficiency of 0.03174%. This thesis describes the structures of the device, and offers a characterization and comparison between different photoelectrodes.

I dedicate this thesis to my wonderful parents and loving sister, whose affection and guidance always lead me to my dreams.

Also to my friend Todd Mckay, whose help cannot be put in words.

And finally to my fiancée, Tamara Zaman, whose love, support and enormous help has always been the driving force behind my every success.

TABLE OF CONTENTS

LIST OF FIGURES

Figures

ACKNOWLEDGEMENTS

This thesis would not have been possible without the support of many people. I express my gratitude to my supervisor, Dr. Massood-Tabib Azar, who was of great help and offered invaluable assistance. My heartfelt gratitude also goes out to the members of my supervisory committee, Dr. Faisal Khan and Dr. Hanseup Kim, for their support. I would also like to thank Dr. Phil Neudeck of NASA Glenn Research Center, Cleveland, Ohio, for providing important samples.

CHAPTER 1

INTRODUCTION AND BACKGROUND

Solar energy delivers renewable, pollution-free power and has done so since ancient times. The primary method of harnessing energy from sunlight relies on photovoltaic (PV) panels, but that energy has limited utility without the robust methods to store it. One method involves converting that energy to hydrogen by diverting the current from PV panels to drive electrolysis, which already accounts for over 4% of worldwide hydrogen production. To split water molecules into hydrogen and oxygen, the change in Gibb's free energy is 237.178kJ/mol [1], or the equivalent electrical potential of 1.229V [1]. Traditionally, solar-powered electrolysis based on PV structure relies on external circuitry to create an electrical potential difference across two electrodes separated by water. Unfortunately, energy is lost in conversion. Photocatalysis decreases this loss by introducing a catalyst through a process called photoelectrolysis.

Photoelectrolysis conducts electrolysis more efficiently than PV methods. While PV cells convert solar energy to electrical energy, which drives a subsequent conversion to chemical energy, photoelectrolysis converts solar energy directly into chemical energy in a process akin to photosynthesis, the process by which plants convert solar energy to chemical energy. The device described in this thesis has the ability to split water molecules with photocatalytic reactions powered by sunlight.

By leveraging nanoarchitecture, the electrodes expose more surface area to sunlight, provide nanochannels for electrons and holes to interact with electrolytes more efficiently, improve photoion generation, and facilitate photoion mobility for electrolysis. Chapters 2 and 3 discuss the structure of the device, its experimental measurement characteristics, and the theories and concepts behind its design.

1.1 History of Hydrogen

In 1766, British scientist Henry Cavendish demonstrated to the Royal Society of London that hydrogen was a distinct element or gas by causing it to separate through a reaction between zinc metal and hydrochloric acid. Cavendish proved that hydrogen is a lighter gas, and, when ignited with a spark, yields water [2].

Later, in 1785, French chemist Antoine Lavoisier studied Cavendish's experiments and concluded that oxygen and hydrogen are the two basic elements of water. Lavoisier named the element hydrogen from two Greek words, hydro, meaning water, and genes, meaning born of, in 1788 [3].

In 1800, scientists William Nicholson and Sir Anthony Carlisle first discovered that applying current to water can produce hydrogen and oxygen, a process which was later termed electrolysis [4]. Around 1839, a Swiss chemist, Christian Friedrich Schoenbein, discovered the Fuel Cell Effect when he found that combining hydrogen and oxygen gases produces water and an electric current [5]. In 1845, another English scientist and judge, Sir William Grove, furthered Schoenbein's discovery on a practical scale by inventing a "gas battery" [6]. This achievement earned him the title "Father of the Fuel Cell" [6].

It was not until 1970 that the phrase "hydrogen economy" was first coined by electrochemists J. O'M Bockris and Neal Triner in a General Motors Technician meeting [7]. Consequently, the late 20th and 21st centuries saw many hydrogen-based industries, hydrogen-powered vehicles, and hydrogen fuel cells. Iceland declared itself to be the first complete hydrogen economy by 2030 [8].

1.2 Hydrogen Economy

Hydrogen economy: it might seem an implausible goal to attain, but attaining this goal is not unprecedented. Even in the beginning of the 20th century, the United States (U.S.) had an energy system based on animals for food and transportation and wood for heat energy. The transition from wood to coal to the increasing contribution of natural gas, petroleum, nuclear energy, hydro-energy, and recently renewable energy has been very significant in the last 150 years among developed countries like the U.S.. The transition to renewable energy reflects more the diversification of energy resources than actual transitions. Due to large-scale environmental concerns and natural energy crises, this century has opted for the advent of technology to provide viable alternatives to meet the ever-increasing domestic demands for energy. It is important to state that up until the end of the 20th century, the U.S. produced all of its required energy by itself. It was not until the 1980s that the consumption of the natural gas surplus in domestic production forced the U.S. to turn to other countries to import natural gas. In the year of 1994, the U.S. imported more petroleum than it produced [9]. This increase in demand was attributed to the industrial and technological revolution in addition to the rising domestic consumption of fossil fuel. Access to energy was always meant to help in the

achievement of advanced technology and to help modernize the standard of living of human kind. In reality, resources such as fossil fuels are limited; if that is not alarming enough, harmful emissions as a result of overproduction cause environmental hazards. These are a handful of the many driving forces behind the transition for coming up with a new, pollution-free and abundant next generation energy resource.

Although a hydrogen economy sounds very promising for solving the energy crisis, the production process of hydrogen has to be kept in mind. Only producing hydrogen using renewable resources can make the idea a successful one. Hydrogen will replace fossil fuel as an energy resource or energy carrier and also any other related feedstock. The theory behind hydrogen economy is that hydrogen and electricity can serve all the energy needs of society, and they would be permanent and independent. In the end, the application of energy will stem from electricity, which in turn will be produced from hydrogen fuel cells or any other means of hydrogen application. Eventually, hydrogen and electricity will transform all aspects of modern day fossil fuel usage so that the transition is successful and effective.

1.3 Hydrogen Production

Hydrogen production from all different processes is based on the separation of hydrogen from hydrogen-containing feedstock. Each type of feedstock requires a different method to extract hydrogen from it. Right now, there are three major technologies behind hydrogen production with their own subcategories. These three major technologies are thermal, electrochemical, and biological. Although the most common method used is the thermal method, it has limitations and poses dangers to the

environment. The first reported commercial technology for producing hydrogen was informed in the late 1920s when pure hydrogen was produced via water electrolysis. Later, the industrial production of hydrogen moved to more fossil-based feedstocks, like oil and coal, which are still the main source of hydrogen production today. There are several feedstocks from which hydrogen can be separated. Figure 1.1 gives an overall idea about different feedstocks available for hydrogen extraction.

In the Sections 1.3.1 through 1.3.3, the three main categories and their subcategories for hydrogen production are discussed.

1.3.1 Thermal

In the thermal process, hydrogen is extracted by simply releasing it from the feedstock by gas reforming and heating.

1.3.1.1 Steam reformation. Using natural gas as a feedstock, steam reforming involves an endothermic conversion of methane (CH_4) and water vapor (H_2O) into hydrogen (H_2) and carbon monoxide (CO) (reaction 1.1). To reform, the required heat is supplied from the combustion of natural gases, where the temperature is around 700°C to 900°C. Following this step, the hydrogen contains CO, which is then put through a water gas shift (WGS) reaction to produce H_2 and carbon dioxide (CO_2) (reaction 1.2).

$$CH_4 + H_2O + (\text{heat}) \rightarrow CO + 3H_2 \quad (1.1)$$

$$CO + H_2O \rightarrow CO_2 + H_2 + (\text{heat}) \quad (1.2)$$

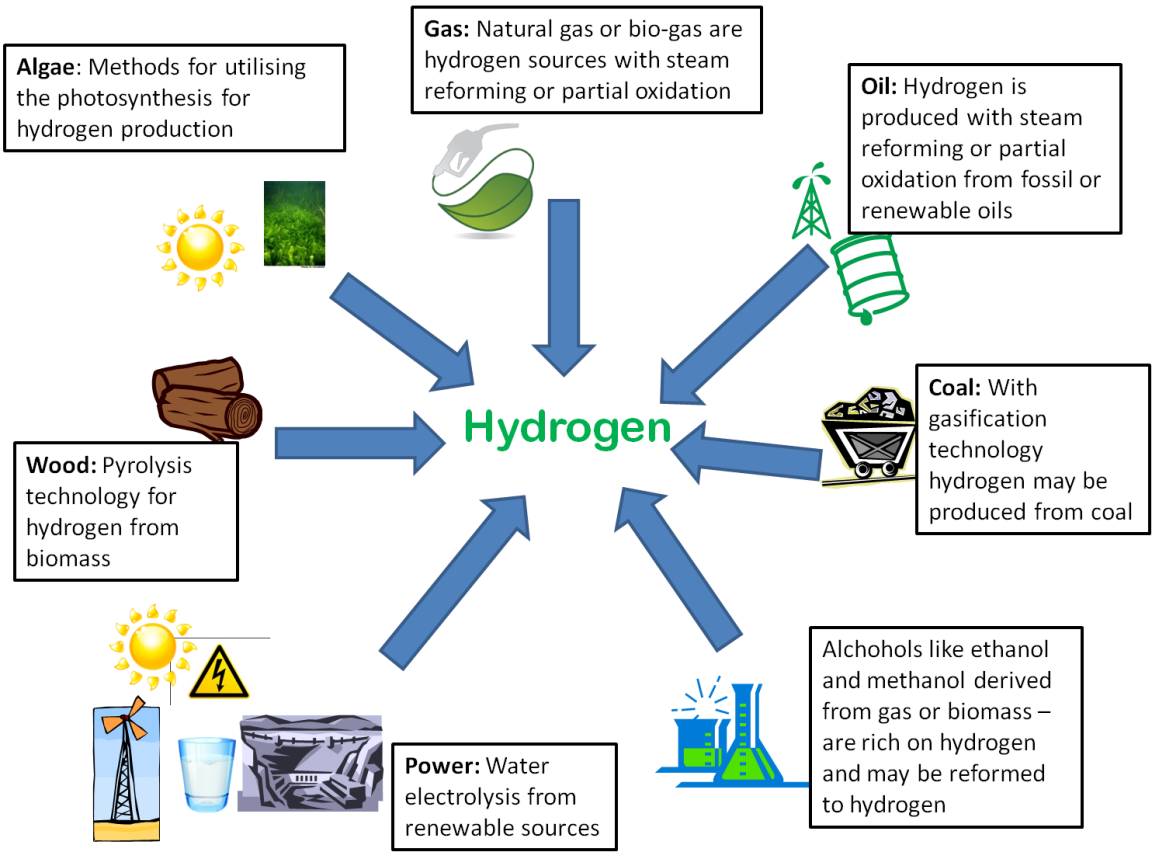

Figure 1.1 Examples of various hydrogen feedstocks

Another method to produce hydrogen through steam reformation is the partial oxidation of natural gas, as CH_4 and O_2 go through a partial combustion to produce H_2 and CO (reaction 1.3) and subsequently go through a WGS reaction (reaction 1.2) to form H_2 and CO_2.

$$CH_4 + ½\ O_2 \rightarrow CO + 2H_2 + (heat) \qquad (1.3)$$

1.3.1.2 Thermochemical water splitting. This process requires a heat-driven chemical reaction to split water into hydrogen and oxygen. Due to the lower requirement

of electrical energy to split water at a high temperature (1000°C) compared to electrolysis (100°C), the high temperature electrolyzer can operate at a rate of processing efficiency higher than low-temperature electrolysis. The electrolyzer is the device setup used to perform the electrolysis.

A typical electrolyzer capable of performing high-temperature water splitting is normally based on a solid oxide fuel cell (SOFC), which operates at the range of 700°C to 1000°C.

1.3.1.3 Gasification. The gasification process follows simple rules of nature where it can break down almost any form of carbon-based feedstock into its chemical components. These days, the modern gasifier exposes coal or biomass (C) in a controlled chamber to high temperatures and pressure in the presence of air or oxygen, which forces the molecules to break down, thus completing the chemical reaction and producing CO and H_2 (reaction 1.4). Next, they go through the WGS reaction (reaction 1.2) to form CO_2 and H_2.

$$\text{C (coal or biomass)} + H_2O + \text{heat} \rightarrow CO + H_2 \qquad (1.4)$$

This gasifier, when used for coal gasification, generates a substantial amount of CO_2. These gasification processes are being optimized for hydrogen production by improving the CO_2 decarbonization, which involves capturing and filtering systems. Also, if biomass is used instead of coal, the emission of CO_2 will decrease significantly.

1.3.1.4 Pyrolysis. Pyrolysis involves the conversion of biomass into hydrogen using a moderately high temperature gas reforming method. Although the field is

conducting research into hydrogen production, ways of making this process work include steam gasification, gasification in supercritical water, and the application of the thermochemical cycle. Additionally, there are bio-liquid feedstock such as sugar, sugar alcohols (ethanol), bio oils, and wood chips.

1.3.2 Electrochemical

Two types of electrochemical processes to produce hydrogen are discussed in this section.

1.3.2.1 Water electrolysis.

Approximately 4% of the world's current production of hydrogen is satisfied by water electrolysis. Although this is a very small statistic, this process is, in fact, a very promising one. The simplest way to explain water electrolysis is that water is split into hydrogen and oxygen with the application of electrical energy (reaction 1.5). In this process, one mole of water produces one mole of hydrogen gas and a half mole of oxygen gas. For the water splitting reaction, at room temperature, 25°C, and 1bar, the change in Gibb's free energy is 237.178kJ/mol [1], and when converted to electrical energy it is 1.229V [1]. This required electrical energy can be applied from any fuel cell, including PV cells.

$$H_2O + \text{electrical energy} \rightarrow H_2 + 1/2\ O_2 \qquad (1.5)$$

Besides simple water electrolysis, there are also Alkaline electrolysis, Polymer electrolyte membrane (PEM) electrolysis [1], high-temperature electrolysis, and more.

1.3.2.2 Photoelectrolysis. Instead of using a PV cell to convert solar energy into electrical energy for electrolysis, Photoelectrolysis uses the same solar energy to directly split the water molecule into hydrogen and oxygen. This form of electrolysis results in the most clean and renewable energy solution in hydrogen production. There are obstacles to this technology, such as the lack of efficient light absorption, the corrosion of semiconductor photoelectrodes, the necessary research on the bandgap shifting of different semiconductors, and surface chemistry modification. Despite these hindrances, reducing the conventional two-step electrolysis process using PV cells into a single-step process proves this technology to be one of the best solutions in hydrogen production.

1.3.3 Biological

Biological production processes for hydrogen are still in exploratory and research phase. This section emphasizes on two methods.

1.3.3.1 Photobiological. There are two major steps in the photobiological production of hydrogen: photosynthesis (reaction 1.6) and catalyzed hydrogen production by hydrogenases (reaction 1.7), for example, green algae and cyanobacteria. During photosynthesis, when plants produce oxygen, these microbes consume water to produce hydrogen as a byproduct.

Photosynthesis: $$2H_2O \rightarrow 4H^+ + 4e^- + O_2 \quad (1.6)$$

Hydrogen Production: $4H^+ + 4e^- \rightarrow 2H_2$ (1.7)

1.3.3.2 Anaerobic digestion. Anaerobic bacteria grow in the dark on carbohydrate-rich substrates, such as biomass. These bacteria break down the biomass, which is high in carbohydrates, very inexpensive, and plentiful. Ongoing extensive research is trying to understand, control and find these specific bacteria which can ferment organic materials to hydrogen.

1.4 Motivation

This section details the aspects that motivated the research for this thesis.

1.4.1 Next-generation energy source

Jules Verne mentioned in his novel, *The Mysterious Island* (1874), "I believe that water will one day be employed as fuel, that hydrogen and oxygen which constitute it, used singly or together, will furnish an inexhaustible source of heat and light, of an intensity of which coal is not capable." [10]

It is interesting to note that Verne observed the potential of water and hydrogen as a substitute for depleting fossil fuels back in the late 1800s. Nonetheless, well over a century later, modern science is yet to claim substantial progress in this field. Electrolysis, as this thesis aims to illustrate, is one of the few innovative and environment-friendly methods for harnessing energy from the abundant resource water.

Unfortunately, the techniques involved are not as simple, and it is the hydrogen in water that scientists are most interested in, as it is strongly believed that hydrogen is

considered to be the next best solution to fossil fuels. The energy crisis and finite natural resources are driving human civilization to the edge of last resorts. In order to uphold and achieve advancement in technology, as well as modernization, a transition to a renewable and clean energy resource is now imperative and only hydrogen can give us the answer. As water is the most abundant resource on this planet, obtaining hydrogen from water is the solution to the energy problem.

1.4.2 Solar-to-hydrogen efficiency

Required electrical energy to split the water molecule is 1.229V [1]. Reported electrolysis potential of a system claiming 70-85% efficiency is 1.9V [11]. So the efficiency margin comes around (1.23/1.9) × 100% = 65%, and the commercially available PV cell's efficiency is around 20% . So coupling the PV cell with electrolysis efficiency gives 0.20 × 0.65 = 13% of solar-to-hydrogen efficiency

Although improving electrolysis efficiency can bring this percentage up, there will continue to be a two-step energy loss due to external energy source, which is the PV cell. Photoelectrolysis combines the technology of PV systems (solar energy harvesting) and an electrolyzer (water splitting) into a single, monolithic device. For a direct conversion system like photoelectrolysis, with a base PV efficiency of 20% and the practical equivalent electrical potential to split water at 1.5V [11], the solar-to-hydrogen efficiency goes up to $0.20\times\left(\frac{1.23}{1.5}\right) = 16.4\%$. This increase provides strong motivation for working in the field of photoelectrolysis to produce hydrogen.

1.5 Literature Survey: Photoelectrolysis for Hydrogen Production

Water splitting using solar photon energy has been studied for a long time, since the first reported photoelectrolysis of water by Fujishima Honda in 1972, using powder and electrode systems [12]. Since that time, the technology related to photoelectrolysis has improved remarkably and has been studied widely.

1.5.1 Photoelectrolysis

The general idea behind photoelectrolysis is similar to that behind the electrolysis cell, where the difference is that at least one of the two electrodes in the electrolyzer is semiconductor material. When photon energy from sunlight hits the surface of the semiconductor photoelectrodes, which are inside an aqueous electrolyte, enough energy is generated to split the water molecule to hydrogen and oxygen. In order for spontaneous photoelectrolysis to occur, some necessary conditions must first be met. Under illumination, the semiconductor conduction band (CB) edge should lie more negative relative to the reduction potential of the water, while the valence band (VB) edge should lie more positive to the oxidation potential referenced to Normal Hydrogen Electrode (NHE). In most cases, the photovoltage developed between the photoelectrodes is less than the voltage required to split the water molecule. For example, in Figure 1.2, a widely studied photoanode material, anatase TiO_2 [1], 3.0eV bandgap generates a 0.7-0.9V when illuminated which is not sufficient and an external electrical bias is needed to make up for the insufficient voltage.

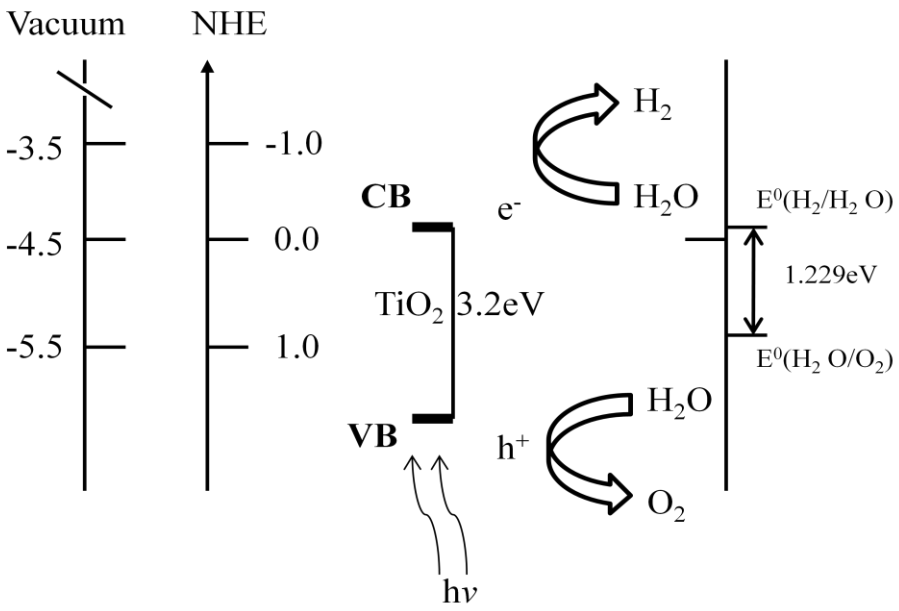

Figure 1.2 Band position of anatase TiO_2 (E_g = 3.2eV), in the presence of a pH 1 aqueous electrolyte. The energy scale is indicated in electron volts (eV), using either an NHE or vacuum level as a reference showing the condition for water splitting

For the meaningful photoelectrochemical decomposition of water to occur, three essential requirements must be met [1]. First, the CB and VB of the semiconductor materials must overlap with the energy levels of hydrogen and oxygen reduction potential. Second, the semiconductor electrodes must be stable under photoelectrolysis conditions. Third, charge transfer from the surface of the semiconductor must be fast enough to prevent corrosion and also to reduce energy loss due to overvoltage or overpotential.

Figure 1.3 shows the forming of liquid junction with the aqueous electrolyte, under illumination, where the electrons from the CB edge in the p-type semiconductor enter the electrolyte, and holes from the VB in the n-type semiconductor also enter the electrolyte.

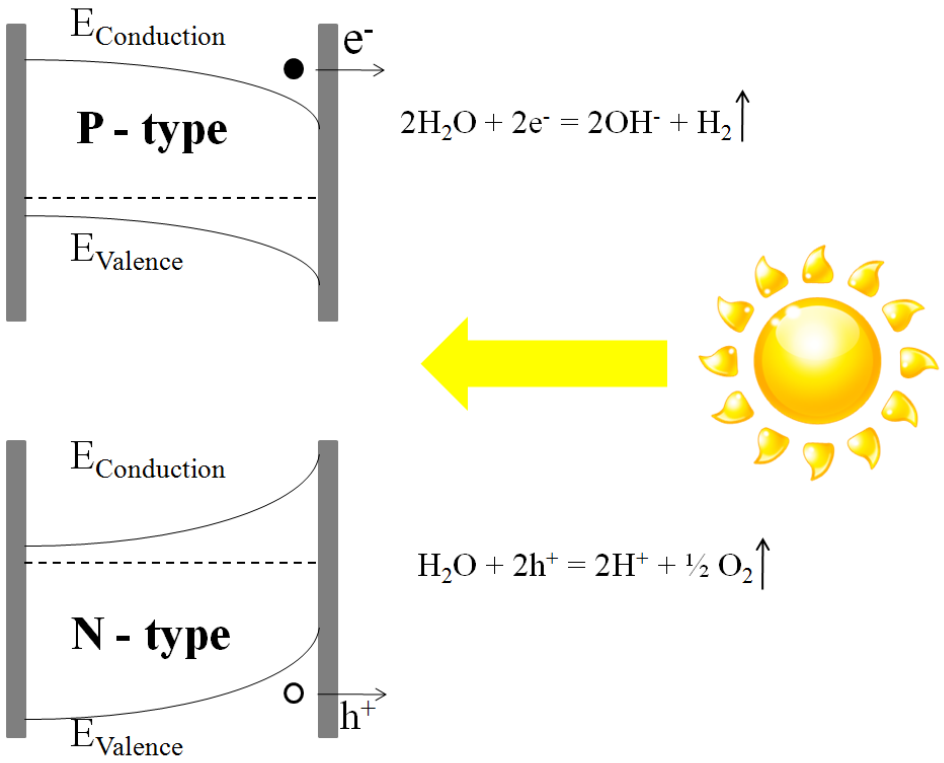

Figure 1.3 Band edges of p- and n-type semiconductors in aqueous electrolyte under illumination

In recent years, articles related to solar energy conversion have drawn a lot of attention, and they have been accumulating in scientific literature. Since 1990, the amount of publication related to this field has increased exponentially, according to Fujishima [12]. The upsurge of interest regarding this solar energy utilization has been fueled by the energy crisis that emerged in recent decades. Table 1.1 includes the most recent work on photoelectrolysis and the photoelectrode description. The table covers the photoanode and photocathode material, electrolyte, incident photon to current efficiency (IPCE), and solar-to-hydrogen conversion efficiency (η_{STH}).

1.5.2 Photocatalysts

The use of photocatalysts to perform photoelectrolysis was first reported between the late 1970s and 1980s. The photocatalysts were mainly TiO_2 and $SrTiO_3$. The TiO_2 photocatalyst is active when another cocatalyst is modified with it and when the electrolyte of the aqueous solution is suitable. Metal cations used to make stable semiconductor oxide photocatalysts usually respond solely to UV light. Thus, band engineering of the photocatalysts is needed to make them responsive to water splitting reaction under visible light.

Table 1.2 is the library [13] of new photocatalysts that have been reported by researchers recently. The main classifications are the overall water splitting into H_2 and O_2 with and without the presence of reagents. Although this photocatalyst library does not contain all reported photocatalysts, it certainly provides an overview of recent and important ones.

1.5.3 Nanostructured surface

For successful photoelectrolysis, the photoelectrodes must absorb significant amounts of sun light energy. Different kinds of inorganic semiconductors besides p-type or n-type silicon, like amorphous silicon (a-Si) or crystalline silicon (c-Si), gallium arsenide (GaAs), cadmium telluride (CdTee), gallium, phosphide (GaP), indium phosphide (InP), copper indium diselenide (CIS), copper indium diselenide (CIGS), and gallium indium phosphide ($GaInP_2$) are popular semiconductors for absorbing and converting solar energy into electrical energy [1].

In this thesis, the photoelectrode for photoelectrolysis emphasizes both the solar spectrum range of semiconductor materials and the new advent of technology with a nanotextured electrode surface. This introduces a whole new window into the surface texture activity of photoelectrodes.

Nanocrystalline nonoxide semiconductors [1], such as CdS nanocrystals, have a high surface-to-volume ratio, making the surface of the lattice full of atoms able to react with the electrolyte. Other steps have been studied including chemical, and electrochemical deposition of nanoparticles on the photoelectrode substrates, as well as immobilization of surface modified nanoparticles with the help of physical interactions and chemical reactions. By implementing these processes, the recombinations of photogenerated electron-hole pairs are minimized, since that would actually hinder the photocurrent generation. So, reduction of the electron-hole recombination enhances the charge separation from the photoelectrode where the electrons from the CB and holes from the VB can advance to the electrode surface.

The substrate used for this thesis's photoelectrode is p- and n-type silicon. The surface coating of p-type silicon (work function ϕ_{Si} =4.88eV) with platinum (work function ϕ_{Pt} =5.28eV) has been reported to have a relatively small Schottky barrier due to little difference in the work function. A 5-10nm of Pt deposition resulted in a very island like topology on the surface of the p-type silicon, and a very thin layer (0.05-0.2nm) of Pt deposition resulted with a photoconversion efficiency of 10% in alkaline solution [1]

Table 1.1 Lists of recently reported photoelectrolysis cells and their efficiencies

Device	Structure	Photocathode	Photoanode	Electrolyte	IPEC	η_{STH}
1.	Multilayer, Multijunction	Si-Pt_{black} [14]	AlGaAs-RuO_2	1M H_2SO_4 pH ~ 1	16 %	18.3 %
2.	Multilayered	p-$GaInP_2$(Pt) / GaAs (substrate) [15]	Pt	3M H_2SO_4 pH ~ 1	-	12.4%
3.	PV-PEC	InGaP/GaAs-Si/PolySi(substrate) [16]	Pt-mesh	1M H_2SO_4 pH ~ 1	-	5.36 %
4.		Pt [17]	$CuGeSe_2$/SnO_2-glass (substrate)	0.5M H_2SO_4 pH ~ 1	-	4.3 %
5.	Nanotube	Pt [18]	Ti-Fe-O (Nanotube)	1M KOH pH ~ 14	-	1.2 %
6.	PV-PEC	aSiGe-Pt/Ti [19]	aSiGe-WO_3	pH ~ 1	-	0.6 %
7.	Multijunction	SiO_2 coated Pt [20]	n-GaN-Cr/Au	0.1M H_2SO_4 pH ~ 1	-	0.35 %
8.	Multilayer	p-SiC [21]	Pt	0.5M H_2SO_4 pH ~ 1	0.17 %	0.27 %
		p-SiC [22]	n-TiO_2		0.06 %	0.27 %
9.	Monolithic	n-TiO_2 [23]	p-GaP	1M H_2SO_4 pH ~ 1	-	0.25 %
10.		Pt [24]	Fe_2O_3/glass – 5% Ti , 5% Al doped	0.1M NaOH pH ~ 14	1.07%	-
			Fe_2O_3/glass – 2% Ti doped		< 1%	

Table 1.2 Photocatalysts' library

Photocatalysts response under visible light			UV light responsive photocatalysts
H_2 evolution (sacrificial)	O_2 evolution (sacrificial)	Overall water splitting	Overall water splitting
$SrTiO_3$:Cr,Sb	TiO_2:Cr.Sb	$SrTiO_3$:Rh-$BiVO_4$	$ZnNb_2O_6$
$SrTiO_3$:Cr,Ta	TiO_2:Ni,Nb	$SrTiO_3$:Rh-Bi_2MoO_6	$Sr_2Nb_2O_7$
$SrTiO_3$:Rh	$PbMoO_4$:Cr	$SrTiO_3$:Rh-WO_3	$Cs2Nb_4O_{11}$
$SnNb_2O_6$	$BiVO_4$		$Ba_5Nb_4O_{15}$
ZnS:Cu	Bi_2MoO_6		$ATaO_3$ (A=Li,Na,K)
ZnS:Ni	Bi_2WO_6		$NaTaO_3$:A
ZnS:Pb,Cl	$AgNbO_3$		(A=Ln,Ca,Sr,Ba)
$NAInS_2$	Ag_3VO_4		ATa_2O_6
$AgGaS_2$	In_2O_3 $(ZnO)_3$		(A=Mg,Ca,Sr,Ba)
$CuInS_2$-$AgInS_2$-ZnS			$Sr_2Ta_2O_7$
$In_2O_3(ZnO)_3$			$K_3Ta_3Si_2O_{13}$
			$K_3Ta_3B_2O_{12}$
			$K_2LnTa_5O_{15}$
			$AgTaO_3$

and 30% in acidic solution [1]. An open circuit voltage (V_{OC}) of 0.685V [1] was reported when Pt dots were deposited on an n-type silicon photoelectrode with a 5-20nm diameter. There are also nanoarchitectured devices with p-type and n-type CdS, CdSe, CdTe and GaN, GaAs, INP [1] reported in various literatures.

CHAPTER 2

HOMOGENOUS SEMICONDUCTING AND METALLIC ELECTRODES

2.1 Introduction

For hydrogen production, it is imperative to investigate different electrode materials and their properties. Here, we investigate metallic electrodes, such as gold (Au), platinum (Pt), palladium (Pd), titanium (Ti), and tungsten (W). In one case, we also studied nanoporous tungsten to examine the effect of a very large electrode area on the electrode hydrogen production efficiency. Semiconducting electrodes, such as titanium dioxide (TiO_2), silicon carbide (SiC) and both p- and n-type single crystal silicon (Si), are also studied and discussed in this chapter. All these electrodes were used to generate hydrogen in acidic as well basic electrolytes, with pH levels ranging from 1-13. The main objective was to find the electrode material that produces the largest amount of hydrogen at the lowest possible turn on voltage (V_{ON}), which is the turn on voltage at which hydrogen is produced in cathode and observed as bubbles.

In Section 2.2, we discuss the experimental setup. Section 2.3 takes a closer look at cathode and anode metal-metal electrodes in our electrochemical fuel cell. The next section, 2.4, focuses on semiconductor-semiconductor electrodes. Section 2.5 talks about the effect of coating the electrodes with various photocatalysts. Finally, Section 2.6 concludes this chapter.

2.2 Experimental Setup

The following sections provide an overview of the experimental setup, the electrical measurements, electrolyte preparation, and electrode materials and preparation processes.

2.2.1 Electrical measurements

The electrical measurements are a crucial component of this project, which is why the setup has to be very precise and neat, so that the results we obtain are accurate. Figure 2.1 shows what components were used to carry out the electrical measurements. First, the electrodes are connected to a Keithley 236 source-measure unit (SMU) that produces current and measures the voltage across the electrodes through two calibrated ports. The SMU is connected to a computer and synchronized with LABVIEW software to monitor the voltammetric measurement of the setup. There is also a separate light source for illuminating the electrode samples inside the electrolyte for different experimental purposes.

2.2.2 Electrolyte preparation

For the voltammetric measurement of the electrodes, we need to prepare electrolytes. In this thesis, the electrodes were studied in both acidic and basic electrolytes at pH levels ranging from 1-11. The pH level of the solution was determined by a digital pH meter, Lutron YK2001PH.

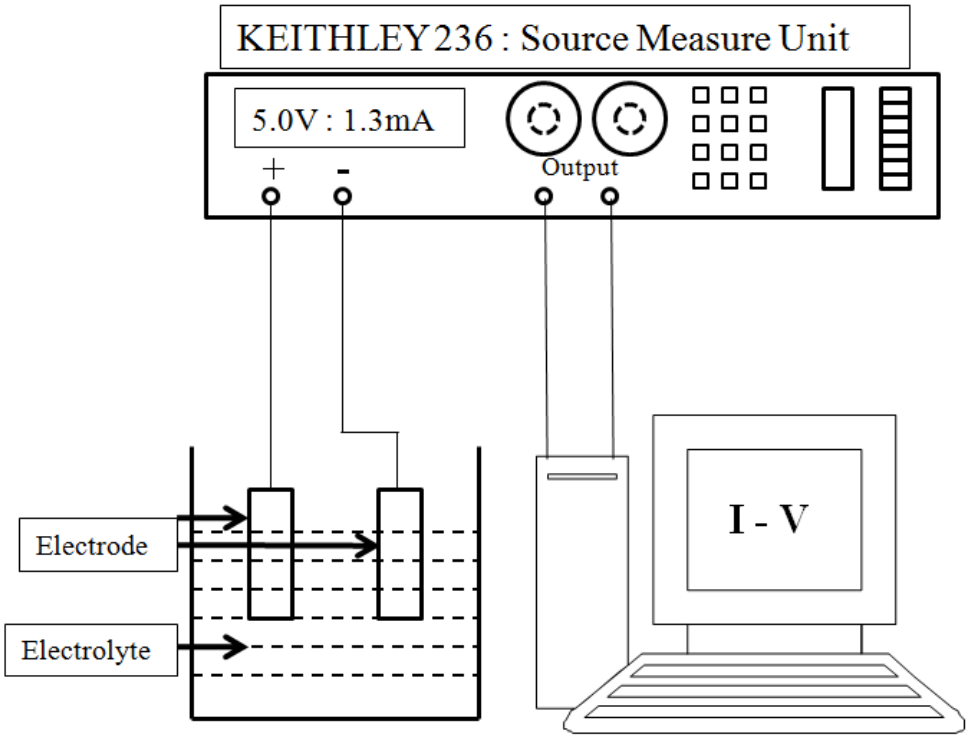

Figure 2.1 Experimental setup used to study different electrodes

Acidic electrolytes were prepared with diluted hydrochloric acid (HCl) mixed with distilled (DI) water. For different pH levels of the acidic electrolytes, ranging from 1-6, the digital pH meter was used to calculate the H^+ ion level of the solution. The higher the concentration of HCl, the more H^+ ions are injected into the electrolyte, and the pH level decreases, thereby making it more acidic. Conversely, the basic electrolyte was prepared with potassium hydroxide (KOH). The KOH injects OH^- ions into the solution, making it rich with hydroxyl ions. This basic electrolyte has a pH level ranging from 8-13. This was determined by the digital pH meter.

2.2.3 Electrode materials and preparation

The electrodes that were used in this thesis were designed and created for experimental purposes. The metal electrodes gold, platinum, palladium, titanium, and tungsten were bought from the company Alfa Aesar^{TM} with 99% purity. Samples were cut and prepared so that the contact surface area of each was the same.

The semiconductor electrodes silicon carbide, gallium nitride and both p- and n-type single crystal silicon were bought from a different manufacturer. Only the TiO_2 was prepared in our laboratory. A 0.5mm thickness of titanium (99% pure) source was purchased from Alfa Aesar^{TM}. Using an electrolyte of 0.5M phosphoric acid (H_3PO_4) and a Keithley 236 SMU, an oxide (anatase) layer of 50-300μm was grown on the titanium sample. [24]

2.3 Metal-Metal Electrodes

Section 2.2 outlines the setup for measuring the characteristics of metal-metal electrodes. In addition, the reason behind selecting gold, platinum, palladium, titanium and tungsten metals as electrodes are also discussed.

In the field of electrochemistry and electroanalytical chemistry, there are different kinds of materials used for electrodes. Among them, gold is widely used. Gold is highly conductive, as the concentration of free electrons is around $5.90\times10^{22}cm^{-3}$ [25]. It is also very resistant to corrosion and oxidation, has good conductivity, ductility, and low toxicity. In semiconductor industries, gold wire is being used to connect semiconductor devices to their packages through a process called wire-bonding. For these reasons, gold has always been a very suitable material for electronic experiments.

Another important and widely used electrode is platinum. Because of its chemical inertness and high corrosion resistance, platinum is frequently used in chemical experiments and other various electronic components. The standard hydrogen electrode (SHE) also utilizes a platinized platinum electrode. Although it is a high-value metal, its promising chemical properties make it an excellent candidate for electrodes.

After gold and platinum, the next suitable candidate for electrodes is palladium. This metal has characteristics similar to gold and platinum, those of being highly corrosion resistant and nontoxic. Palladium has been used for electronics besides electrodes. The palladium-hydrogen electrode (Pd/H_2) is one of the common reference electrodes in electrochemical studies, similar to SHE (with platinum). Although palladium is known for its hydrogen absorption characteristics, this feature is applicable only in high temperature.

Titanium has the physical qualities of strength, durability, high resistance to corrosion, low density, and biological compatibility. These characteristics make titanium a very useful element for various applications. Titanium's most common compound, titanium dioxide (TiO_2), is one of the most popular photocatalysts, and is also used as a compound for industrial white pigments. Even though titanium gets oxidized during anode-cathode experimentation when exposed to aqueous electrolytes, its chemical properties and other various characteristics make titanium a very promising candidate for electrode testing.

Tungsten is the last metal listed in this thesis as a candidate for electrode testing. Most commonly known as tungsten-filament, this metal has the highest tensile strength among metals in pure form. It is also very brittle, which makes it hard to work with. Due

to high covalent bonds formed between tungsten atoms and the 5d electrons, tungsten has low thermal expansion and the highest melting point (3,422 ^{o}C, 6192 ^{o}F) in pure form. Because of its strength at high temperatures and relative chemical inertia, tungsten is used as electrodes in different electronic applications, which makes it a suitable transitional metal for electrodes.

Due to the repetitive nature of the voltammetric behavior of metal-metal electrodes, only the setups for gold-gold and gold-platinum electrodes are discussed in Sections 2.3.1 and 2.3.2. For the other metal electrode combinations, which are gold-palladium, gold-titanium, gold-tungsten, platinum-titanium, platinum-palladium, platinum-tungsten, palladium-tungsten, and titanium-tungsten, setups have been included in Appendix A.

2.3.1 Gold-gold electrodes

This section studies the gold-gold electrodes in acidic and basic (pH 1-11) electrolytes both under illumination and in the dark. The surface areas of the gold electrodes were 40mm^2 (10mm [L] x 4mm [W]) on both sides, creating a total contact area of 80mm^2.

Figure 2.2 presents a graph of the voltammetric analysis of the gold-gold electrode setup in a pH 11 basic solution The voltage level was raised from 0V to 3V, then lowered to -3V and finally brought up to 0V again. The SMU calculated the current level in the electrolyte, and this level was stored using the LABVIEW program on the computer. This experiment was conducted with different pH levels ranging from 1-11. Extrapolating the data from this set of experiments, Figure 2.3 was constructed.

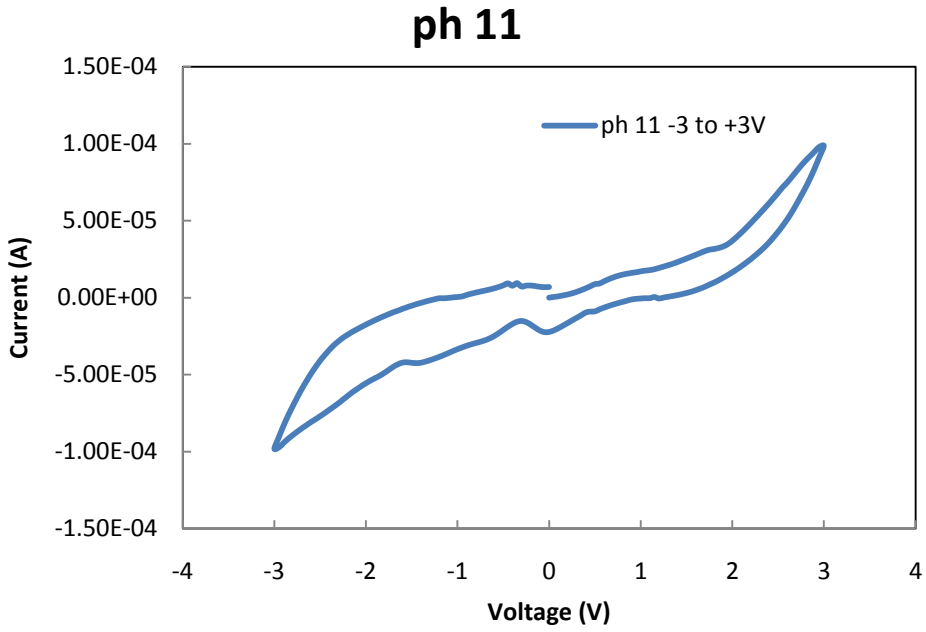

Figure 2.2 Current vs. voltage graph of gold-gold electrodes in a basic solution of pH 11

In Figure 2.3, the V_{ON} is shown against the pH level of the electrolytes. From different graphs generated during the experiments, similar to the one shown in Figure 2.2, the V_{ON} was measured for the same electrodes in electrolytes ranging from pH 1-11. The V_{ON} was extracted by taking the voltage that corresponded to 10% of the maximum current (I_{MAX}) produced inside the electrolyte.

V_{ON} is the minimum voltage required to generate hydrogen from the electrolyte solution. Studying the V_{ON} vs. pH graph gives some interesting information about the behavior of the electrodes related to the pH electrolytes used. The V_{ON} has two minimum values around pH 1 (where V_{ON} is 0.45V) and pH 10 (where V_{ON} is around 0.55V). The maximum V_{ON} registers at 1.65V where pH is 7. This indicates that around pH 1 and 10 the H^+ and OH^- ions, respectively, are plentiful in the electrolytes, which is necessary to complete the photoelectrochemical cell reactions.

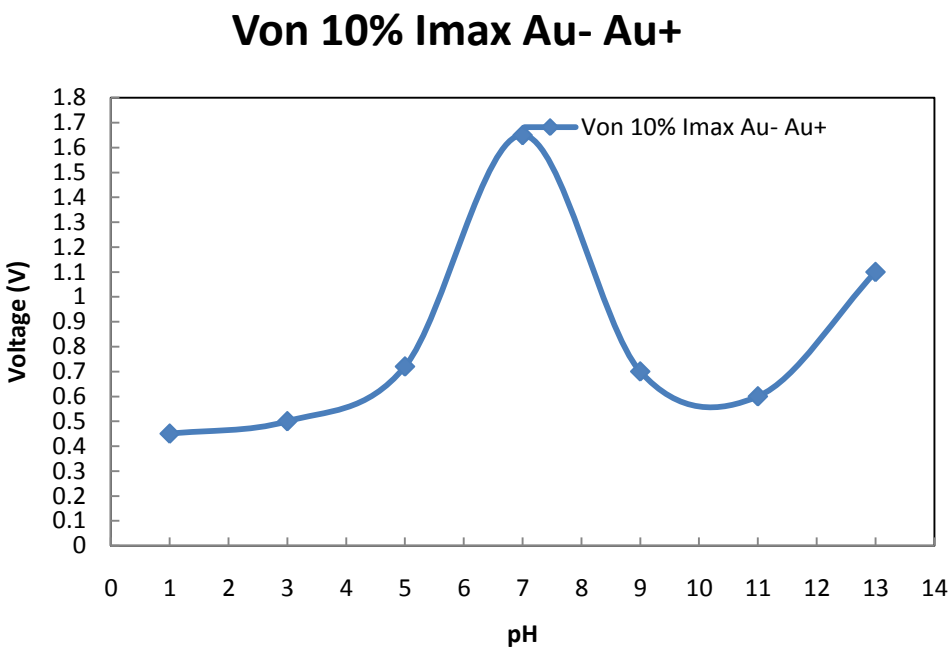

Figure 2.3 V_{ON} vs. pH graphs for gold-gold electrodes

2.3.2 Gold-platinum electrodes

Combinations of gold and platinum were used as test electrodes for the experiments discussed in this section of the thesis. Here two kinds of setup are done. In the first one, the gold is used as the cathode and platinum is used the anode. In second setup, platinum is used as the cathode and gold as the anode. Figure 2.4 presents a graph of a voltammetric analysis of a gold-platinum electrode setup in a pH 9 basic solution. The voltage level was raised from 0V to 3V, then lowered to -3V and finally brought up to 0V again. The SMU calculated the current level in the electrolyte, and this level was stored in LABVIEW on the computer. This experiment was conducted at different pH levels ranging from 1-11. Figure 2.5 was constructed by extrapolating data from LABVIEW plots.

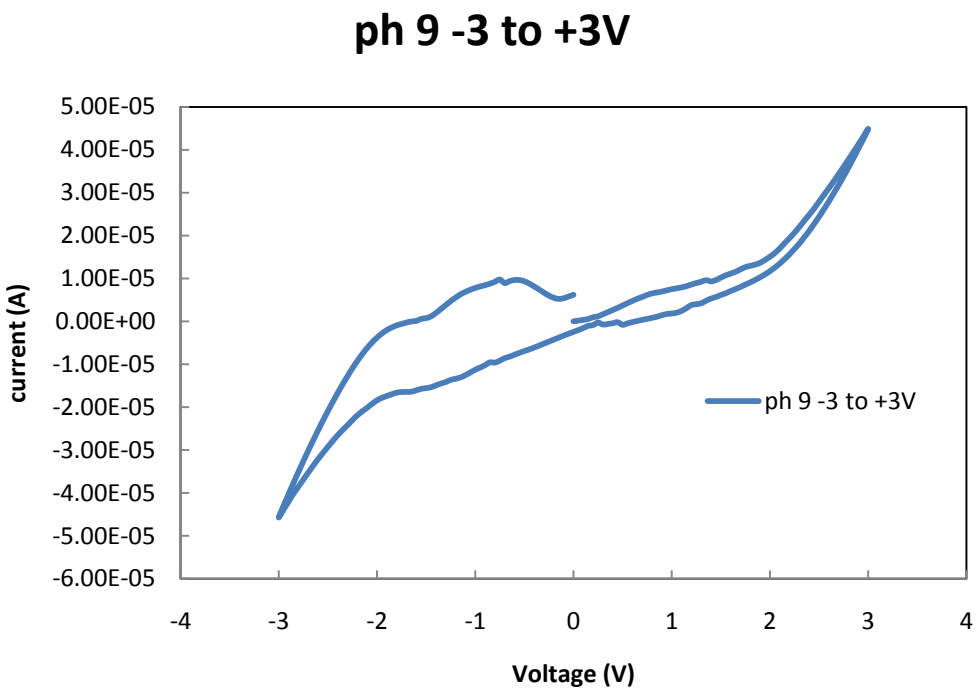

Figure 2.4 Current vs. voltage graph of gold-platinum electrodes in a basic solution of pH 9

In Figure 2.5, the V_{ON} vs. pH graph was extrapolated from different current vs. voltage graphs for pH level 1-11 solutions for gold-platinum electrodes. The first setup was done such that the gold electrode was connected to the negative terminal, and the platinum electrode connected to the positive terminal. In the next setup, the electrodes were connected in the opposite order, which is explained in Figure 2.6.

Observing the V_{ON} vs. pH graph in Figure 2.5 shows that around pH 3 and pH 10, the V_{ON} gives the lowest values of 0.65V and 0.55V respectively. It is necessary to mention that in this setup, the gold was connected as negative electrode, where, during the electrochemical reaction, electrons were released into the electrolyte thus reducing the hydrogen to H^+ ions, concurrently producing hydrogen gas. The platinum, which was

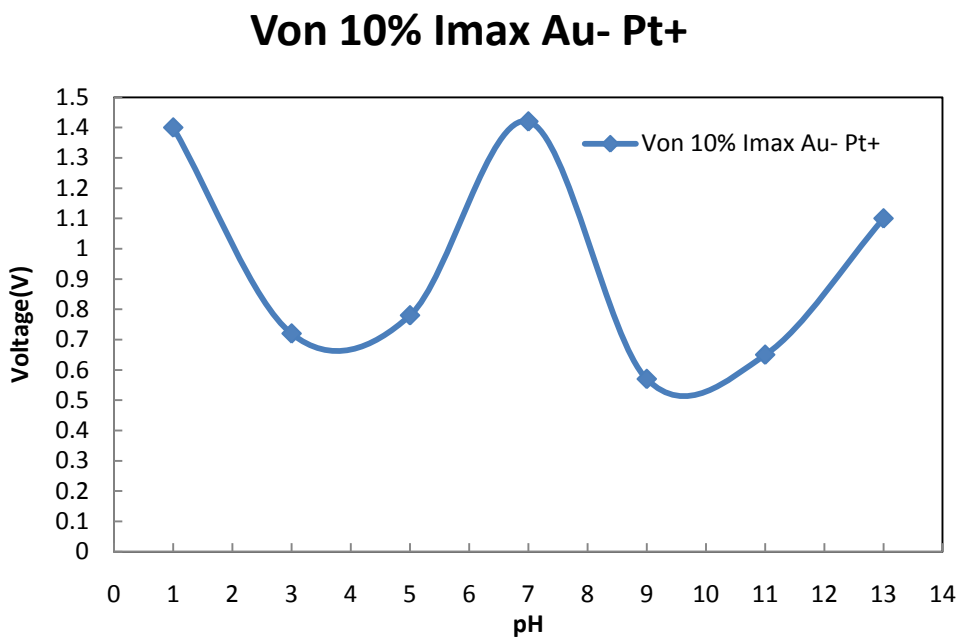

Figure 2.5 V_{ON} vs. pH graph for gold-platinum electrode

connected as positive electrode, produced oxygen as corresponding to the other half of the photoelectrochemical reaction.

Here, in Figure 2.6, V_{ON} vs. pH was plotted in the same way as the previous plot, by extrapolating data from current vs. voltage graphs for pH 1-11 electrolytes, where the gold was connected as positive electrode, and platinum was connected as negative electrode. From characteristics depicted in Figure 2.6, it is clear that, near pH 3 and pH 10, the corresponding V_{ON} shows 0.3V and 0.75V. This means that when platinum is used for negative electrodes, the tendency for it to give electrons to the electrolyte solution, thus generating hydrogen gas in the cathode, is higher than gold when used as a negative electrode.

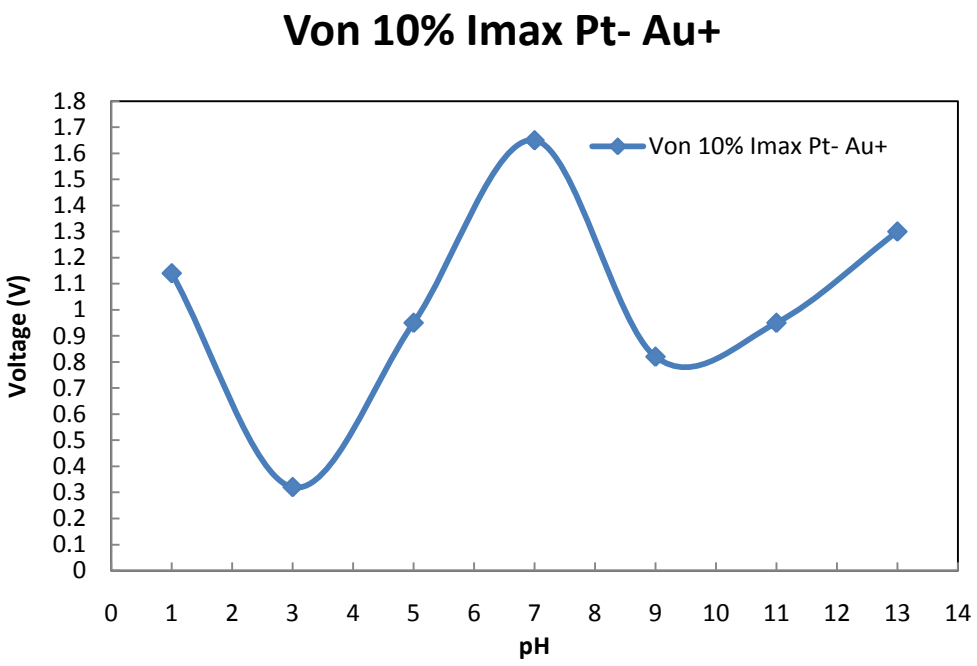

Figure 2.6 V_{ON} vs. pH graph for platinum-gold electrode

2.4 Semiconductor-semiconductor electrode

In section 2.3, various types of metal-metal electrodes were studied in order to determine the best metal electrode for producing hydrogen from different pH levels of aqueous solutions. In this chapter, three types of semiconductor-semiconductor electrodes were studied: silicon (p- and n-type), silicon carbide (4HN-type), and titanium dioxide.

Certain criteria must be met for a spontaneous water-splitting reaction to occur, for any kind of electrolysis. For example, under illumination, the semiconductor CB edge should be at a position negative to the reduction potential of water, while the VB edge should be at a positive position compared to the oxidation potential. Figure 2.7 explains the necessary position for a bandgap with respect to the reduction and oxidation

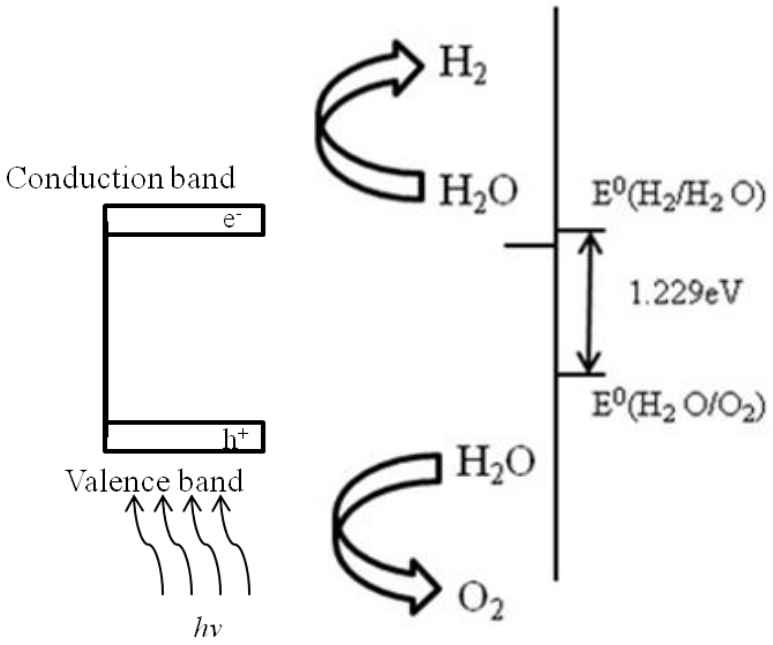

Figure 2.7 Band position of semiconductor with respect to the oxidation reduction potential of water splitting electrical equivalent energy 1.229eV

potentials of water.

In Figure 2.8, it is shown that when the photoactive semiconductor electrodes are illuminated with photon energy (*hv*) equal to or larger than the bandgap of the semiconductors, what results is a formation of electronic charge carriers, electrons in the CB, and holes in the VB. The favorable positioning of the Fermi levels in this kind of semiconductor allows the electron and holes to move in and out from the CB and VB. Here the p- and n-type semiconductors are our first candidate as electrodes. Two more semiconductors are discussed in this thesis to observe their semiconductor-semiconductor electrode characteristics.

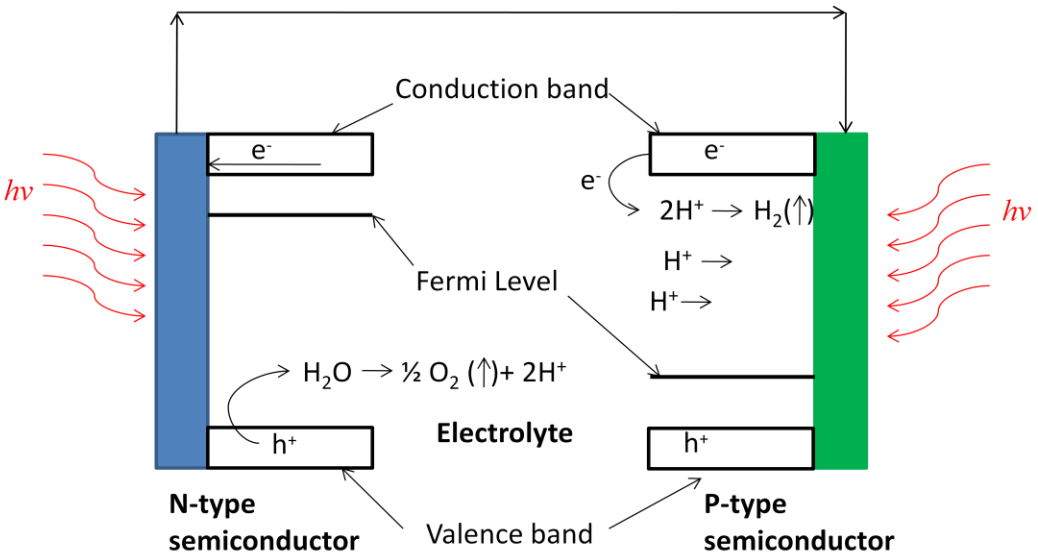

Figure 2.8 Simple diagram of photoactive semiconductor electrode se up for water photoelectrolysis

2.4.1 Silicon

Both p- and n-type silicon have been studied and used as semiconductor electrodes. The electrode samples were made by dicing 4" p- and n-type silicon wafers of <100> orientation with a doping concentration of ~$10^{15}$$cm^{-3}$. In Figure 2.9 two 4" p- and n-type silicon wafer are shown and Figure 2.10 illustrate how the electrodes were prepared.

Standard silicon wafers have a polished side and an oxide back-sealed side. The wafer was diced into a 1cm × 1cm piece, and the back side was scratched with diamond-tipped scribe to reveal the bare silicon. A covered copper wire was then cut on both ends. One end was placed on the scratched back surface of the silicon and sealed with silver paint for conductivity. After that the entire device was covered with melted black wax and the polished side was kept open for photon energy from the sunlight.

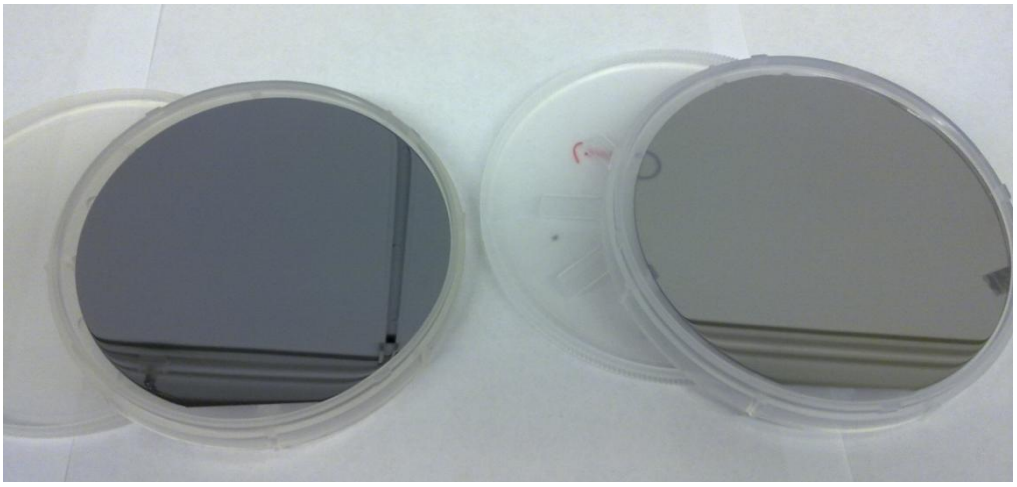

Figure 2.9 P- and n-type 4” silicon <100> wafers

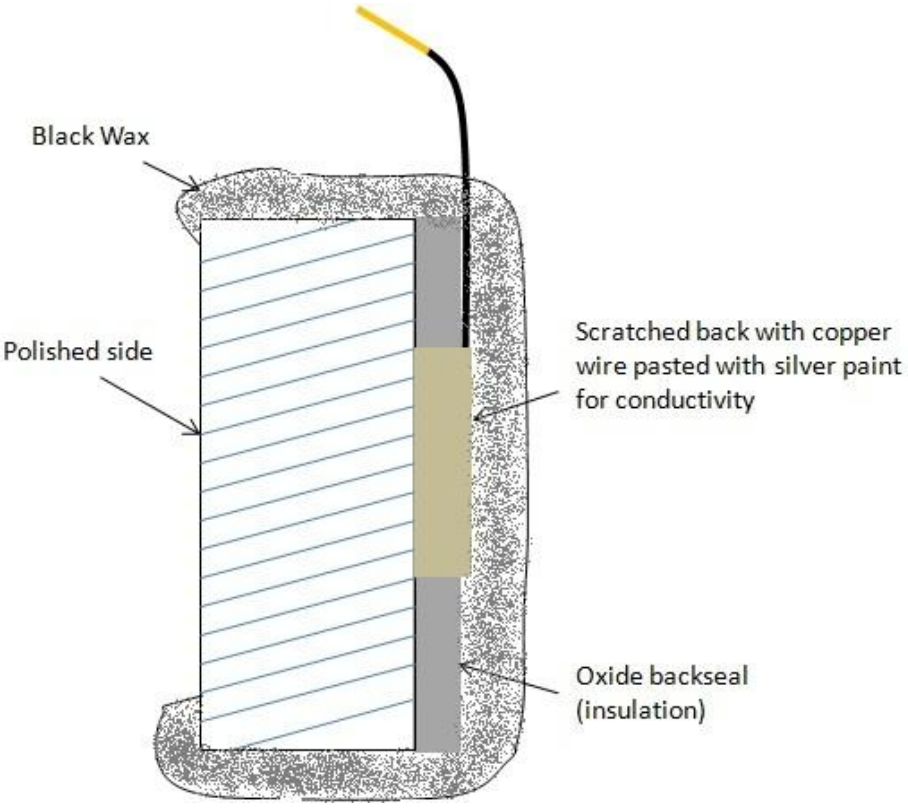

Figure 2.10 Silicon semiconductor electrode sample preparation

2.4.2 Titanium dioxide (TiO_2)

Interest in TiO_2 as a photocatalyst has been growing rapidly in the last few decades. TiO_2 is one of the most widely used photocatalysts for the decomposition of various organic pollutants. Its optical properties of high activity and chemical stability have made it a prime component in the study of photocatalysis of water.

The TiO_2 was prepared by anodic oxidation on a 5mm thick, 99.99% pure sheet of titanium foil. The foil was cut into small pieces where the total surface area of the foil was kept the same with all other counter electrodes that were used. The titanium dioxide grown on the titanium foil was an n-type, Figure 2.11. This process is detailed in Atusushi Nakahira's [24] paper. The synthesis of the TiO_2 films was done by anodic oxidation in phosphoric acid under various conditions (several different acid concentrations and applied voltages). The applied voltage ranged from 150V to 350V. The concentration that was used for the growth of TiO_2 in this study was 0.25M phosphoric acid. The expected thickness of the TiO_2 films was in the range of 50-300nm.

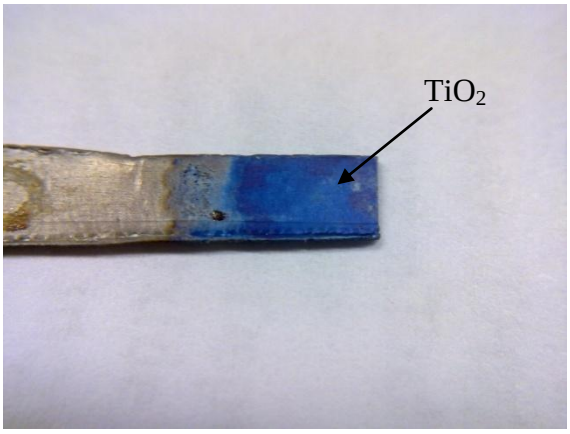

Figure 2.11 TiO_2 films grown on Ti foil by anodic oxidation in 0.25M phosphoric acid

2.4.3 Silicon carbide (SiC)

Silicon carbide (SiC,4HN type) is a wide bandgap with 3.23eV at room temperature semiconductor with a hardness close to that of diamond (9-10mohs) and corrosion resistant, which has very suitable conduction band energy relation to the formation of hydrogen in water. Photogenerated electrons absorb the energy of photons, which have more energy than they do, and jump from VB to CB, which then enter the water to form hydrogen.

A 3", 4HN-type SiC wafer was diced into 1cm × 1cm squares and prepared as an electrode in the same way as silicon electrodes in Figure 2.12.

2.4.4 Silicon-silicon electrodes

There are two semiconductor electrodes, both of which are silicon semiconductors, discussed in this section. The difference between the two electrodes is that one of them is a p-type and the other an n-type silicon wafer. In Section 2.4.1, it is

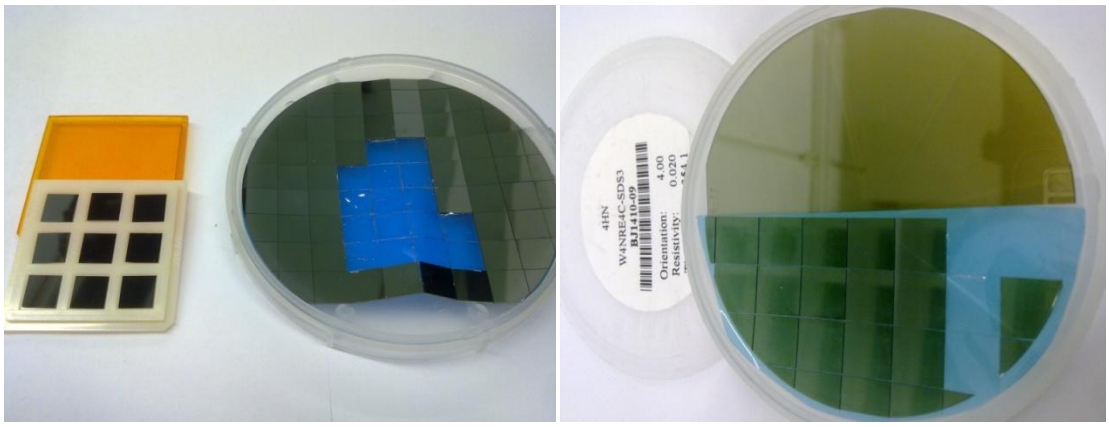

Figure 2.12 1cm x 1cm diced SiC wafer for electrode

mentioned that p- and n-type semiconductor are the first choice as photoelectrodes due to its suitable bandgap structure and Fermi level positioning for photogenerated electron-hole pair. That is why p- and n-type silicon semiconductor is the first candidate for semiconductor electrode testing. The electrolytes used in this experiment also range from pH 1 acidic to pH 13 basic solutions. However, for convenience, only two kinds of pH solutions are discussed in this section, acidic pH 1 and basic pH 11 solutions.

In order to explain the photoactive semiconductor electrodes' characteristics, voltammetric analysis was conducted under two conditions. First, the electrodes were put inside the electrolytes and the current vs. voltage analysis was run under no illumination. After the analysis was done, the electrodes were taken out and put inside a diluted BOE (buffered oxide etch) to get rid of the thin layer of oxide formation on the surface due to the anodizing effect. Once the oxide was etched off, both electrodes were put into the electrolytes again and the current vs. voltage analyses were conducted under illumination. The intensity of the light source was $197.35 W/\mathrm{m}^2$.

As mentioned earlier the p-type silicon electrode was used as a photocathode where H^+ ions were reduced to hydrogen. The n-type silicon electrode was used as a photoanode, where, due to water oxidation, oxygen gas was generated and H^+ ions were released.

Figures 2.13 and 2.14 show current vs. voltage plots both in pH 1 and pH 11 electrolytes for p- and n-type semiconductor electrodes. The current vs. voltage plot without illumination (blue line) shows. In the figures the p-type silicon photocathode was under negative bias (reverse bias), and the p-type silicon photoanode was under positive bias (forward bias) when voltage was raised from 0V to 3V and brought down to 0V.

Conversely when the voltage was lowered from 0 to -3V then brought up to 0V, the biasing of the electrodes was reversed. The p-type was used as a photoanode, which was under positive bias (forward bias), and the n-type as a photocathode, which was under negative bias (reverse bias). The blue line shows the condition where the current vs. voltage plot were taken without illumination. As there was no light energy projected onto the surface of the electrode, there was no noticeable photoreaction happening inside the semiconductor, the blue line does not show any significant difference in forward or reverse bias

However, when the electrodes are illuminated with a bright light source, the current vs. voltage graph shows some significant change in its behavior. When photon energy from the light source hits the surface of the semiconductor electrodes on the surface of the n-type photoanode, water oxidation occurs due to the holes (h^+) acceptation in the valence band from the electrolytes. Oxygen gas is generated and, at the same time, H^+ ions are released. Concerning the p-type photocathode under illumination, the electrons (e^-) from the conduction band are released into the electrolytes, which then reduce the H^+ ions to H_2 gas.

In studying Figures 2.13 and 2.14, it is clear that when the photogenerated hydrogen experiment was conducted in the pH 1 acidic, in contrast to the pH 11 basic solution, the maximum current measured was 2.50 E-04A. In the basic solution, the highest current was 1.50E-04A. This is expected because, in the acidic solution, there are more H^+ ions than in the basic solution. In the basic solution, there are more OH^- ions. H^+ ions give more electrons for reducing hydrogen than producing hydrogen and more flow in the electron concentration.

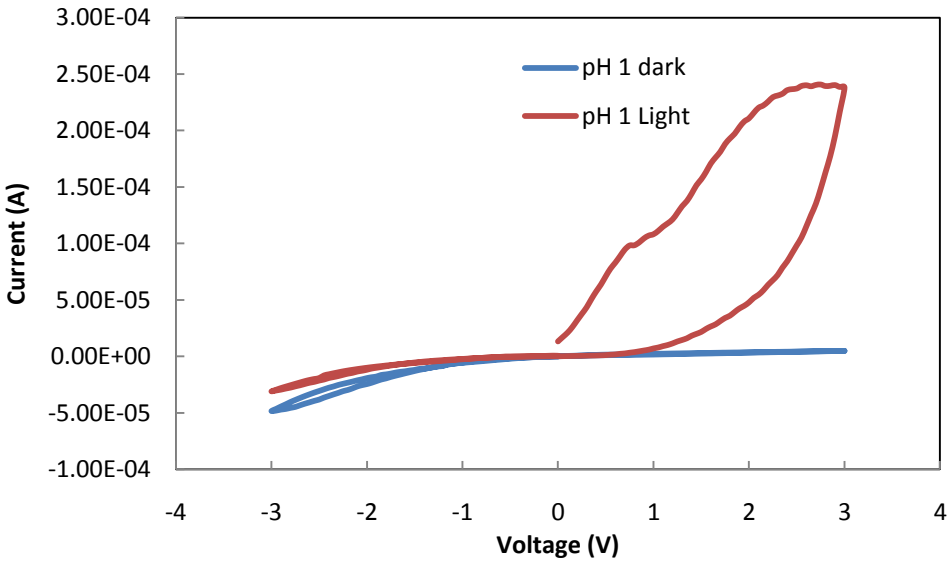

Figure 2.13 Current vs. voltage graph of p-type silicon as cathode and n-type silicon as anode under dark and illuminated condition in pH 1 acidic solution

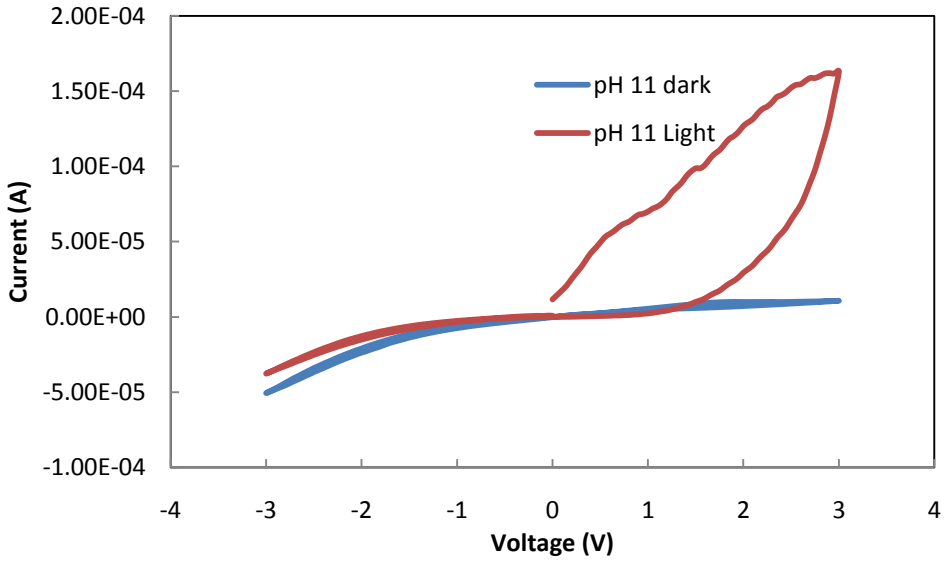

Figure 2.14 Current vs. voltage graph of p-type silicon as cathode and n-type silicon as anode under dark and illuminated condition in pH 11 basic solution

2.4.5 Silicon-titanium dioxide electrodes

In this section two different kinds of semiconductor electrodes are used. For the photocathode, p-type silicon was used. For the photoanode, an n-type TiO_2 was used. The TiO_2 was grown on a 5mm thick, pure titanium foil using anodic oxidation. In previous sections, it was explained how the n-type TiO_2 was grown on the titanium foil.

TiO_2 is a very popular photocatalyst in the field of photogenerated hydrogen for water electrolysis. It is thus a good candidate for a potential electrode for the purpose of generating oxygen in the photoanode.

In Figure 2.15 a pH 9 basic electrolyte was used to study the characteristics of n-TiO_2 for producing oxygen. This would prove TiO_2 to be a suitable candidate for a photoanode paired semiconductor photocathode. The current vs. voltage analysis was run from -3V to 3V. When the current vs. voltage analysis was done under the dark condition (blue line), it became clear that in forward bias mode, there were no photogenerated holes being accepted in the photoanode, TiO_2. Therefore, there is no noticeable current being generated. However, under illumination (red line), it becomes clear that current is generated around 1E-04A. This indicates that the TiO_2 photoanode is accepting holes generated due to photon energy from the electrolytes, and releasing H^+ ions for the photocathode to be reduced and produce hydrogen gas. It can also be seen that, in the dark condition under the reverse bias, the electrodes are accepting and releasing holes and electrons, therein generating a maximum 2E-04A current, but this is not due to photon energy from the light source as both the blue and red line show the same plots of data.

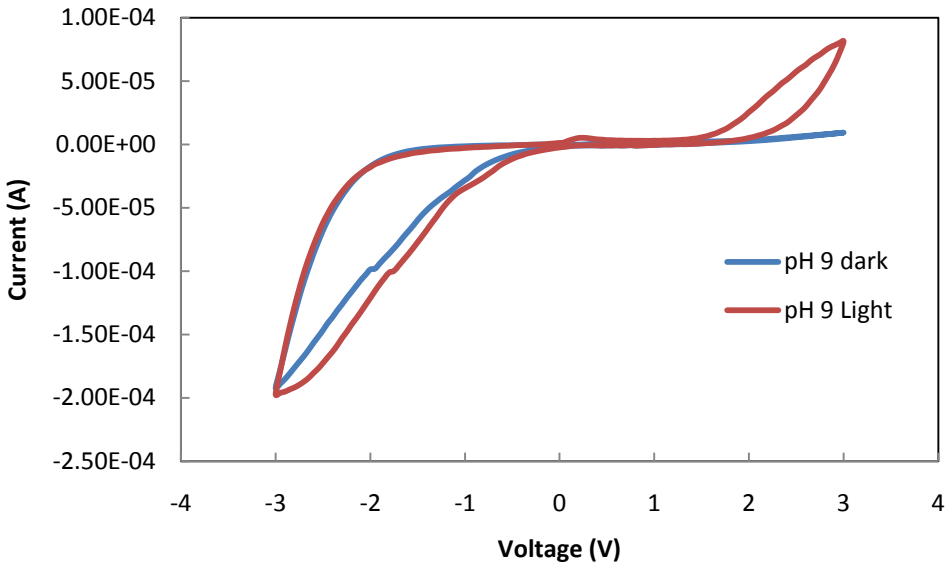

Figure 2.15 Current vs. voltage graph of p-type silicon as cathode and n-type TiO_2 as anode under dark and illuminated condition in pH 9 basic solution

2.4.6 Silicon carbide-titanium dioxide electrodes

The last sets of semiconductors that were used for the photoelectrolysis of water are a 4HN-SiC and an n-TiO_2. It might be confusing to observe that both of the electrodes that are used here are N-type semiconductors, where it is clear that, in order to produce hydrogen in the photocathode, an n-type semiconductor is required. The reason this combination is used is to understand and study the ability of these two n-type semiconductors to generate oxygen under illumination, where it could be easier to determine which semiconductor would be better suited for a photoanode with a photocathode. Figure 2.16 is the current vs. voltage graph of these two photoelectrodes in pH 1 electrolyte.

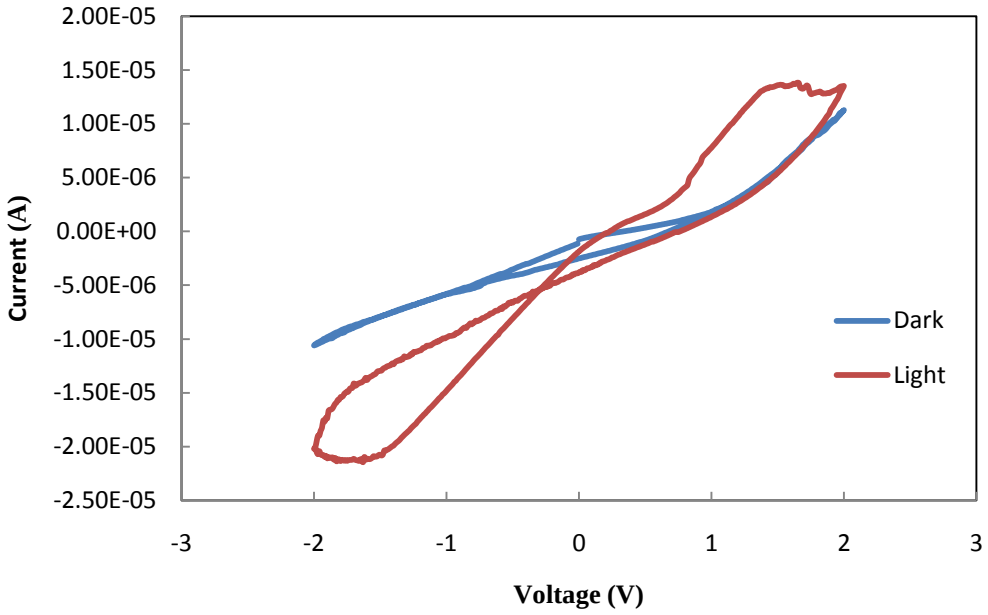

Figure 2.16 Current vs. voltage graph of 4HN SiC as cathode and n-TiO_2 as anode under dark and illuminated condition in pH 1 acidic solution

In this setup, the 4HN-types SiC was used as a photocathode and the n-type TiO_2 was used as the photoanode. In closely examining Figure 2.16, it is clear that, under no illumination, the current vs. voltage curve shows very few signs of generating current. Yet, under illumination it is visible that both of the N-type semiconductor electrodes showed potential characteristics for producing oxygen as they accepted holes from the electrolyte and oxidized water to release H^+ ions.

The Table 2.1 summarizes the data collected through the experiments outlined between sections 2.3 and 2.4.

Table 2.1 Summary of maximum current I_{MAX}, Lowest V_{ON} and pH level for metal-metal electrodes and semiconductor-semiconductor photoelectrodes

	Cathode(-ve) , Anode (+ve)	I_{Max} (A), pH (at 5V)	Lowest V_{On} (V), pH
Metal Electrodes	1. Au – Au	1.0E-04 (pH 11)	0.5 (pH 1)
	2. Au(-ve) – Pt(+ve)	4.5E-05 ((pH 9)	0.3 (pH 3)
	3. Au(-ve) – Pd(+ve)	6.0E-04 (pH 9)	0.5 (pH 10)
	4. Au(+ve) – Ti(-ve)	2.2E-05 (pH 3)	0.9 (pH 3)
	5. Au(-ve) – W(+ve)	7.2E-04 (pH 11)	0.2 (pH 3)
	6. Pt(-ve) – Pd(+ve)	1.5E-04 (pH 11)	0.5 (pH 11)
	7. Pt(-ve) – W(+ve)	8.0E-04 (pH 3)	0.3 (pH 3)
	8. Pt(-ve) – Ti(+ve)	6.0E-05 (pH 11)	0.8 (pH 11)
	9. Pd(+ve) – W(-ve)	1.5E-04 (pH 3)	0.5 (pH 3)
	10. Ti(-ve) – W(+ve)	2.0E-04 (pH 3)	0.3 (pH 3)
	Photocathode(-ve) , Photoanode (+ve)	I_{Max} (A), pH (at 3V)	Lowest V_{On} (V), pH
Semiconductor Electrodes	1. P-Si(-ve)–N-Si(+ve)	6.0E-06 (pH 1) Dark 2.5E-04 (pH 1) Illuminated	0.2 (pH 1) Illuminated
	2. P-Si(-ve) - N-TiO_2(+ve)	7.0E-06 (pH 9) Dark 9.5E-05 (pH 9) Illuminated	1.5 (pH 9) Illuminated
	3. N-SiC(-ve) – N-TiO_2(+ve)	1.0E-05 (pH 1) Dark 1.5E-05 (pH 1) Illuminated	0.5 (pH 1) Illuminated

2.5 The Effect of Photocatalyst Coating on Electrodes

In this section, the effect of the photocatalyst on a semiconductor was studied in order to locate a possible candidate for use as a photoelectrode in water electrolysis using light energy. Sections 2.5.1 and 2.5.2 discuss what photocatalysts are and why we need them.

2.5.1 What is a photocatalyst?

Catalysts work by changing the activation energy for a reaction, in other words, the minimum energy needed for the reaction to occur. This is accomplished by providing a new mechanism or reaction path through which the reaction can proceed. When the new reaction path has lower activation energy, the reaction rate is increased and the reaction is said to be catalyzed.

Photocatalysis happens when a photoreaction is accelerated in the presence of a catalyst. The activity of the photocatalysis depends completely upon the ability of the catalyst to create an electron-hole pair, which generates free radicals (hydroxyl radicals: OH^-) capable of undergoing secondary reactions. Figure 2.17 shows a simple illustration of photocatalyst. Due to the photon energy (*hv*) hitting the band energy, an electron is knocked from the valence band to conduction band. The electron e^- is then released to form a reduction reaction and, due to the absence of an electron, a hole h^+ undergoes an oxidation reaction by accepting an electron e^-.

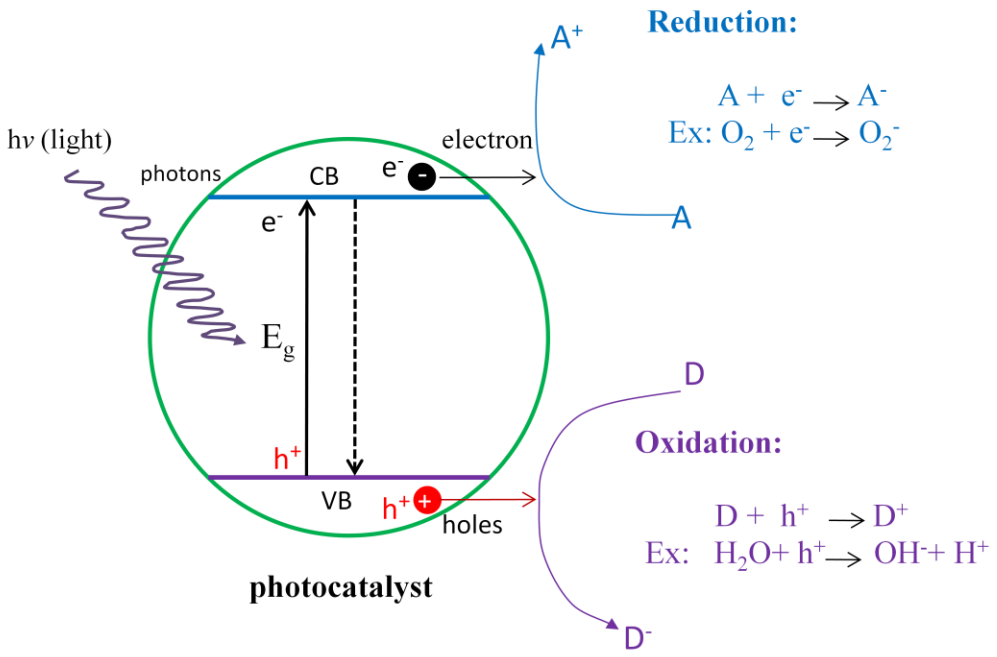

Figure 2.17 Simple diagram showing the work of a photocatalyst

2.5.2 Why are photocatalysts needed?

Although using photocatalysts to split water seems very intriguing, there are a number of parameters to be concerned with. In Figure 2.18, some of the properties of photocatalysts important to study are given. When light energy generates electrons and holes, these have to migrate to the surface separately or else they will recombine with each other. This again depends on the crystal property of the material. The better the crystalline structure of the material, the fewer defects there are because the more defects present in the material, the higher the chance of the photo-generated electrons and holes recombining at certain sites due to those defects. Moreover, there is also a concern about the number of active sites available on the surface for the photogenerated electrons and holes to conduct redox reactions. This means that even if the electrons and holes have

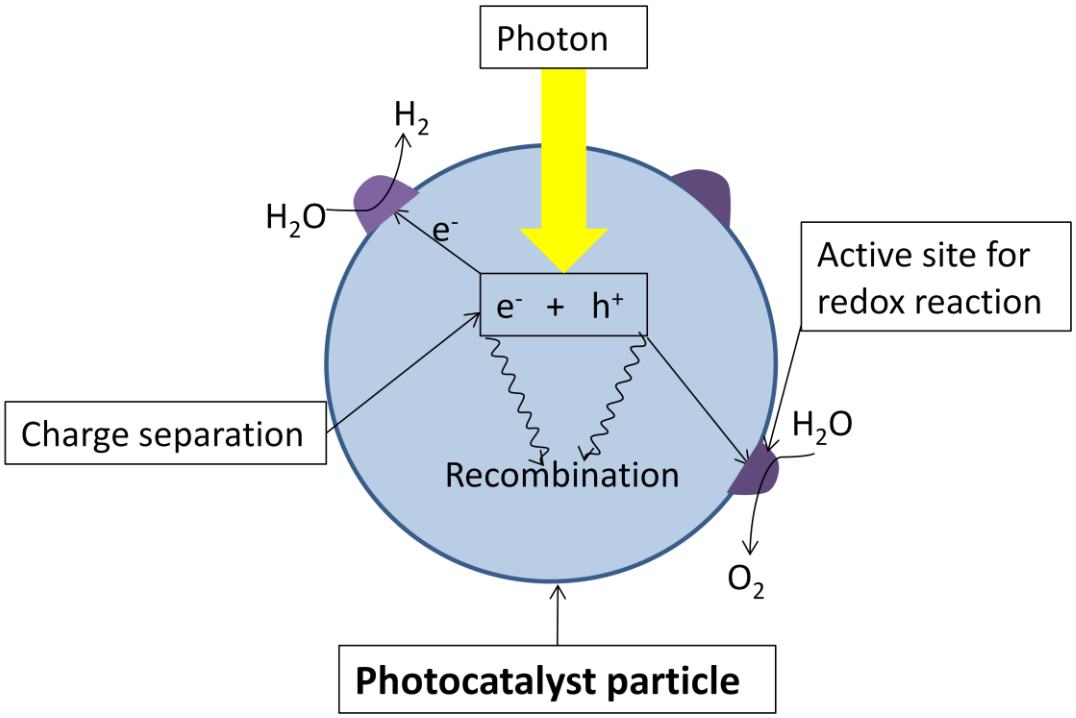

Figure 2.18 Photocatalytic process of powdered photocatalyst

sufficient thermodynamic energy to split water molecules, there have to be enough sites on the surface for them to complete the redox reaction. That is why other photocatalysts, such as Pt, NiO, TiO_2, RuO_2, etc., are introduced on the surface to increase the availability of active sites.

Chapter 3 contains a detailed discussion regarding some photocatalytic material used on semiconductor photoelectrodes in order to enhance their characteristics.

2.6 Conclusion

In this chapter, we investigated different suitable metal-metal and semiconductor-semiconductor electrodes in order to understand their role as a potential photoelectrode for water photoelectrolysis. In studying the different results and data, it is concluded that

silicon (p- and n-type) yield the best results among photoelectrode test results. Platinum and tungsten were more photoactive as metal electrodes, generating hydrogen through the photoelectrolysis of water.

CHAPTER 3

MULTILAYER DEVICES AND ELECTRODES

3.1 Introduction

This chapter focuses on the multilayer photoactive semiconductor electrodes, their principles, and the device that was designed for this thesis. In the field of hydrogen production that uses photoactive semiconductor electrodes, there are two kinds of approaches: one being a single layer electrode and the other a multilayer electrode. Multilayer device electrodes have been reported to exhibit a much more efficient performance than the former. In this thesis, the multilayer device was constructed using a silicon substrate, an atomic layer deposition of Al_2O_3, doped polysilicon and tungsten nanopores (TNP) layers. The voltammetric and efficiency analyses were conducted and are reported.

In Sections 3.1.1 and 3.1.2, the differences between single and multilayer photoactive semiconductor electrodes and basic examples of multilayer device structures and mechanisms are discussed.

3.1.1 Simple electrodes vs. multilayer electrodes

Single layer structure was the main concept behind the first solar device which was constructed with p- and n-type semiconductors. It is known that p-type silicon has impurities with 3 valence electron (such as boron), which when introduced to intrinsic

silicon semiconductors, create a vacant space for electrons where boron forms covalent bonds using its 3 outer shell electrons with the 4 outer shell electrons of silicon. This vacant space for electrons, which is also known as holes, makes the p-type extrinsic silicon semiconductor. Additionally, in p-type semiconductors, the Fermi level lies close to the VB, as there are more holes in a p-type semiconductor. When impurities with 5 valence electrons (such as phosphorous) are introduced to the intrinsic silicon, the 5 electrons in the outer shell try to make covalent bonds with the 4 outer shell electrons of silicon. After creating 4 covalent bonds with the 4 outer shell electrons of silicon, there is 1 extra electron from the phosphorous that remains free. This extra electron can then roam in the semiconductor, making the silicon an n-type semiconductor. In n-type, the Fermi level lies close to the CB. Now, when these two p- and n-type silicon semiconductors are used as photoactive electrodes to perform electrolysis of water, the photon energy from sunlight knocks the electron from the VB to the CB, which then enters the electrolyte.

Figure 3.1 explains the phenomenon of photon energy directing the flow of electrons and holes inside the p- and n-type silicon semiconductors. This structure thus represents the basic single layer semiconductor structure for photoactive electrodes. In multilayer semiconductor electrodes, however, while the concept is nearly the same, the structure is usually different. Instead of using 1 semiconductor (p- or n-type), various layers of materials are used to ease the flow of electrons and holes to and from the electrolyte.

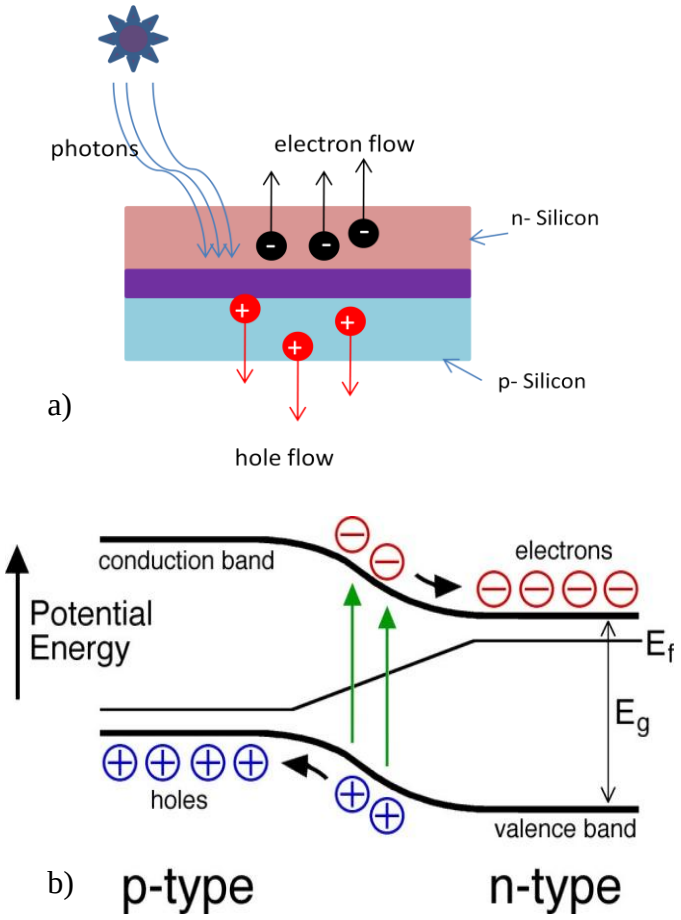

Figure 3.1 The photon energy from sunlight energizing the electrons and holes to flow in a) opposite directions; The schematic diagram of b) bandgap structure of p- and n-type silicon semiconductor and the flow directions of electrons and holes

3.1.2 Multilayer electrodes and devices

As discussed in Section 3.1.1, in multilayer semiconductor electrode devices, different combinations of structures have been reported. Multilayer solar cells have recently reached an efficiency of 41% [27], which exceeds the previous record of 40% [27] efficiency.

The multilayer solar cell, which comes from the concept of multiband cells, was conceptualized by Martin Wolf who proposed the PV effect in 1960 [28]. In 1999, at a Berkeley lab, Wladek Walukiewicz and others were working with solar cell designers at

Department of Energy's National Renewable Energy Laboratory (NREL). Researchers there were working on building a three-junction solar cell. When researchers from NREL were trying to make semiconductor material with a 1eV bandgap using gallium indium arsenide nitride alloys to achieve the desired bandgap, they created the first PV semiconductor with a split bandgap.

Figure 3.2 is a simple diagram that explains the advantages of multiband cells. This kind of structure consists of different layers. Each layer is a different alloy or semiconductor with a different bandgap, which responds to a different frequency of sunlight. Multiband structures involve multiple bandgaps with only a single layer of material, whereas a multilayer solar cell comprises various layers of materials. The device that has been reported in this thesis is a multilayer photoactive solar device.

3.2 Multilayer Structures

In this section, the structure of the multilayer device is discussed and the construction process is described. Sections 3.2.1 and 3.2.3 focus on the silicon substrate, the reason for the choice of silicon, Atomic Layer Deposition (ALD) of Al_2O_3 and doped polysilicon.

3.2.1 Silicon (p- and n-type) substrate.

So far, the importance of silicon semiconductors (both p- and n-type) has been discussed in terms of electrode purposes. Even though it is a poor absorber of the full spectrum of light and requires a thick (several hundred microns) material coating, crystalline silicon (c-Si) has always been used as a light absorbing semiconductor in

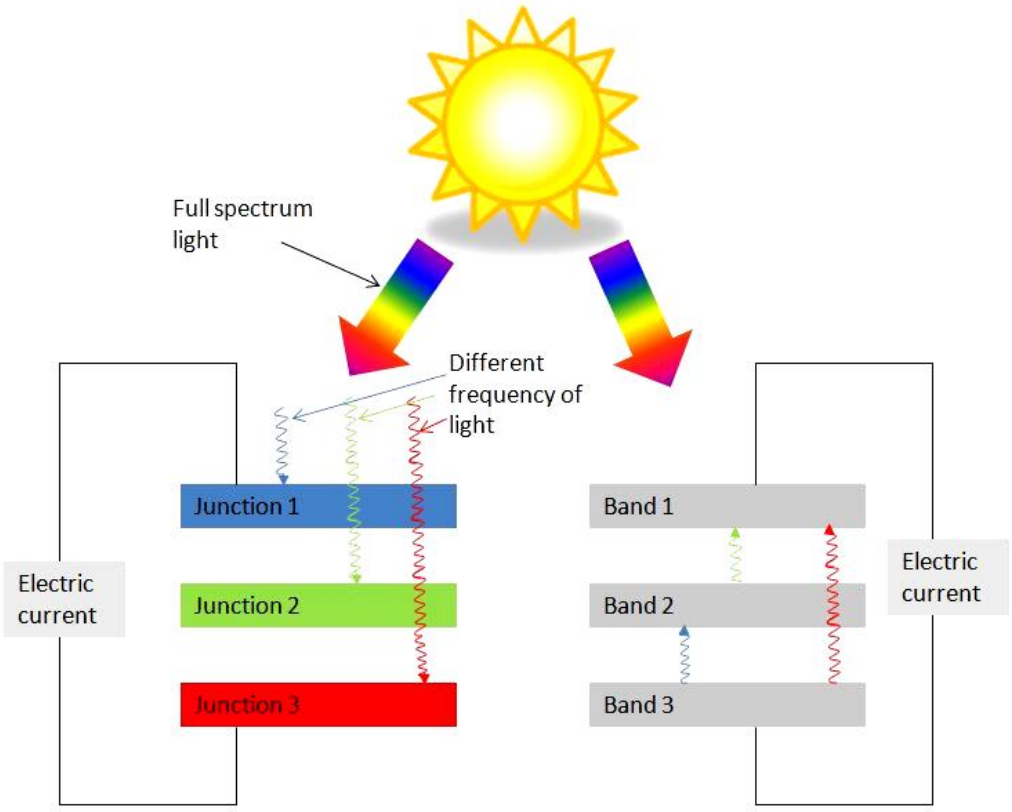

Figure 3.2 Multilayer (left) and multigap (right) solar cell responses to different frequencies of sunlight

most solar cells. Because of its standard performance in solar cells with good efficiency (12-18%, half to two-thirds of the theoretical maximum) and abundance on earth silicon is always the first choice when it comes to microelectronics and semiconductor industries.

Two types of crystalline silicon are being produced in industries. One is monocrystalline silicon, which is made by slicing wafers up to 200mm in diameter and 500μm thick from a high-purity, single crystal boule. The other type is multicrystalline silicon, which is made by first sawing a cast block of silicon into bars and then into wafers.

The bandgap energy (E_g) of silicon crystalline is around 1.12eV, which corresponds to the 1107nm wavelength (λ) of light ($\lambda_g = 1.24 / E_g$). Although the freqency of the wavelength is near that of infrared light, the bandgap and the Fermi level positions of both p- and n-type silicon semiconductors are nonetheless very suitable for solar device structures.

Both p- and n-type c-Si wafers used were doped with phosphorous and boron impurities, and their concentrations were around ~$10^{15}cm^{-3}$.

3.2.2 Atomic layer deposition (ALD)

The device reported in this thesis has a multilayer structure. In order to enhance the mobility and generation of electron-hole pairs, a thin layer (0.1µm) of doped polysilicon was deposited on the silicon substrate. Due to the structural design, which will be explained later in this chapter, oppositely doped polysilicon was deposited on both p- and n-type silicon substrates. It is known that if doped polysilicon (for example, n^+ polysilicon) was deposited on top of the p-type silicon, a p-n junction would form in between. A p-n junction in semiconductor will act as a diode and will have an opposite electric field, preventing the free electrons or holes from moving between the layers. Therefore, in order to prevent the p-n junction, a very thin layer of Al_2O_3 (1nm) was first deposited on both p- and n-type silicon substrates using ALD. This also reduces the leakage current from the reported device.

3.2.3 Polysilicon

The polysilicon was deposited using a Low Pressure Chemical Vapor Deposition (LPCVD) on the silicon substrate. The silicon substrate had a thickness of 500µm and the Al_2O_3 layer was 1nm thick. Polysilicon does not have a crystalline orientation-based structure like that of c-Si, which plays a very important role in the part of electrons' and holes' mobility and directions. This shortcoming is compensated for by depositing a very thin layer of doped polysilicon (0.1µm) on top of Al_2O_3 layer.

In Figure 3.3, the parameters of the doped polysilicon and Al_2O_3 layers are shown. The reason behind the polysilicon deposition is when P-type silicon and

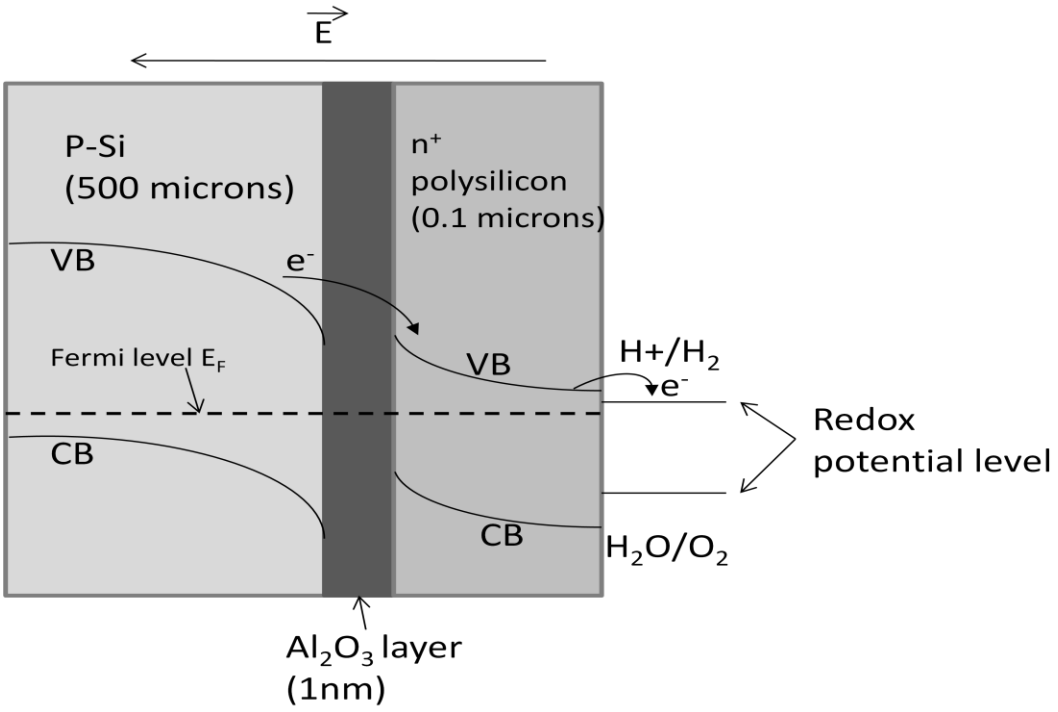

Figure 3.3 Diagram showing the polysilicon deposition on c-Si substrate and the VB and CB position and the flow of electrons

n^+-polysilicon (highly doped ~$10^{20}cm^{-3}$) are joined together, there is an electric field ($\bar{E}$) created due to the surplus of holes in p-type silicon and electrons in n^+-polysilicon; however, due to the ALD layer of Al_2O_3 (1nm) in between them, the p-n junction cannot form. Now, because of the presence of an electric field, the VB and CB bend downwards in the p-type silicon and upwards in the n^+-polysilicon near the ALD layer. This creates a very suitable path for the electron to move against the electric field through the polysilicon into the electrolyte. In the same way, the other electrode with the n-type silicon, Al_2O_3 layer and p^+-polysilicon structure was constructed where the physics behind the design is similar to that of the p-silicon based electrode explained above.

The structure of polysilicon is not the same as that of c-Si, which has an orientation-based planar structure that helps the electrons and holes generated by the photon energy to move through the structure easily. Polysilicon has a granular structure, which means that there are random fissures that could act as a recombination site for the electrons and holes generated. This problem was taken care of by making the polysilicon layer very thin (0.1µm).

3.3 Tungsten Nanopores (TNP)

After the electrodes were prepared with a multilayer structure, they were finally ready to be tested. In this step, in order to enhance the electrodes' surface reaction with the electrolyte and sunlight, and also to enhance the mobility of electron-hole pairs generated from photon energy, the surface of the electrodes were nanotextured with TNP.

The following sections, 3.3.1 to 3.3.4, discuss tungsten material, its usefulness, the process of how to grow TNP, and SEM images of the TNP.

3.3.1 Tungsten

Tungsten (W) is the last metal listed in this thesis as a candidate for metal electrode testing. Most commonly known as tungsten-filament, this metal has the highest tensile strength among metals in pure form and is very brittle, which makes it difficult to work with. Due to strong covalent bonds formed between tungsten atoms and its 5d electrons, tungsten has a low thermal expansion and the highest melting point (3422°C, 6192°F) among metals in pure form. Therefore, because of its strength at high temperatures and relative chemical inertia, tungsten is used for electrodes in different electronic applications, which makes it a suitable transitional metal for electrodes.

3.3.2 Process to grow TNP

Growing the TNP required several steps in a microfabrication facility. The steps for growing the TNP on the surface of the polysilicon are as follows:

1. Sputtering 20nm of tungsten (W) on the target surface
2. Applying 1813 positive photoresist on the top of the sputtered tungsten surface
3. Spinning the photoresist for 200rpm for 60 seconds.
4. Prebaking the photoresist for 2 minutes in 110°C on a hot plate.
5. Exposing it to ultraviolet (UV) light for 30 seconds
6. Developing the photoresist in 352 developer for 45 seconds
7. Post baking for 3 minutes in 120°C

8. Dipping the photoresist in hydrogen peroxide (H_2O_2) for 40 seconds
9. Using oxygen plasma to remove the photoresist for 12 minutes

3.3.3 SEM images

The SEM images of the TNP are discussed in this section. Figure 3.4 shows the top view of the TNP grown on one of the electrode surfaces. In the magnified version of the image, it can be seen that the nanopores are in the range of 5-10nm in diameter. Next, Figure 3.5 is a cross section of the photoelectrode with p-type silicon, Al_2O_3, n^+-polysilicon, and TNP on its surface. Although the purpose and function of the Al_2O_3 layer between the silicon and polysilicon were to prevent the p-n^+ junction from forming, the phosphorus dopant seems to penetrate through the Al_2O_3 layer and move to the n-silicon layer for about 0.05μm. However, the structure should still serve the purpose of the Al_2O_3 layer.

3.3.4 Device structure

In this section, Figure 3.6 illustrates reported device structure. The electric field will be strong between the silicon (p- and n-) and oppositely, plus highly doped (n^+- and p^+-) polysilicon, and suitable for the electrons and holes to move according to the direction of the electric field. To prevent the p-n junction from forming and to reduce the electric field, a thin layer of Al_2O_3 was introduced between the silicon and polysilicon layers. This layer is so thin (1nm) that it does not hamper the electric field from forming due to the (p- and n-) silicon and oppositely doped (n^+- and p^+-) polysilicon, thus making it easy for the photogenerated electron-hole pairs to move through the thin Al_2O_3 layer..

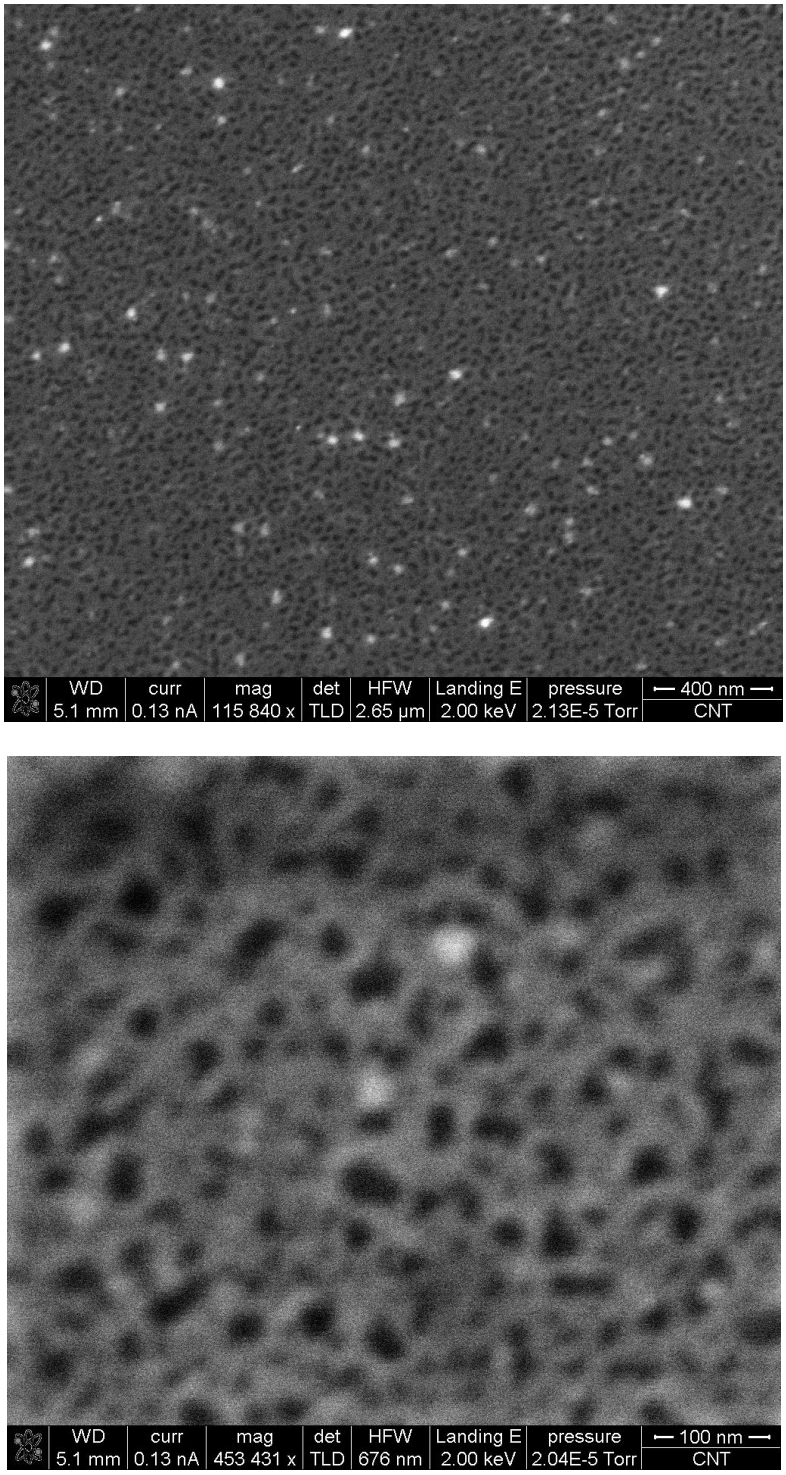

Figure 3.4 SEM images of TNP on the surface of n-silicon, Al_2O_3 and p^+-polysilicon (top), magnified (bottom)

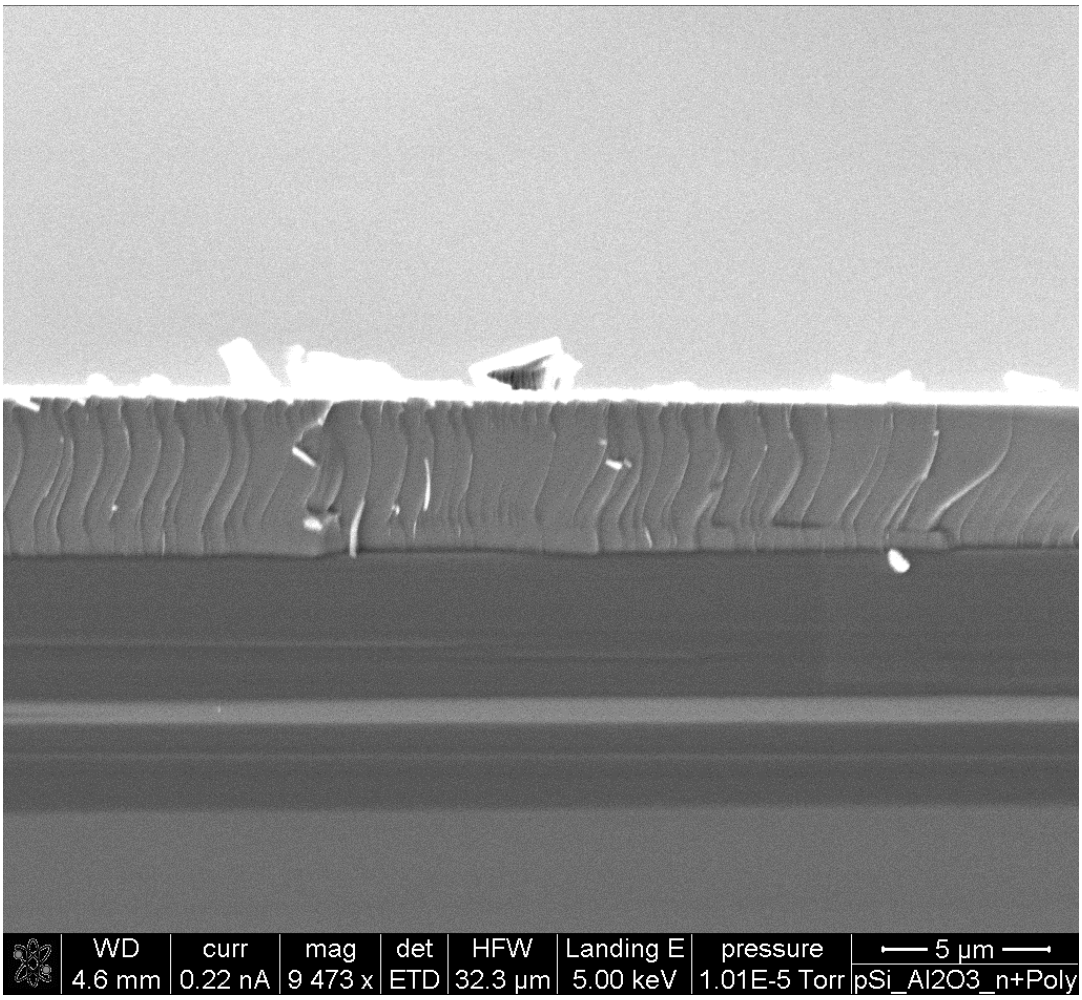

Figure 3.5 Cross sectional SEM image of the silicon-Al_2O_3-polysilicon-TNP layered photoelectrode

The TNP increases the total surface area of the electrodes and also provide a nanochannel for the electrons or holes to move in or out of the electrode into the electrolytes

Figure 3.7 is a pictorial representation of the core final device of this thesis. It portrays the production of hydrogen and oxygen through photoelectrolysis as the result of a water splitting reaction, which has been detailed in the greater part of Chapter 3. The effects of the electron-hole pair generation through the photocathode and photoanode are also illustrated

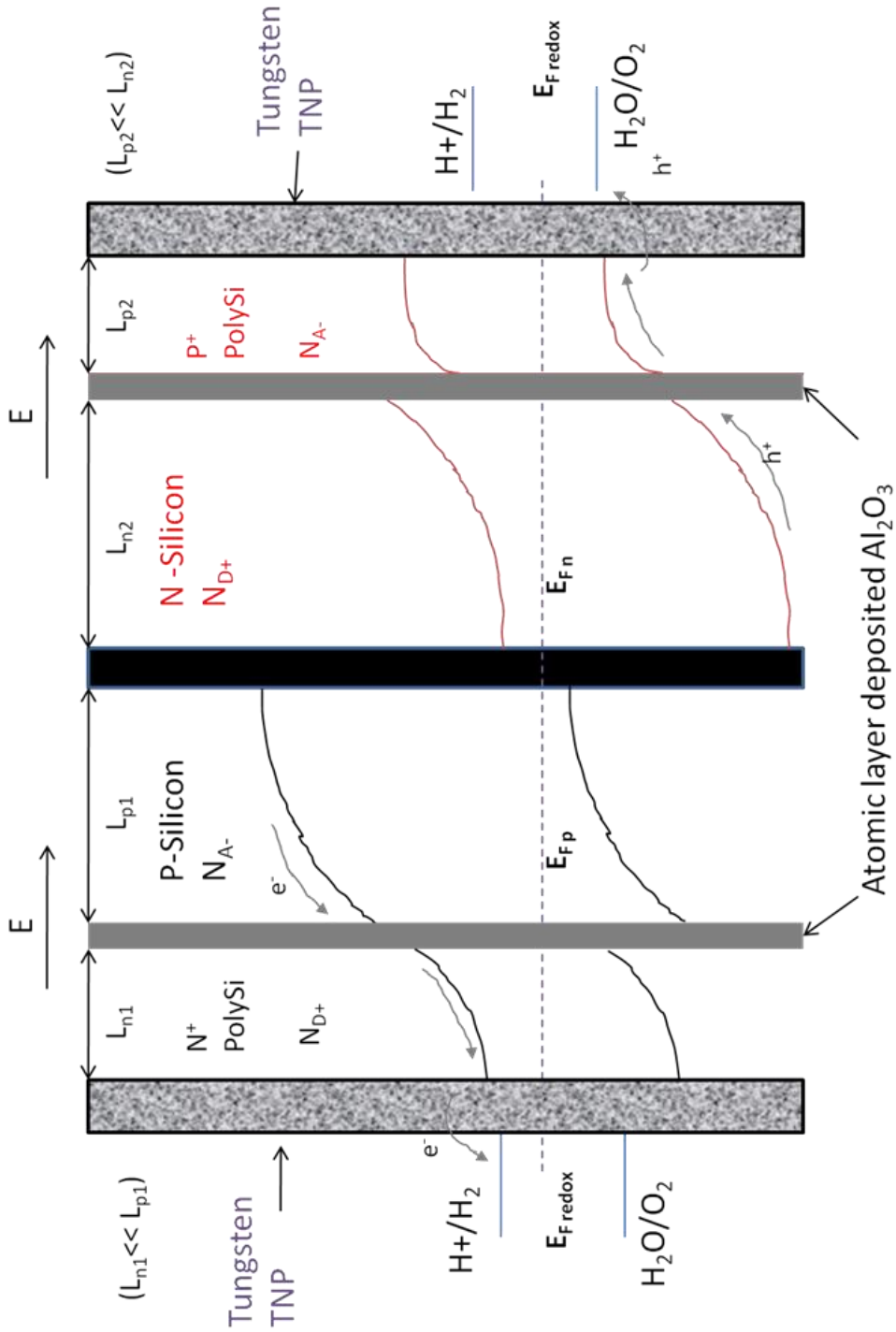

Figure 3.6 The device structure of the two photoelectrodes with p- / n- silicon, the Al_2O_3 layer, n^+ - / p^+ - polysilicon, and TNP on the surface

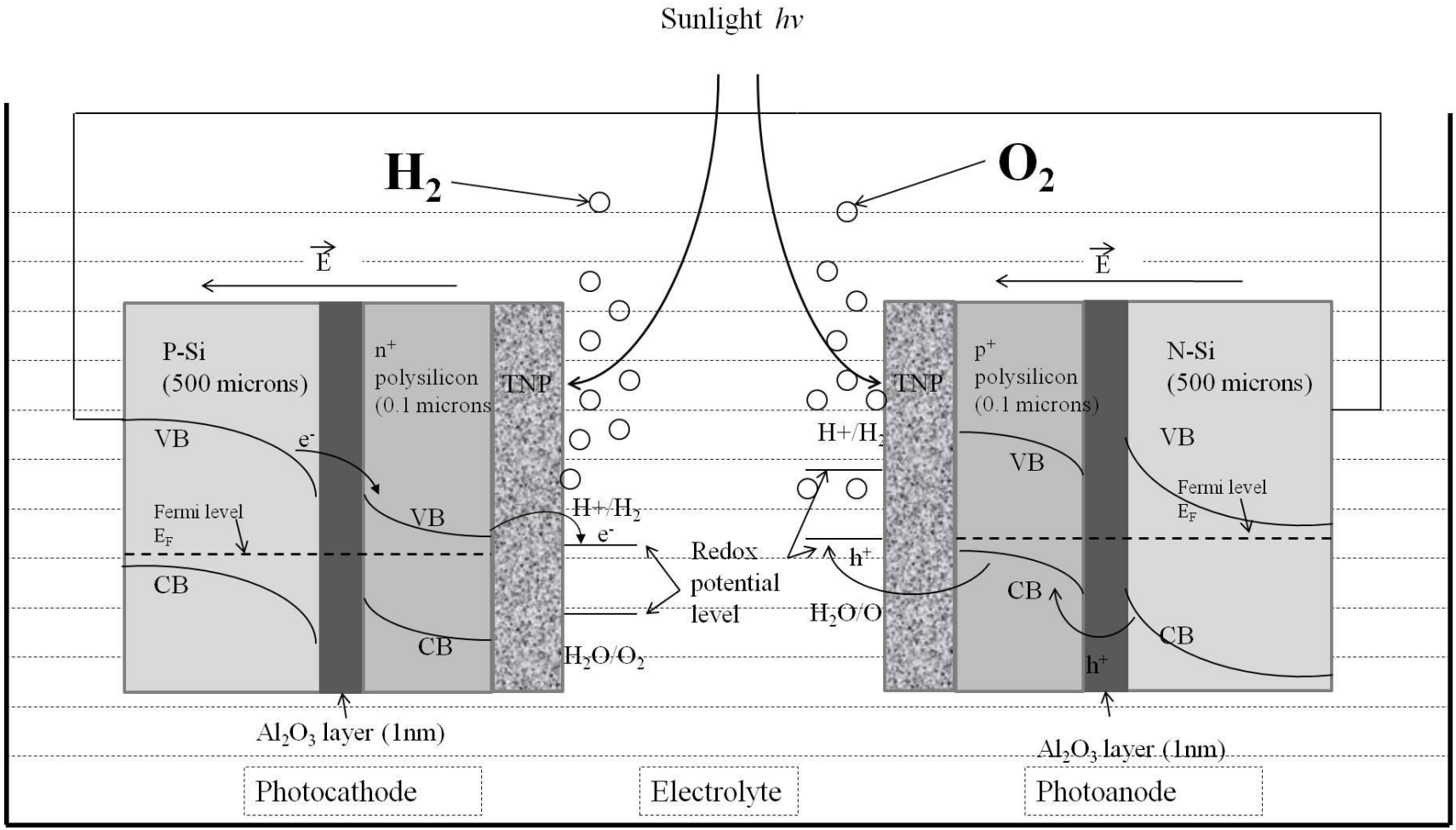

Figure 3.7 Photocathode (left) producing hydrogen and photoanode (right) producing oxygen through photogenerated electron-hole pairs with the aid of sunlight and water molecule splitting

3.4 Comparison Between Different Electrodes, Devices, Electrolyte Systems

For the experiments mentioned in this section, the multilayer device structure was used and three different approaches for designing the photoelectrodes were studied. Section 3.4.1 talks about the electrodes having a (p- / n-) silicon substrate with an oppositely doped (n^+- / p^+-) polysilicon layer on top of it, and two photocatalyst metals, titanium and platinum, were deposited on the surface of the electrode. In Section 3.4.2, the TNP were grown directly on the silicon (p- / n-) with oppositely doped (n^+- / p^+-) electrode structure and studied thoroughly. The next section, 3.4.3, also consists of the same silicon (p- / n-), polysilicon (n^+- / p^+-), and TNP structures as in 3.4.2, only this time there is an Al_2O_3 layer introduced between the silicon and polysilicon layers via the ALD method. In the last section, Section 3.4.4, discusses the V_{ON} of the devices mentioned with respect to the different pH levels of electrolytes.

The experimental setup consists of a low-range Keithley 236 SMU, a light source, different pH electrolytes ranging from acidic to basic (1-11), and a computer. Acidic and basic pH solutions were made using HCl and KOH. The power of the light source was about 100mW, and the area of the incident light was $Area = \pi(0.0127)^2 = 5.0671 \times 10^{-4}\text{m}^2$; thus, the intensity of the light source was 100mW/Area = $197.35 W/\text{m}^2$. The area of the sample electrodes was 1cm × 1cm = $1\times 10^{-4}\text{m}^2$. A voltage sweep was done in a unilateral manner, where the sweep was started from -5V to 5V with 100ms of delay time. Two kinds of data were measured: one sweep was done without any illumination, and the other was done under illumination. Figure 3.8 shows the setup for the measurement with the light source, SMU, photoelectrodes, and computer on the left. On

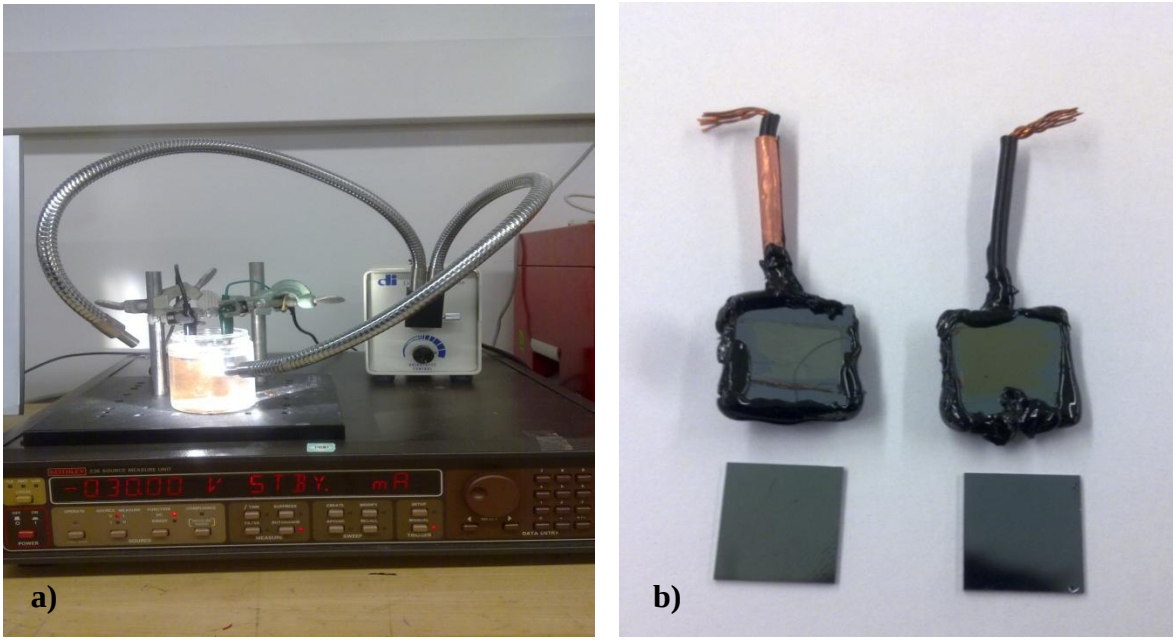

Figure 3.8 Equipment setup for the a) current vs. voltage and efficiency measurement of the photo electrodes; b) prepared sample electrodes

the right, it shows the electrode samples (1cm × 1cm) and the preparation of the electrodes with black wax and connecting wires.

3.4.1 Silicon, polysilicon, and photocatalyst metal coated electrodes

In this section, the photoelectrode consists of the multilayer structure that has been discussed in Section 3.4. For the photocathode, the electrode was prepared on a 0.5mm p-Si substrate on top of which a doped n^+-polysilicon (0.1µm) was deposited by LPCVD method. On top of the polysilicon, a thin layer of platinum (5nm) photocatalyst metal was deposited using sputtering method. For the photoanode, a 0.5mm n-type silicon substrate was used on which a doped p^+-polysilicon (0.1µm) was deposited by LPCVD method. A thin layer of titanium (5nm) was deposited using a sputtering method.

Figure 3.9 represents the voltammetric analysis of the two photoelectrodes. Figure 3.10 depicts the quadrant of the voltammetric analysis where, due the photogenerated electrons and holes, the red line (under illuminated condition) shows more current generation than the blue line (under dark condition). These red and blue lines represent the data of current vs. voltage measurements. The green line is the power curve of the red line which was used to calculate the %FF and the efficiency of the photoelectrodes.

The blue line shows an almost diode-like characteristic of the two photoelectrodes, and the red line shows the excess current generation due to the photogenerated electron-hole pairs. The maximum current reached under illumination for

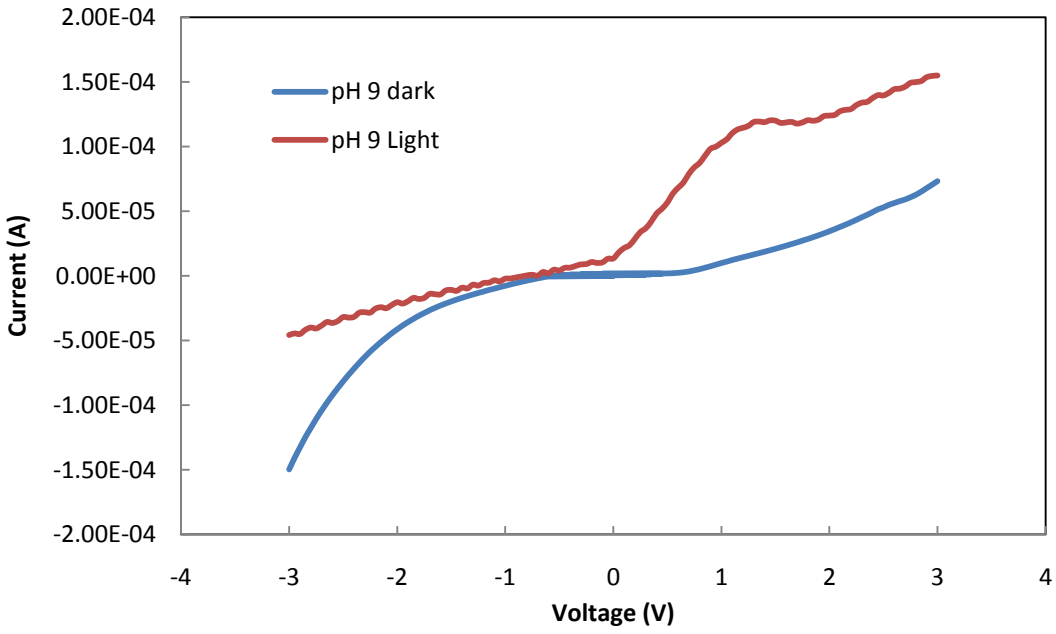

Figure 3.9 Current vs. voltage graph of p-Si, n^+-polysilicon, Pt and n-Si, p^+-polysilicon, Ti photoelectrodes in pH 9 basic solution with and without illumination

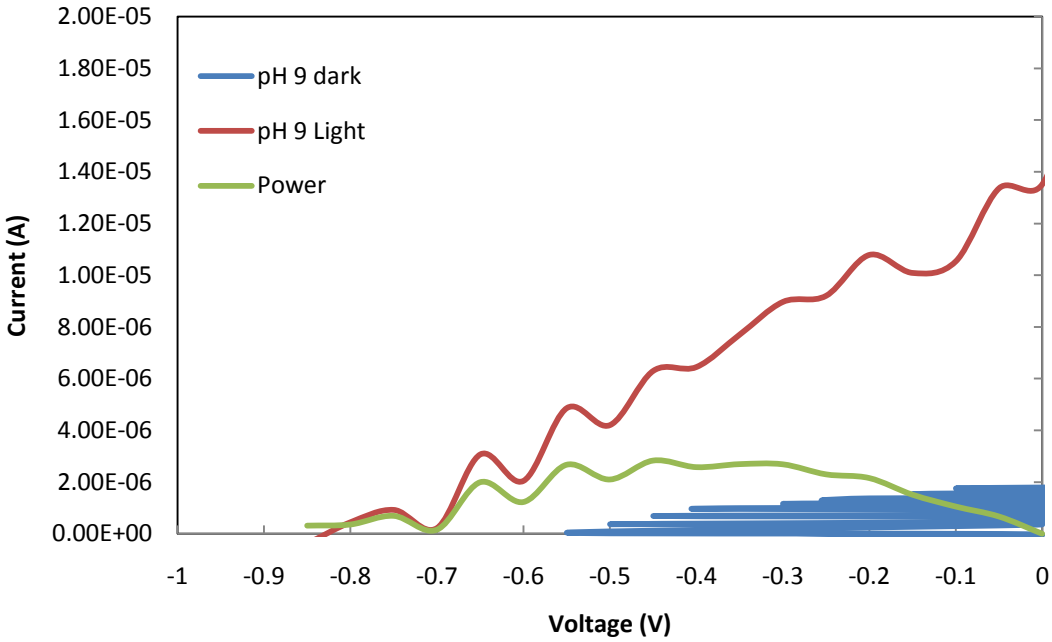

Figure 3.10 The quadrant showing the voltammetric analysis of the p-Si, n^+polysilicon Pt and n-Si, p^+-polysilicon, Ti photoelectrodes' blue (dark), red (illuminated) and green (power) plots

positive bias 5V is 1.50E-04A. Here, the photocathode (p-Si, n^+-polysilicon, Pt) is under negative bias and the photoanode (n-Si, p^+-polysilicon, Ti) is under positive bias.

From Figure 3.10, the open circuit voltage V_{OC} = 0.82V and short circuit current I_{SC}= 1.38E-05A and from the power curve the V_{MAX}= 0.45V and I_{MAX}= 6.30E-06A were extracted. So the %FF is:

$$\%FF = \frac{V_{max} \times I_{max}}{V_{OC} \times I_{SC}} \times 100\%$$

$$= \frac{0.45V \times 6.3\mu A}{0.82V \times 13.8\mu A} = \times 100\% \quad = 25.6\%$$

For the efficiency calculation, as mentioned earlier in this section, the intensity of the lamp was 197.35 W/m^2 (power input), and the area of the photoelectrode samples was 1cm × 1cm = 1× 10^{-4} m^2. Therefore, the power output was

$$= \frac{Power\ out\ put}{area\ of\ the\ electrode} = \frac{0.45V \times\ 6.3\mu A}{1 \times 10^{-4}\ \mathrm{m}^2} = 0.02835\ W/\mathrm{m}^2\ .$$

The efficiency of the photoelectrode, IPCE:

$$\eta = \frac{Photoelectrode\ Power\ out\ put}{Incident\ light\ power\ input} \times 100\ \%$$

$$\eta = \frac{0.02835\ W/\mathrm{m}^2}{197.35\ W/\mathrm{m}^2} \times 100\ \% = \mathbf{0.01437}\%$$

3.4.2 Silicon, polysilicon with TNP electrodes

In this section, the photoelectrode consists of the multilayer structure that has been discussed in the previous section. For the photocathode, the electrode was prepared on a 0.5mm p-Si substrate on top of which a doped n^+-polysilicon (0.1µm) was deposited by LPCVD method. On top of the polysilicon the TNP were grown. Consequently, for the photoanode, a 0.5mm n-Si substrate was used on which a doped p^+-polysilicon (0.1µm) was deposited by LPCVD method, and the TNP were grown on the electrode surface.

Figure 3.11 represents the voltammetric analysis of the two photoelectrodes. Figure 3.12 depicts the quadrant of the voltammetric analysis where, due the

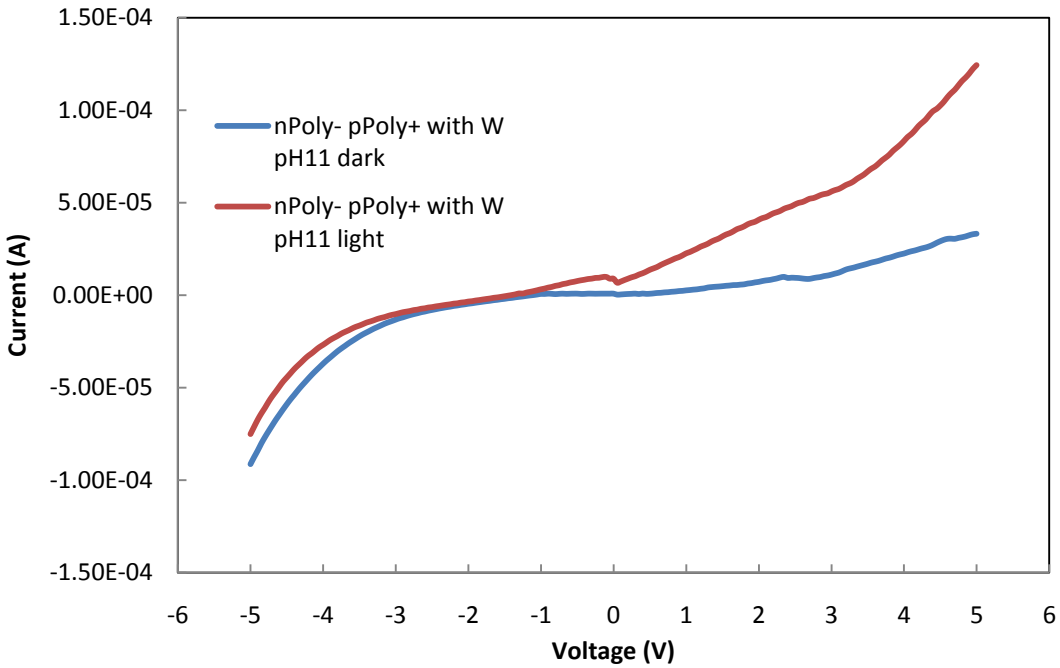

Figure 3.11 Current vs. voltage graph of p-Si, n^+-polysilicon, TNP, and n-Si, p^+-polysilicon, TNP photoelectrodes in pH 11 basic solution with and without illumination

photogenerated electrons and holes, the red line shows more current generation than the blue line. The green line (power curve) was used to calculate the %FF and the efficiency of the photoelectrodes.

Without illumination, the blue line shows an almost diode-like characteristic of the two photoelectrodes, and under illumination the redline shows the excess current generation due to the photogenerated electron-hole pairs. The maximum current reached under illumination for positive bias of 5V is 1.30E-04A. Here the photocathode (p-Si, n^+-polysilicon, TNP) is under negative bias and the photoanode (n-Si, p^+-polysilicon, TNP) is under positive bias.

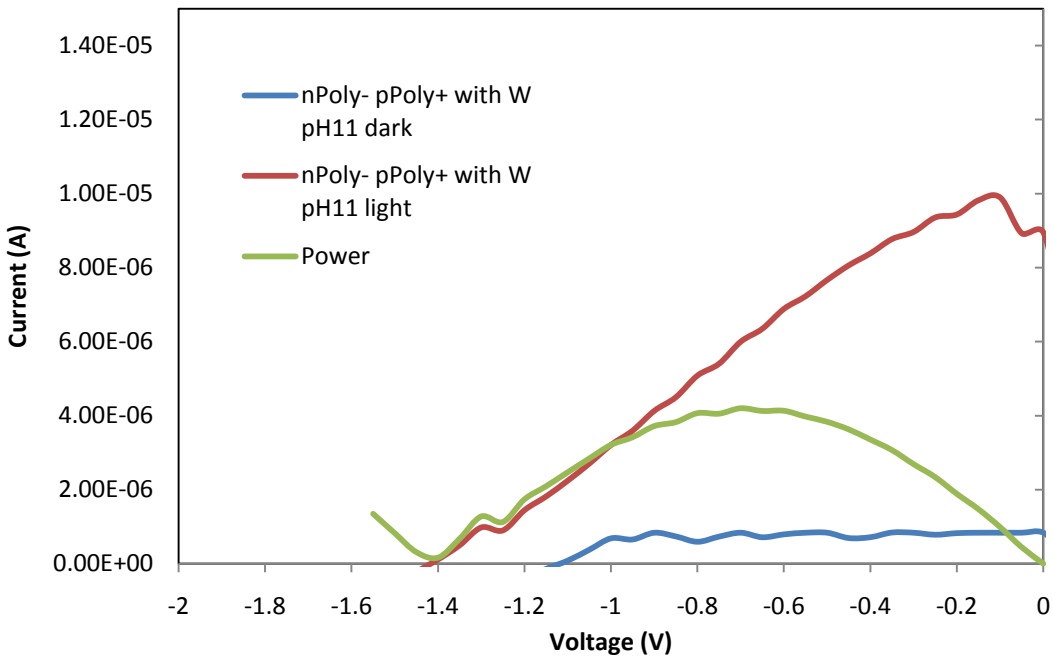

Figure 3.12 The quadrant showing the voltammetric analysis of the p-Si, n^+-polysilicon, TNP, and n-Si, p^+-polysilicon, TNP photoelectrodes' blue (dark), red (illuminated) and green (power) plots

From Figure 3.12, the V_{OC} = 1.4V and I_{SC}= 1.00E-05A and from the power curve, the V_{MAX}= 0.7V and I_{MAX}= 6.00E-06A were extracted. So the %FF is:

$$\%FF = \frac{V_{max} \times I_{max}}{V_{OC} \times I_{SC}} \times 100\%$$

$$= \frac{0.7V \times 6\mu A}{1.4V \times 10\mu A} = \times 100\% \quad = 30\%$$

For the efficiency calculation, as mentioned earlier in this section, the intensity of the lamp was 197.35 W/m^2 (power input), and the area of the photoelectrode samples was 1cm × 1cm = 1×10^{-4} m^2. Hence, the power output was

$$= \frac{Power\ out\ put}{area\ of\ the\ electrode} = \frac{0.7V \times 6\mu A}{1 \times 10^{-4}\ \mathrm{m}^2} = 0.042\ W/\mathrm{m}^2\ .$$

The efficiency of the photoelectrode, IPCE:

$$\eta = \frac{Photoelectrode\ Power\ out\ put}{Incident\ light\ power\ input} \times 100\ \%$$

$$\eta = \frac{0.042\ W/\mathrm{m}^2}{197.35\ W/\mathrm{m}^2} \times 100\ \% = \mathbf{0.02128}\%$$

3.4.3 Silicon, polysilicon with TNP and Al_2O_3 layer electrodes

In this section, the photoelectrode consists of the multilayer structures discussed in previous sections. For the photocathode, the electrode was prepared on a 0.5mm p-Si substrate on top of which a doped n^+-polysilicon (0.1µm) was deposited by LPCVD method. On top of the polysilicon, the TNP were grown. Consequently, for the photoanode, a 0.5mm n-Si substrate was used on which a doped p^+-polysilicon (0.1µm) was deposited by LPCVD method, and the TNP were grown on the electrode surface.. An Al_2O_3 (1nm) layer was introduced between the Silicon and polysilicon layer to prevent the leakage current from passing through and to prevent the p-n junction from forming and thus reducing the electric field.

Figure 3.13 represents the voltammetric analysis of the two photoelectrodes. Figure 3.14 depicts the quadrant of the voltammetric analysis where, due the photogenerated electrons and holes, the red line shows more current generation than the

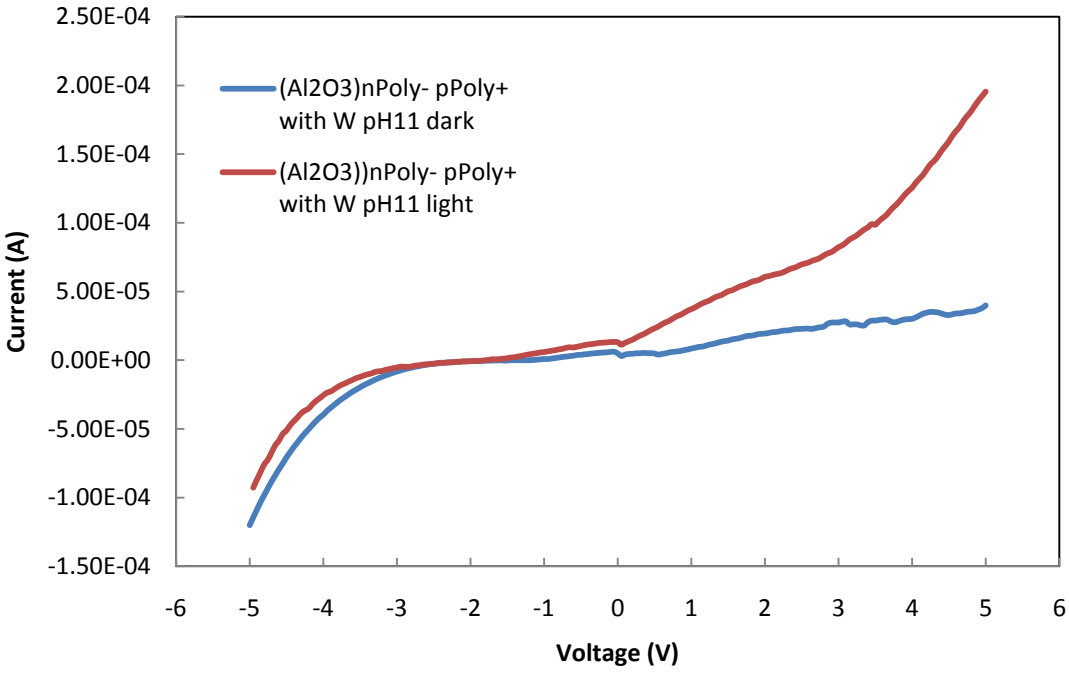

Figure 3.13 Current vs. voltage graph of p-Si, Al_2O_3, n^+-polysilicon, TNP, and n-Si, Al_2O_3, p^+-polysilicon, TNP photoelectrodes in pH 11 basic solution with and without illumination

blue line. The green line (power curve) was used to calculate the %FF and the efficiency of the photoelectrodes.

Without illumination, the blue line shows an almost diode-like characteristic of the two photoelectrodes, and under illumination the red line shows the excess current generation due to the photogenerated electron-hole pairs. The maximum current reached under illumination for positive bias of 5V is 2.00E-04A. Here the photocathode (p-Si, Al_2O_3, n^+-polysilicon, TNP) is under negative bias and the photoanode (n-Si, Al_2O_3, p^+-polysilicon, TNP) is under positive bias.

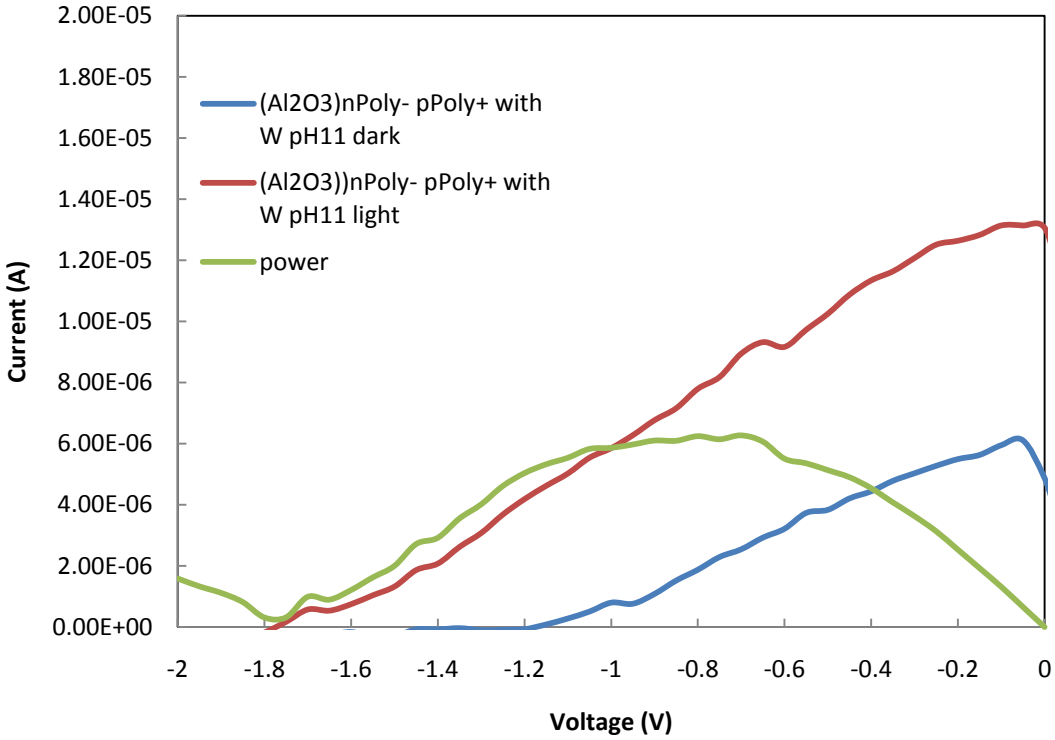

Figure 3.14 The quadrant showing the voltammetric analysis of the p-Si, Al_2O_3, n^+-polysilicon, TNP, and n-Si, Al_2O_3, p^+-polysilicon, TNP photoelectrodes' blue (dark), red (illuminated) and green (power) plots

From Figure 3.14, the V_{OC} = 1.8V and I_{SC}= 1.30E-05A and from the power curve the V_{MAX}= 0.7V and I_{MAX}= 8.95E-06A were extracted. So the %FF is:

$$\%FF = \frac{V_{max} \times I_{max}}{V_{OC} \times I_{sc}} \times 100\%$$

$$= \frac{0.7V \times 8.95\mu A}{1.77V \times 13\mu A} = \times 100\% = 27.22\%$$

For the efficiency calculation mentioned, the intensity of the lamp was 197.35 W/m^2 (power input), and the area of the photoelectrode samples was 1cm × 1cm = $1\times 10^{-4}\mathrm{m}^2$. Therefore, the power output was:

$$= \frac{Power\ out\ put}{area\ of\ the\ electrode} = \frac{0.7V \times\ 8.95\mu A}{1 \times 10^{-4}\ \mathrm{m}^2} = 0.06265\ W/\mathrm{m}^2$$

The efficiency of the photoelectrode, IPCE:

$$\eta = \frac{Photoelectrode\ Power\ out\ put}{Incident\ light\ power\ input} \times 100\ \%$$

$$\eta = \frac{0.06265\ W/\mathrm{m}^2}{197.35\ W/\mathrm{m}^2} \times 100\ \% = \mathbf{0.03174}\%$$

3.4.4 Comparison of turn on voltage (V_{ON})

In this section, the V_{ON} of four different photoelectrodes is compared and the best performing electrodes were determined based on this measurement. Figures 3.15 and 3.16 show the V_{ON} of the four photoelectrode pairs under dark and illuminated condition respectively. The V_{ON} was extrapolated from the current vs. voltage curves of each electrode pair in electrolytes ranging from acidic to basic (pH 1-13). The voltammetric analysis was first run without illumination and then with illumination. V_{ON} was measured from the corresponding voltage of 10% of I_{MAX} from the electrolytes at each pH level. The V_{ON} vs. pH graph was then plotted.

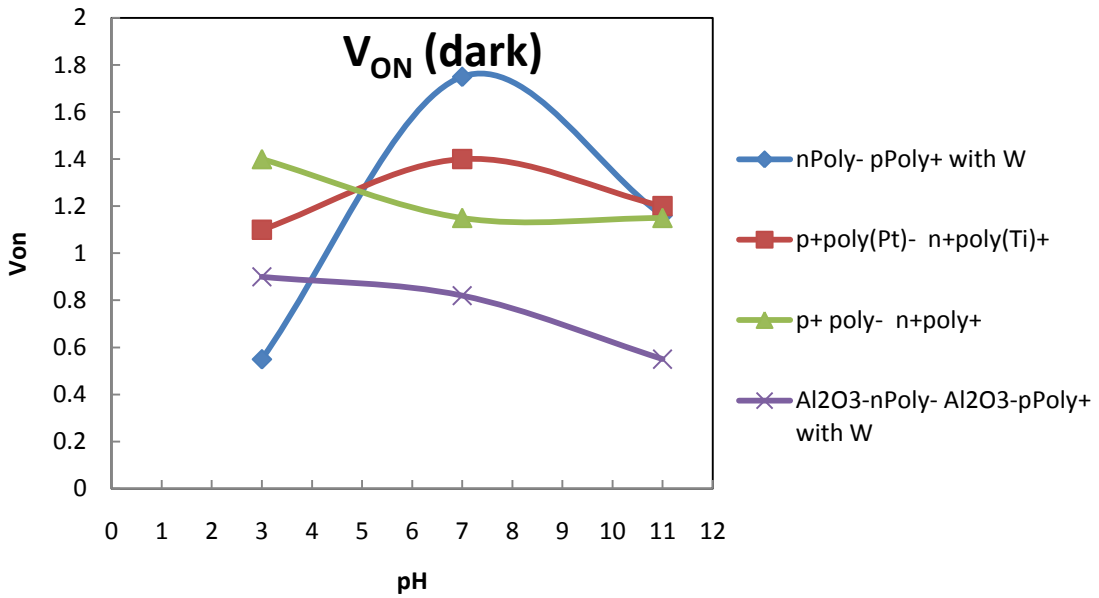

Figure 3.15 V_{ON} vs. pH graphs under dark conditions for the photoelectrode pairs

The four different electrode pairs which were studied were p- / n- silicon with n^+- / p^+- polysilicon and TNP grown on the surface (blue line), p- / n- silicon with n^+- / p^+- polysilicon with Ti / Pt photocatalyst metal coated on surface (red line), p- / n- silicon with n^+- / p^+- polysilicon (green line) and p- / n- silicon with a 1nm Al_2O_3 layer between n^+- / p^+- polysilicon and TNP grown on the surface (purple line).

In Figure 3.15, the V_{ON} was measured for the four types of photoelectrode pairs under dark conditions. On studying the graph, it is clear that the photoelectrode with Al_2O_3 layer between the silicon and polysilicon layer (purple line) shows the lowest V_{ON} voltage 0.5V around pH 11, a basic electrolyte. All the other photoelectrode pairs show lowest V_{ON} voltage above 1V.

However, in the Figure 3.16, the VON was measured under illumination of the four photoelectrodes. When we study the figure, it is observed that the photoelectrode with the Al_2O_3 layer between the silicon and polysilicon (purple line) again gives the

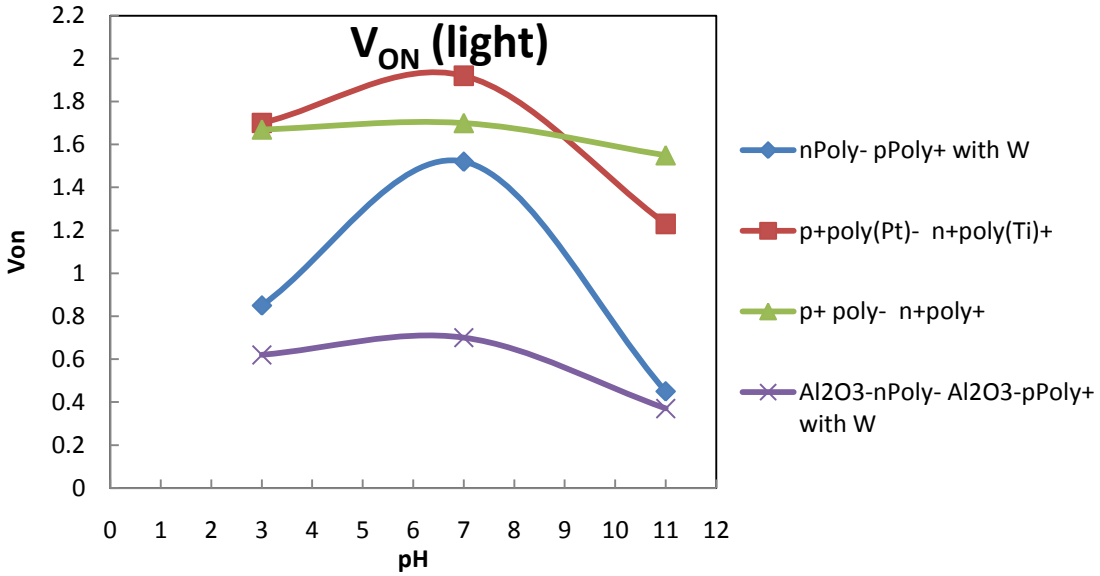

Figure 3.16 V_{ON} vs. pH graphs under illumination for the photoelectrode pairs

lowest turn on V_{ON} voltage, around pH 11 basic electrolyte which under illumination is reduced to 0.3V. The next lowest V_{ON} is 0.4V measured using the photoelectrode with Silicon and polysilicon with TNP grown on the surface (blue line), but it should also be mentioned that the steep tendency of the V_{ON} vs. pH curve for the latter photoelectrode pairs makes it unsuitable for different experimental purposes. This is especially true where there is any chance of change in pH level in the electrolyte due to various reasons.

3.5 Final Summary

The reported device was not set up to measure the quantity of hydrogen produced. Instead, solar-to-Hydrogen (STH) efficiency ηSTH was calculated from solar-to-photocurrent generation, using the following formula [12]

$$\eta_{STH} = \frac{I_{ph} \times (1.23V - V_{ext})}{I_O}$$

where I_{ph} is the photocurrent density (A/m^2), V_{ext} is the external potential applied and I_O is the light intensity (W/m^2). The STH efficiency measurement for our device was performed under no external bias condition V_{ext} = 0V. Table 3.1 summarizes the data gathered from all three reported photoelectrode pairs from this thesis. A total of three photoelectrode (PE) pairs had been studied: Silicon, Polysilicon and Photocatalyst Metal Coated Electrodes (PE -1), Silicon, Polysilicon with TNP Electrodes (PE -2) and Silicon, Polysilicon with TNP and Al_2O_3 Layer Electrodes (PE -3).

3.6 Conclusion

This chapter discusses the advantages of multilayer structures for photoelectrodes and also describes different examples. The multilayer structure that has been used to construct the devices in this thesis, were explained in detail. Furthermore, to understand the design and to observe its performance, three kinds of photoelectrode structures were studied for %FF and efficiency. From the study and calculation, the reported device with a thin layer of Al_2O_3 between the silicon and polysilicon with the TNP on the surface showed the maximum efficiency (0.03174%) among the three photoelectrodes. Also, to further justify the finding, the V_{ON} of four different photoelectrodes including the reported device, were studied. It was concluded that the device with the Al_2O_3 layer between silicon and polysilicon gives the lowest V_{ON}, which indicates that the reported device is superior to the other tested devices.

Table 3.1 Summary of %FF, IPCE (η), ηSTH and lowest V_{ON} for all three kinds of photoelectrode pairs

Devices	pH	%FF	IPCE, η	η_{STH}	Lowest V_{ON}
PE - 1	Acidic - 1	40 %	0.02 %	0.065 %	1.1 (pH11)
	Neutral - 7	31 %	0.0118%	0.036 %	
	Alkaline - 9	25.6 %	0.0144%	0.04 %	
PE - 2	Acidic - 3	25 %	0.01 %	0.033 %	0.5 (pH 11)
	Neutral - 7	33 %	0.014 %	0.031 %	
	Alkaline - 9	30 %	0.0213 %	0.04 %	
PE - 3	Acidic - 3	33 %	0.023 %	0.042 %	0.4 (pH 11)
	Neutral - 7	22 %	0.01 %	0.034 %	
	Alkaline - 9	27.22%	0.03174 %	0.084 %	

CHAPTER 4

CONCLUSION

A novel photoelectrode has been reported in this thesis to perform photoelectrolysis with multilayer semiconductor devices having nanotextured surface.

Different photocatalyst metals were studied to find a metal layer suitable for the photoelectrode device. Although the platinum and tungsten were found to be the most photoactive metals, this thesis reported a TNP surface for the device built. The multilayer semiconductor structure used in this thesis with p- / n- silicon substrate with n^+- / p^+-polysilicon layer on top of it was the base design for three different photoelectrode devices that were studied. Among the three, the device made of silicon and polysilicon layer with an Al_2O_3 layer in between (to prevent the forming of a p-n junction, thus reducing the leakage current) and the TNP on the surface reported the highest photo conversion efficiency (0.032%).

Voltammetric analysis was done to determine the current vs. voltage analysis of the different metal and semiconductor electrode experiments. The semiconductor electrode experiments for photoelectrode selection established the p- and n-type silicon as the best choice for photo conversion of solar-to-electrical energy.

4.1 Future Work

Despite the magnitude of technological progress in today's global economy, the concept of relying on nanotechnology to provide a feasible and sustainable solution to the energy crisis is ambitious but gaining momentum. The field is young and much research is yet to be undertaken in order to develop innovations to address modern society's high demands for fossil-fuel based energy. A hydrogen economy is envisioned to be a solution to all problems, so it is imperative to come up with a renewable energy source based on hydrogen. Electrolysis of water to produce hydrogen accounts for 4% of hydrogen production worldwide. Photoelectrolysis, as described in this thesis, is one of the cleanest and most renewable forms of electrolysis which yields hydrogen. There are many obstacles that are yet to be overcome before studies can be furthered and major advances can be made to meet industrial and domestic consumption needs. The outcomes of research in the field of photoelectrolysis to produce hydrogen attest a very important transition in the area of energy resource for the next generation civilization, the hydrogen economy.

The photoelectrode reported in this thesis has multilayer semiconductor structure and a new concept ALD of a thin layer of insulator (Al_2O_3) between the silicon and oppositely doped polysilicon. This insulating layer prevents the formation of p-n junction between the two layers; also, due to its very thin deposition (1nm) it does not hamper the electric field formed between the silicon and polysilicon. This ALD step can be used with different types of material to reduce the leakage current effect in multilayer structured photoelectrodes or PV cells.

Tungsten was used to form nanopores on the surface of the electrodes to enhance the surface area and form nanochannels to improve mobility of electron-hole pairs in and out of the electrolyte. This approach is still under extensive research. There is more material to be studied to understand the nanopores' implementation on the surface of photoelectrodes.

APPENDIX

ADDITIONAL DATA PERTAINING TO CHAPTER 2

The metallic electrodes used in this chapter for the voltammetric analysis were gold, platinum, palladium, titanium and tungsten. Each of the metals was combined with another for the test. So, the combinations made were gold-gold, gold-platinum, gold-palladium, gold-titanium, gold-tungsten, platinum-titanium, platinum-palladium, platinum-tungsten, palladium-tungsten, and titanium-tungsten. The first two combinations were discussed in Chapter 2. During the current vs. voltage measurement, two kinds of setups were used. For example, in the gold-platinum setup, first the gold was used as a cathode and the platinum as an anode. In the second step, gold was used as the anode and platinum as the cathode.

The metallic electrode combinations were tested in acidic and basic electrolytes, with pH level ranging from 1-11. For each of the combinations a V_{ON} vs. pH plot was generated where the data was extrapolated from the current vs. voltage graphs. In this appendix, the graphs for the rest of the metal electrode pair, gold-palladium, gold-titanium, gold-tungsten, platinum-titanium, platinum-palladium, platinum-tungsten, palladium-tungsten, and titanium-tungsten are shown in Figures A.1 to A.23.

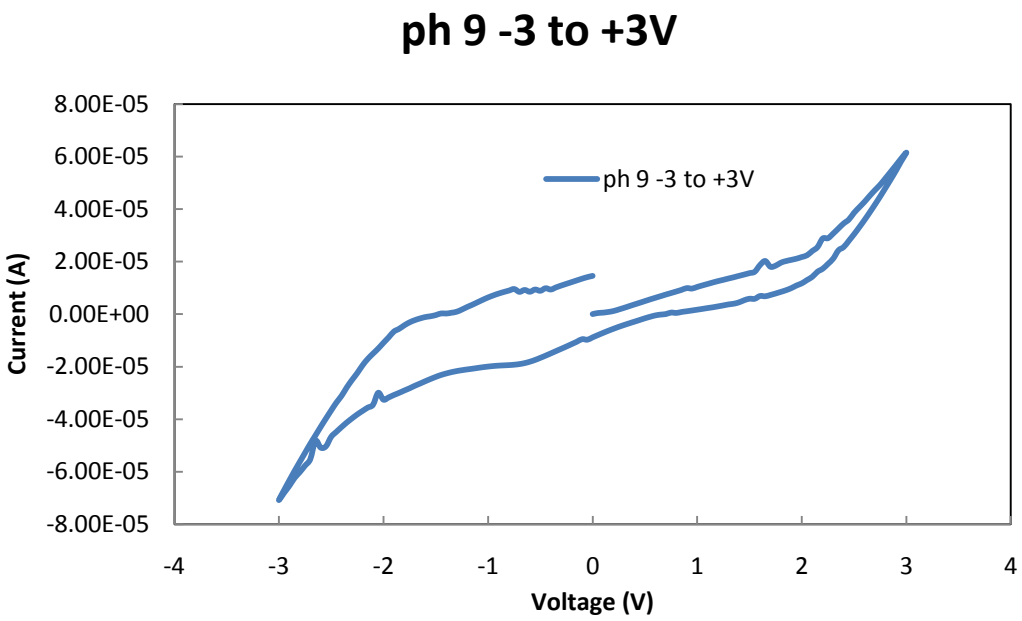

Figure A.1 Current vs. voltage graph gold-palladium electrodes in a basic solution of pH 9

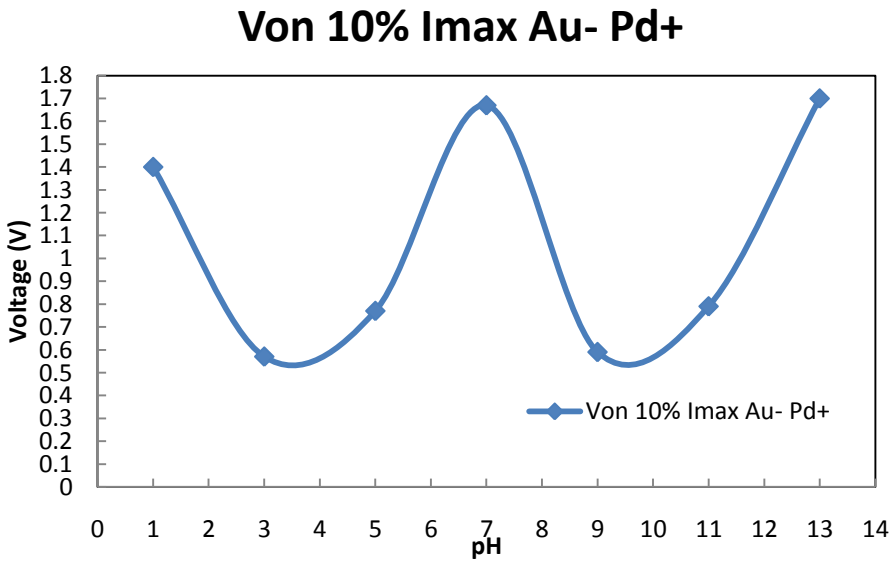

Figure A.2 V_{ON} vs. pH graph for gold-palladium electrode

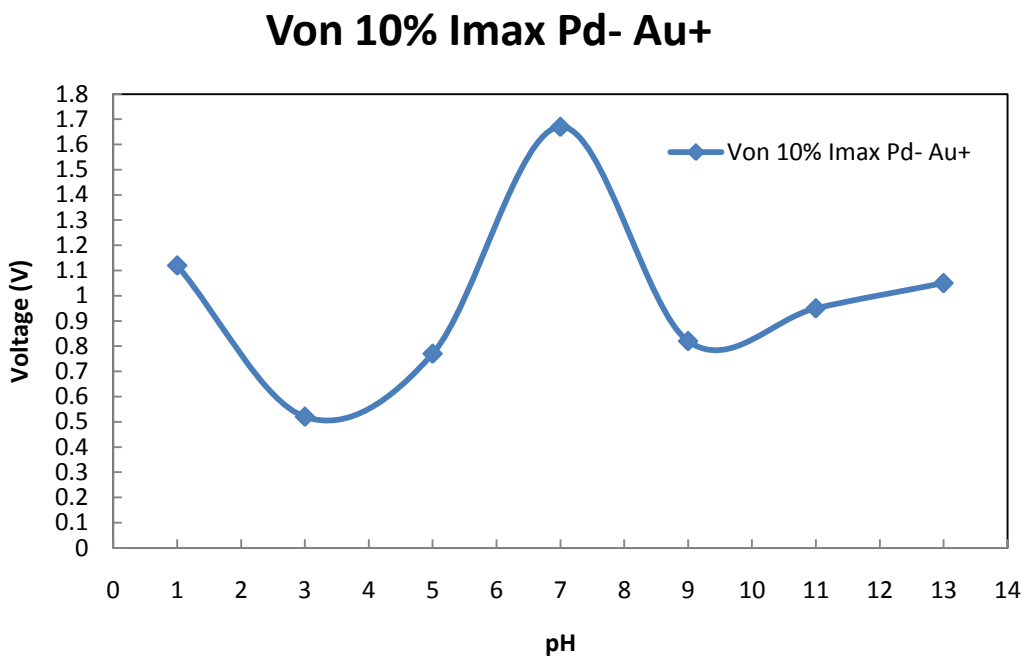

Figure A.3 V_{ON} vs. pH graph for palladium-gold electrode

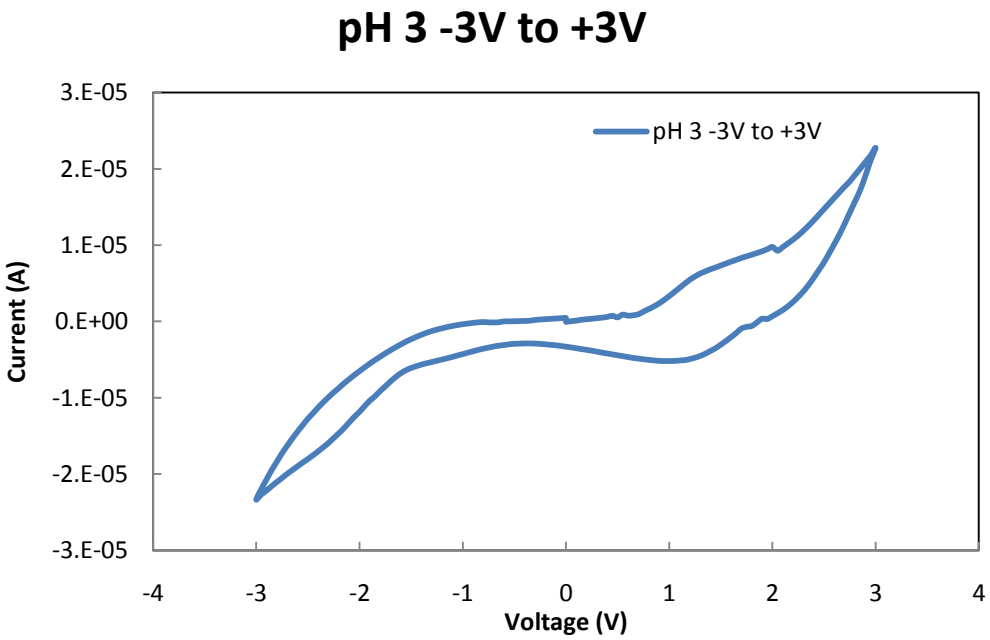

Figure A.4 Current vs. voltage graph gold-titanium electrodes in a basic solution of pH 3

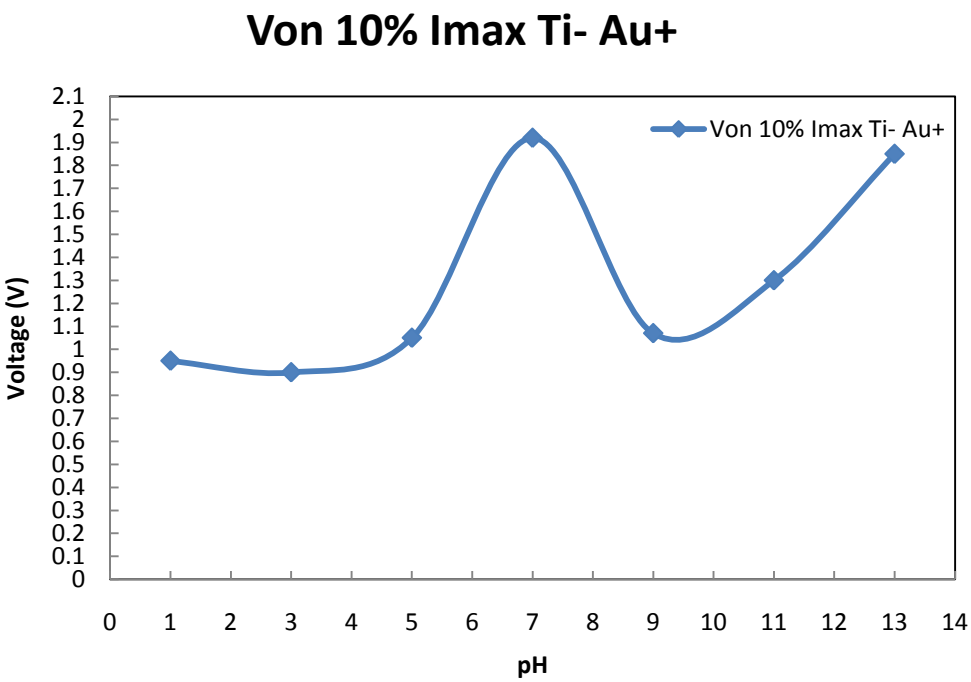

Figure A.5 V_{ON} vs. pH graph for titanium-gold electrode

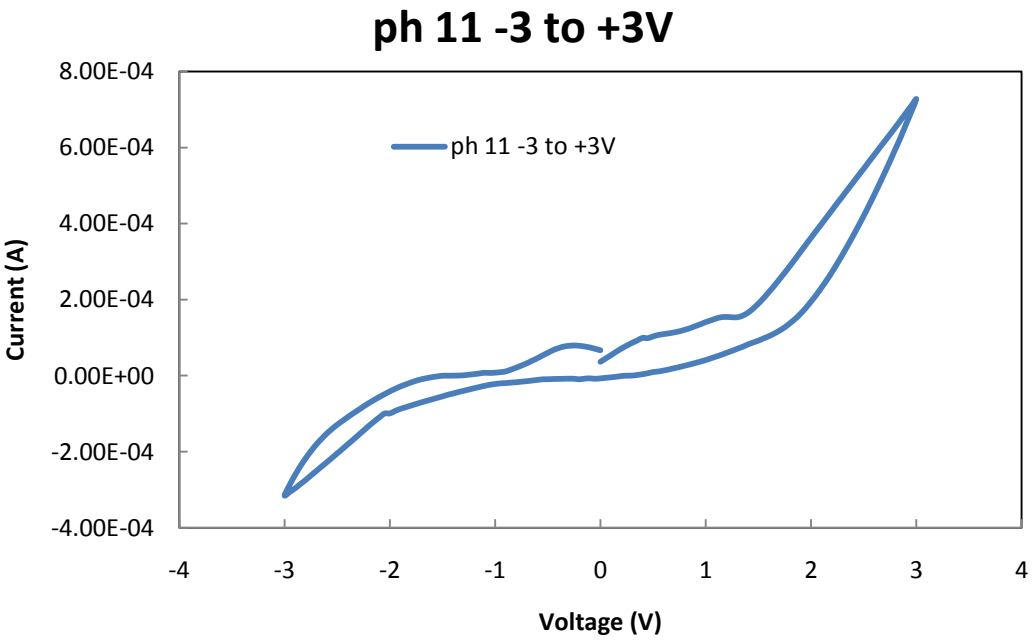

Figure A.6 Current vs. voltage graph gold-tungsten electrodes in a basic solution of pH 11

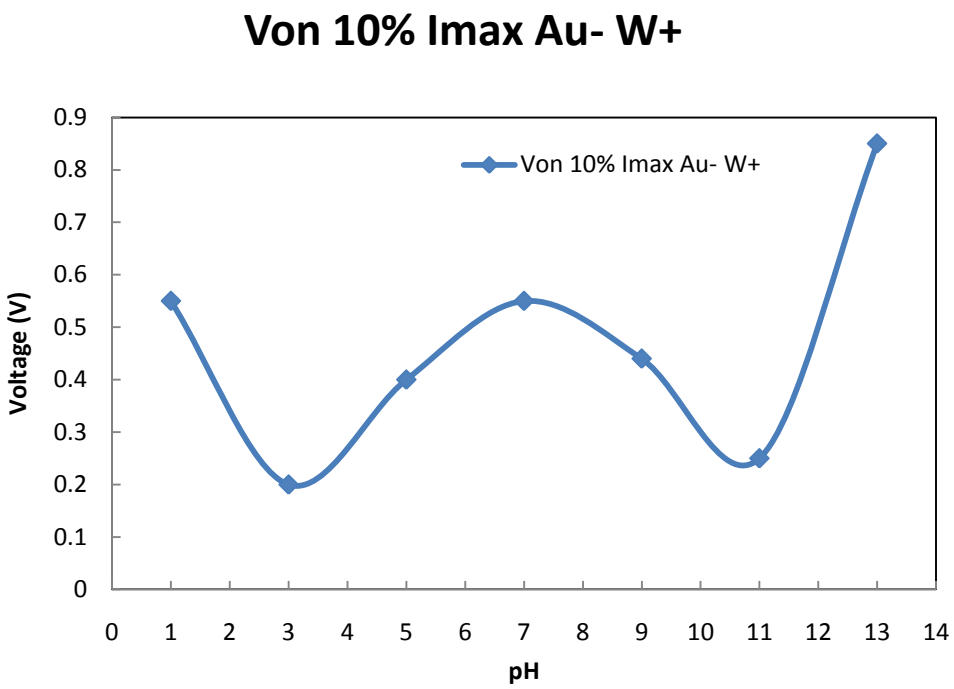

Figure A.7 V_{ON} vs. pH graph for gold-tungsten electrode

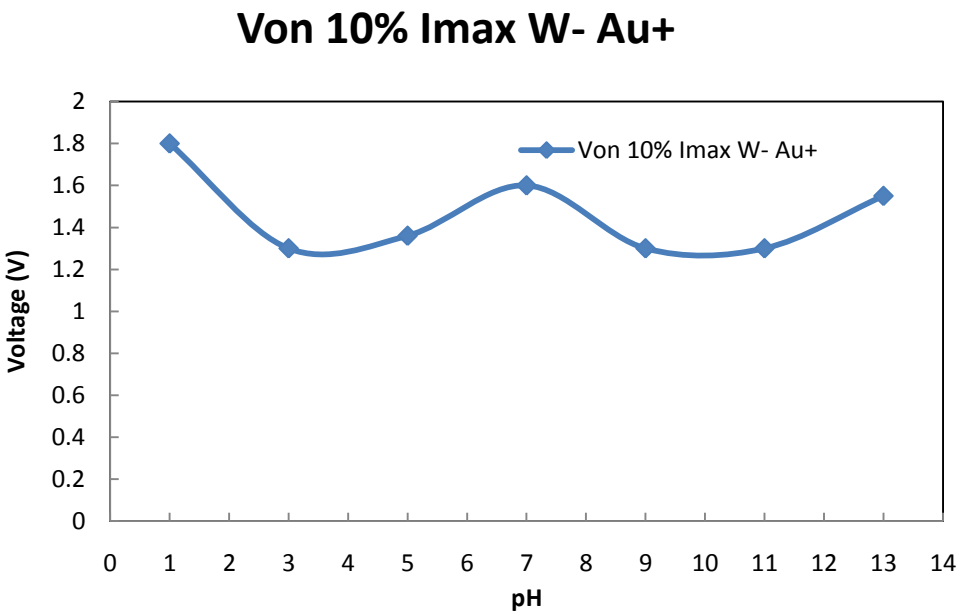

Figure A.8 V_{ON} vs. pH graph for tungsten-gold electrode

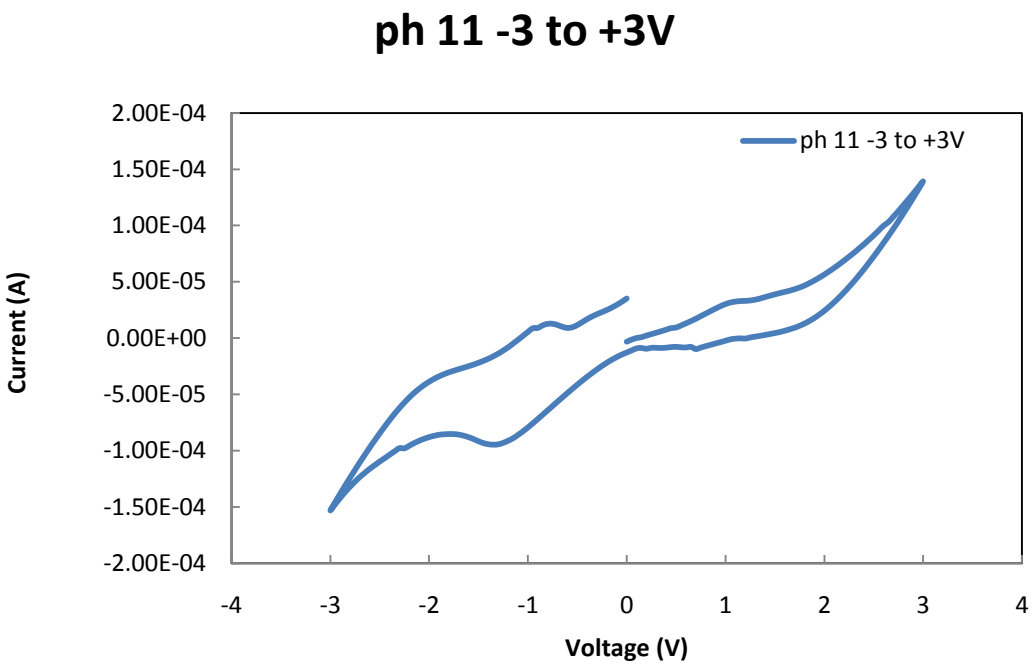

Figure A.9 Current vs. voltage graph platinum-palladium electrodes in a basic solution of pH 11

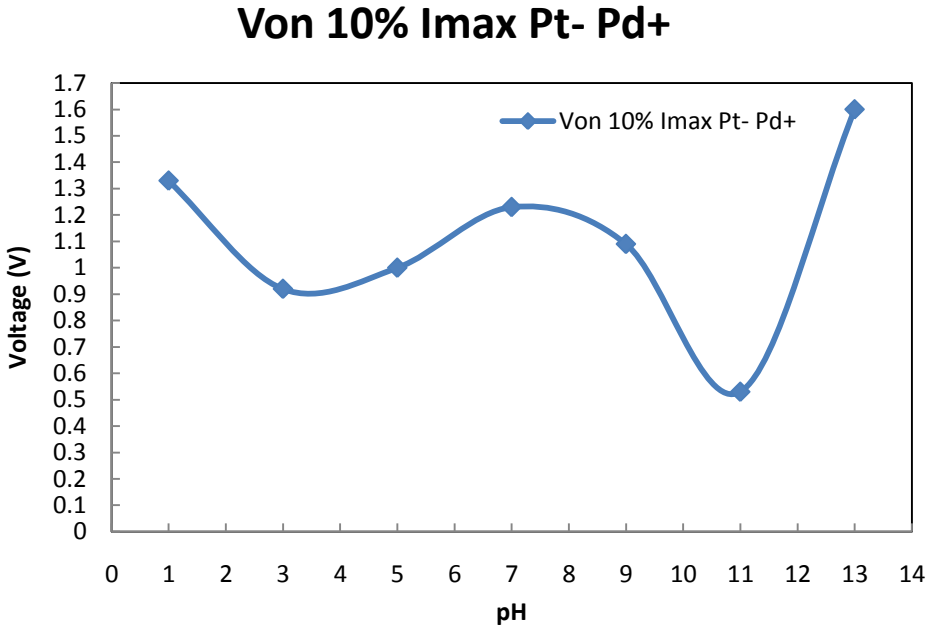

Figure A.10 V_{ON} vs. pH graph for platinum-palladium electrode

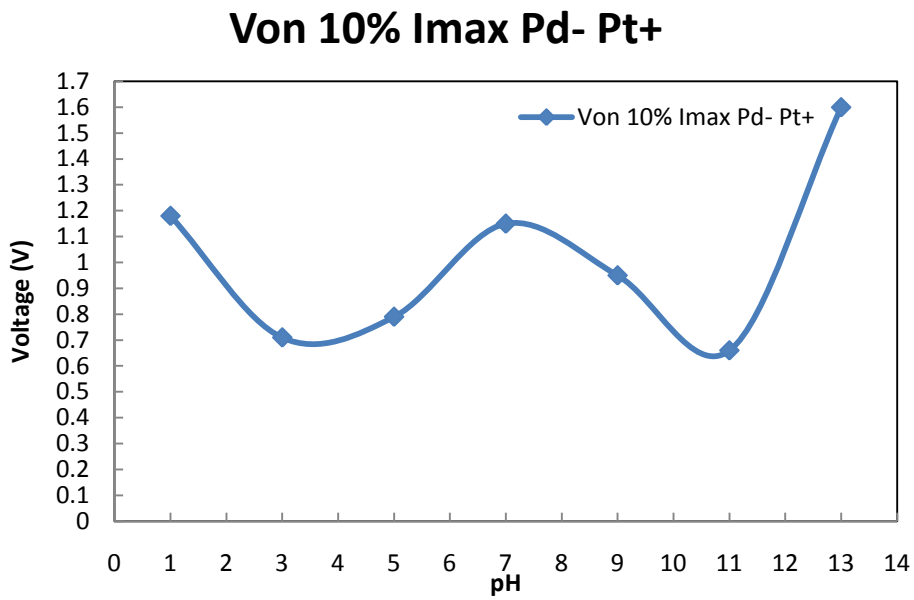

Figure A.11 V_{ON} vs. pH graph for palladium-platinum electrode

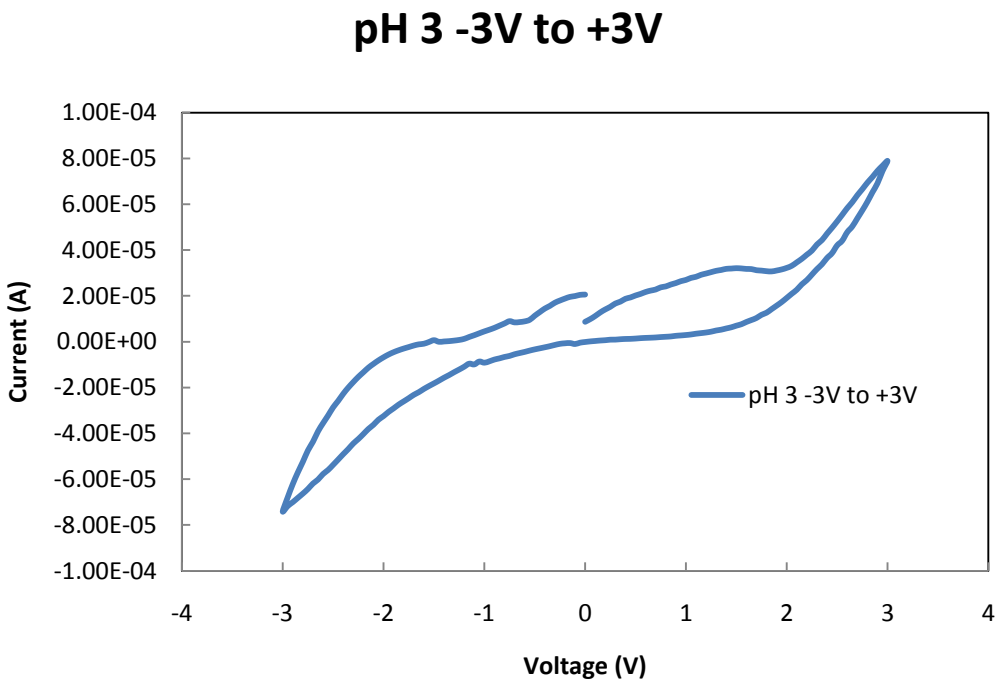

Figure A.12 Current vs. voltage graph platinum-tungsten electrodes in a basic solution of pH 3

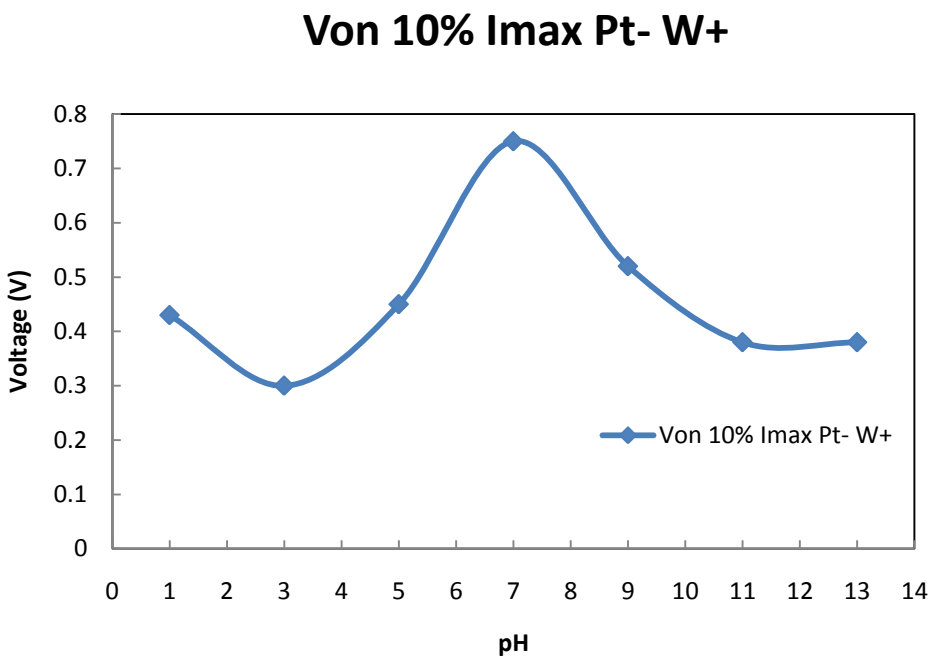

Figure A.13 V_{ON} vs. pH graph for platinum-tungsten electrode

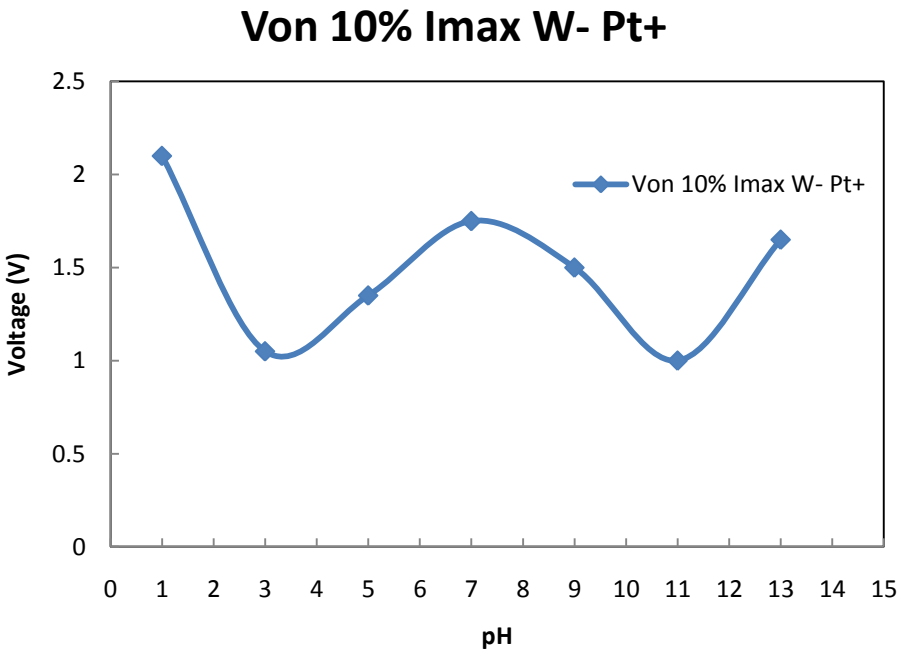

Figure A.14 V_{ON} vs. pH graph for tungsten-platinum electrode

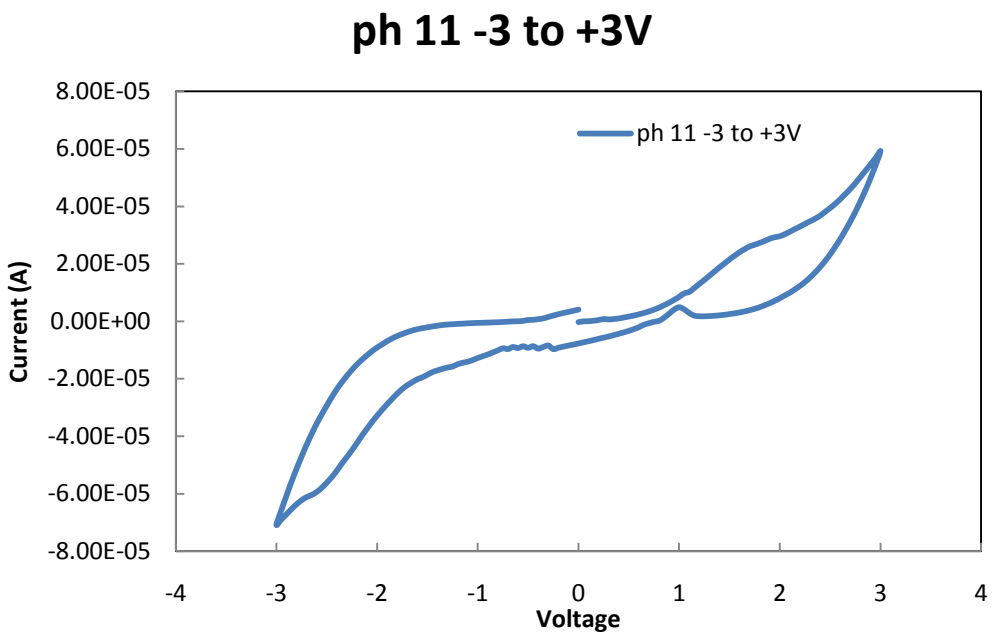

Figure A.15 Current vs. voltage graph platinum-titanium electrodes in a basic solution of pH 11

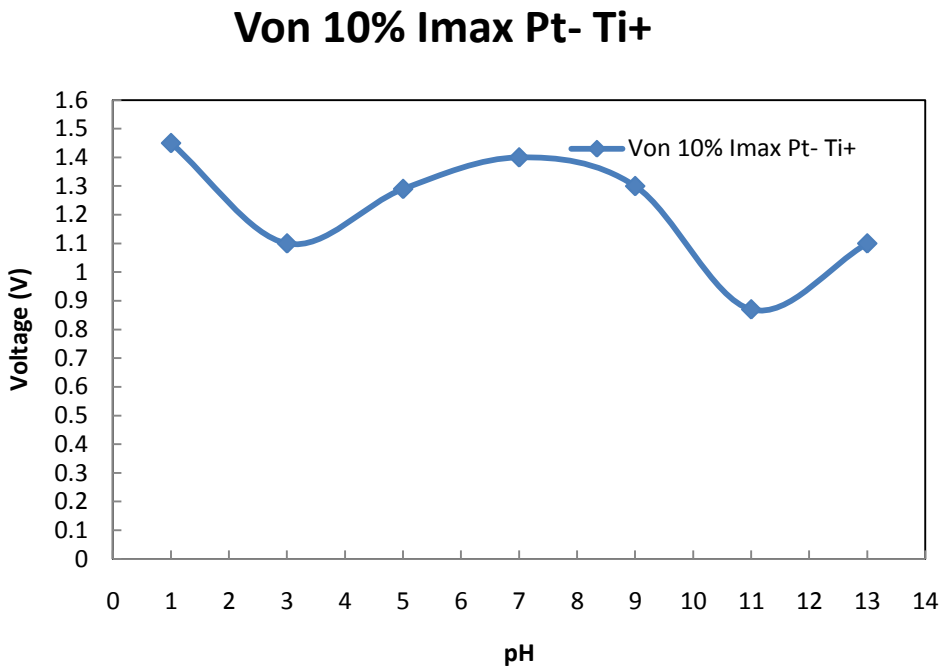

Figure A.16 V_{ON} vs. pH graph for platinum-titanium electrode

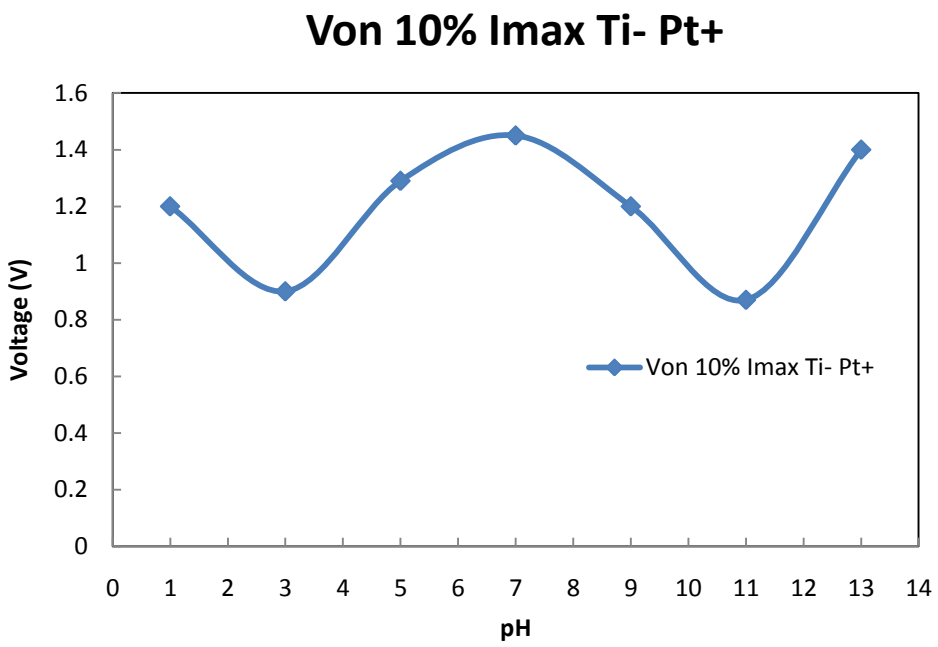

Figure A.17 V_{ON} vs. pH graph for titanium-platinum electrode

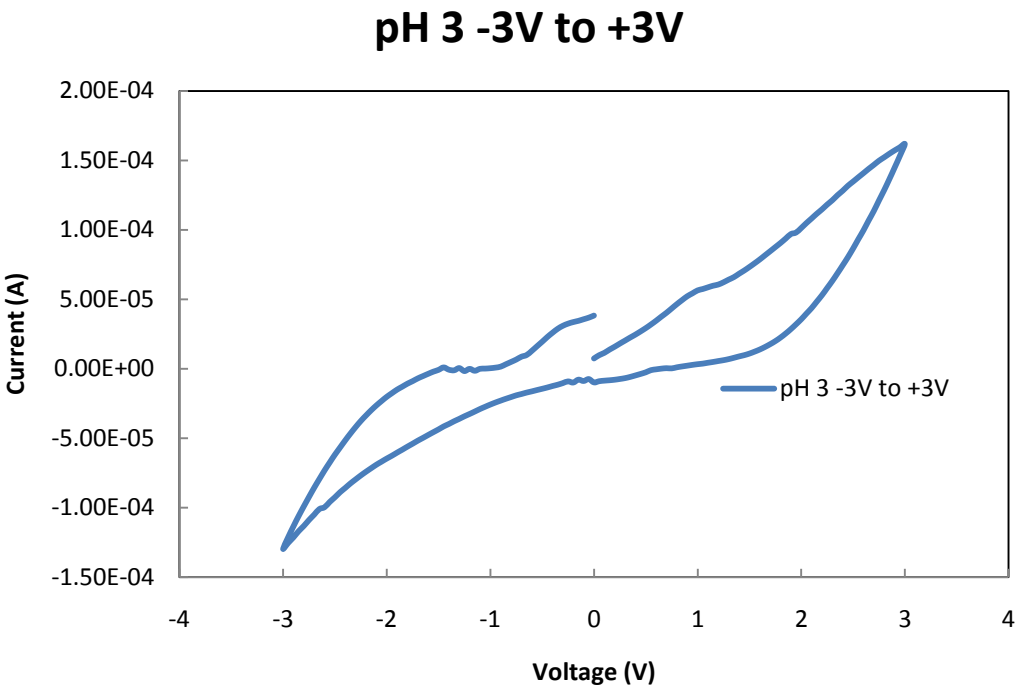

Figure A.18 Current vs. voltage graph palladium-tungsten electrodes in a basic solution of pH 3

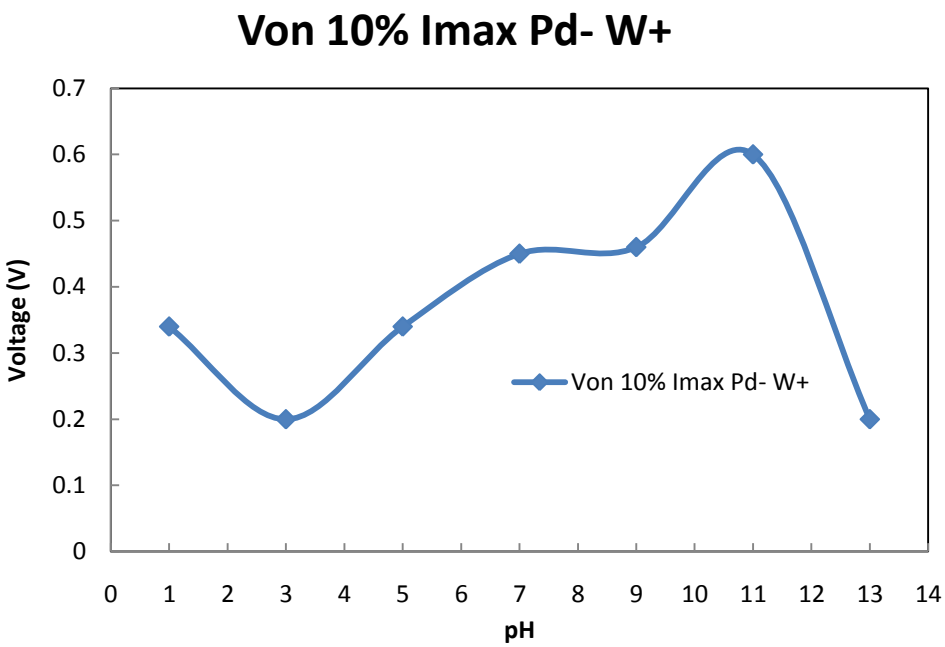

Figure A.19 V_{ON} vs. pH graph for palladium-tungsten electrode

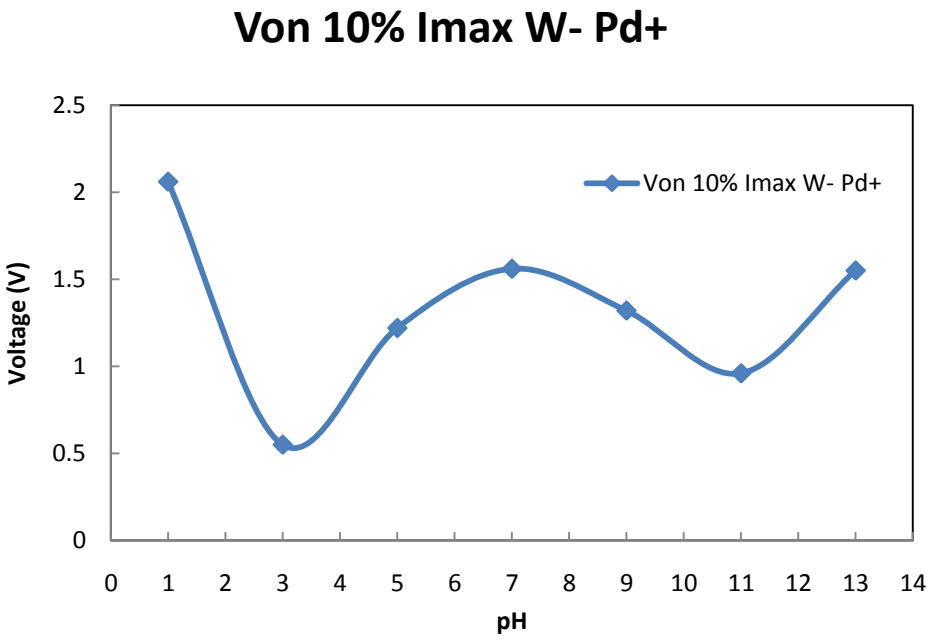

Figure A.20 V_{ON} vs. pH graph for tungsten-palladium electrode

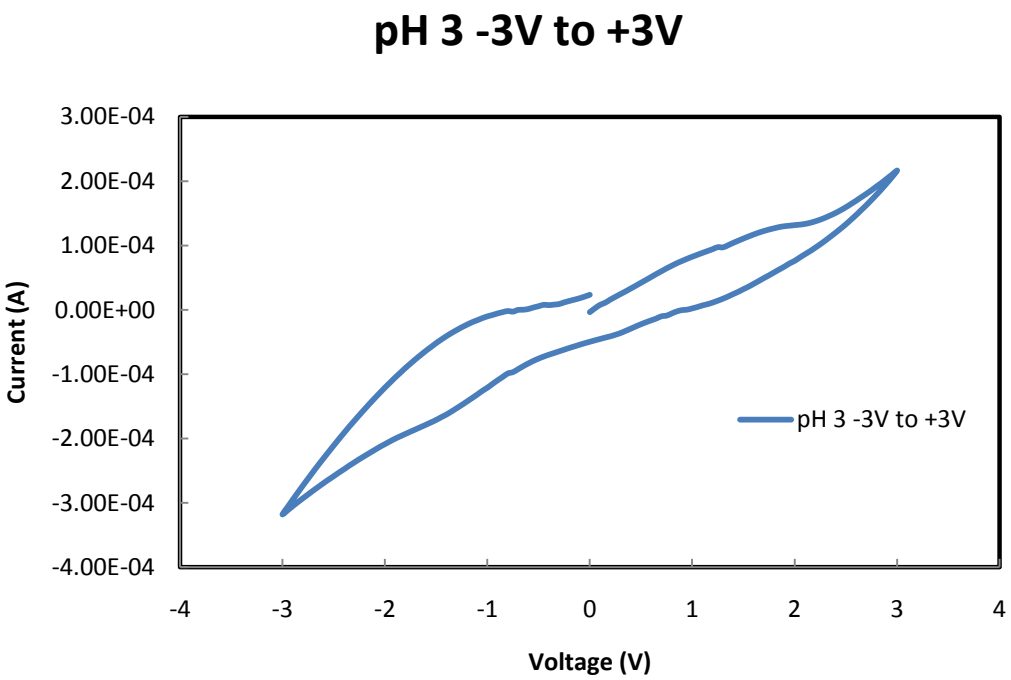

Figure A.21 Current vs. voltage graph titanium-tungsten electrodes in a basic solution of pH 3

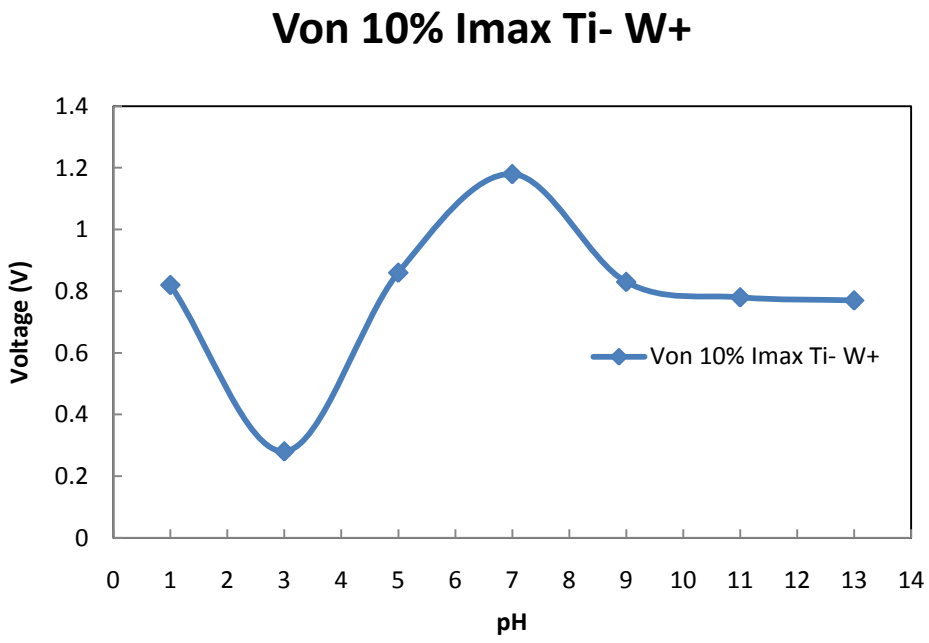

Figure A.22 V_{ON} vs. pH graph for titanium-tungsten electrode

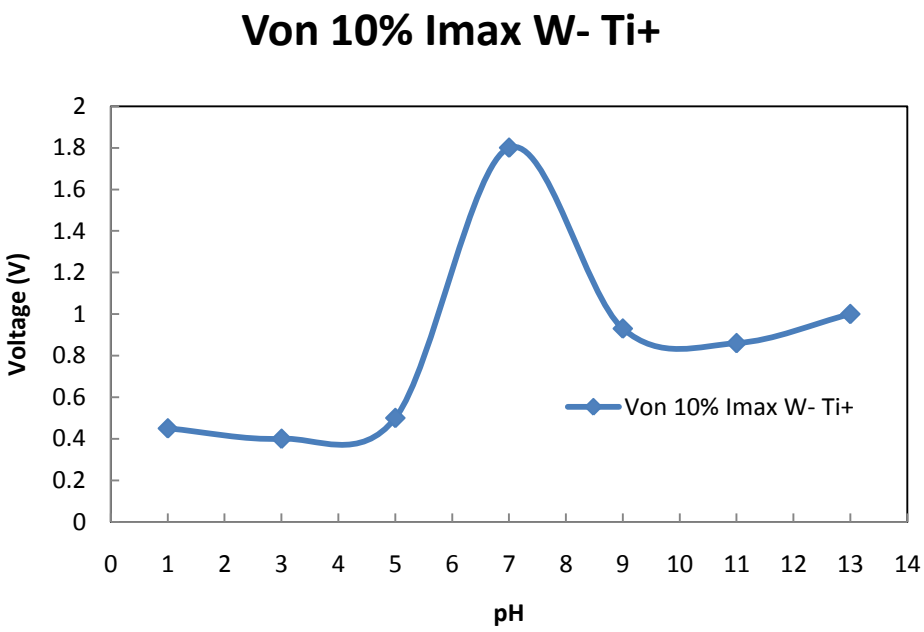

Figure A.23 V_{ON} vs. pH graph for tungsten-titanium electrode

REFERENCES

1. Craig A. Grimes, Oomman K. Varghese, Sudhir Ranjan. *Light, Water, Hydrogen – The Solar Generation of Hydrogen by Water Photoelectrolysis*– A. Grims, 2007

2. Henry Cavendish, (1766). "Three Papers Containing Experiments on Factitious Air, by the Hon. Henry Cavendish." *Philosophical Transactions* (The University Press) 56: 141 – 184. doi:10.1098/rstl.1766.0019. Retrieved 6 November 2007.

3. "Hydrogen." Chemicool Periodic Table. Chemicool.com. 24 Feb. 2011. Web. 4/10/2011 <http://www.chemicool.com/elements/hydrogen.html>

4. http://www.rsc.org/chemistryworld/Issues/2003/August/electrolysis.asp *Enterpris e and electrolysis...* Chemistry World,2003, Royal Society of Chemistry

5. Wikipedia. Retrieved 2011January. http://en.wikipedia.org/wiki/Fuel_cell# History

6. William Robert Grove, "On a Gaseous Voltaic Battery." *Philosophical Magazine and Journal of Science* vol. XXI (1842), pp 417-420.

7. National Hydrogen Association; United States Department of Energy. "The History of Hydrogen".*hydrogenassociation.org*. National Hydrogen Association. p. 1. Retrieved 17 December 2010

8. Hjálmar W. Hannesson, (2.8.2007). "Climate Change as a Global Challenge." Iceland Ministry for Foreign Affairs. Retrieved 2008-05-09

9. Fact Sheet Series: The Hydrogen Economy, U.S. Department of Energy, Washington D.C., Rep. 1.008, 2011

10. Jules Verne. "Ch XI" in *The Mysterious Island*, vol. II. Middletown CT 06459: Wesleyan University Press, 2001, pp. 327

11. Krishnan Rajeshwar, Robert D. McConnell, Stuart Licht. *Solar Hydrogen Generation: Toward a Renewable Energy Future.* Springer 2008, p 57

12. Fujishima Akira; Honda Kenichi (1972). "Electrochemical Photolysis of Water at a Semiconductor Electrode." *Nature* 238 (5358): 37

13. Akihiko Kudo, "Photocatalysis and Solar Hydrogen Production." *Pure Appl. Chem.,* Vol. 79, No. 11, pp. 1917–1927, 2007

14. S. Licht, B. Wang, S. Mukerji, T. Soga, M. Umeno, H. Tributsch, "Efficient Solar Water Splitting, Exemplified by RuO2-Catalyzed AlGaAs/Si Photoelectrolysis." *J. Phys. Chem. B* 2000, *104,* 8920-8924

15. Oscar Khaselev, Jhon A. Turner, "A Monolithic Photovoltaic – Photoelectrochemical Device for Hydrogen Production via Water Splitting." *Science* 17 April 1998 Vol. 280 no. 5362 pp. 425-427 DOI: 10.1126/ science.280.5362.425

16. Michael G. Mauk, Anthony N. Tata, Bryan W. Feyock, "Selectively-grown InGaP/GaAs on Silicon Heterostructures for Application of Photovoltaic-Photoelectrolysis Cell." *Journal of Crystal Growth* 225 (2001) 359–365

17. Bjorn Marsen , Brian Cole, Eric L. Miller, "Photoelectrolysis of Water Using Thin Copper Gallium Diselenide Electrodes." *Solar Energy Materials & Solar Cells* 92 (2008) 1054– 1058

18. Gopal K. Mor, Haripriya E. Prakasam, Oomman K. Varghese, Karthik Shankar, Craig A. Grimes, "Vertically Oriented Ti-Fe-O Nanotube Array Films: Toward a Useful Material Architecture for Solar Spectrum Water Photoelectrolysis." *Nano Letters* 2007 Vol. 7, No. 8 2356-2364

19. Eric L. Miller, Bjorn Marsen, Daniela Paluselli, and Richard Rocheleau, "Optimization of Hybrid Photoelectrodes for Solar Water-Splitting." *Electrochemical and Solid-State Letters,* 8 ~5! A247-A249 (2005). 1099-0062/2005/8~5!/A247/3 © The Electrochemical Society, Inc

20. Shu-Yen Liu,a J. K. Sheu,a,z Chun-Kai Tseng,a Jhao-Cheng Ye,a K. H. Chang,a M. L. Lee, W. C. Laia, "Improved Hydrogen Gas Generation Rate of n-GaN Photoelectrode with SiO2 Protection Layer on the Ohmic Contacts from the Electrolyte." *Journal of The Electrochemical Society,* 157 _2_ B266-B268 (2010). 0013-4651/2010/157_2_/B266/3 © The Electrochemical Society

21. Jun Akikusa, Shahed U.M. Khan, "Photoelectrolysis of Water to Hydrogen in p-SiC/Pt and p-SiC/n-TiO2 Cells." *International Journal of Hydrogen Energy* 27 (2002) 863 – 870

22. A. J. Nozik, "*p*-n Photoelectrolysis Cells." PACS numbers: 84.6O.Rb, 82.50.Et, 85.80.Dg, 73.4O.-c 1976

23. C. Jorand Sartoretti a, M. Ulmann a, B.D. Alexander a, J. Augustynski a, A. Weidenkaff b, "Photoelectrochemical Oxidation of Water at Transparent Ferric Oxide Film Electrodes." *Chemical Physics Letters* 376 (2003) 194–200

24. Atsushi Nakahira, Koichi Konishi, Koji Yokota, Tetsuo Honma, Hirofumi Aritani, Katsuhisa Tanaka, "Synthesis and Characterization of TiO_2 Doped with P Ions by Anodic Oxidation of Titanium in Acid Solution." *Journal of the Ceramic Society of Japan* 114 [1] 46-50, 2006

25. Wikipedia, August 2001 [update April 2011] [Online] Avalaible: http://en.wikipedia.org/wiki/Gold [Accessed: 20 September 2010]

26. http://www.pvsolarchina.com/multilayer-solar-cell-conversion-efficiency-as-high-as-41-1.html"

27. Andreas W. Bett, Frank Dimroth, Wolfgang Gutter, Raymond Hoeisel, Eduard Olivia, Simon P. Philipps, Jan Schone, Gerald Siefer, Marc Steiner, Alexander Wekkeli, Elke Welser, Matthias Meusel, Wolfgang Kostler, Gerhard Strobl "Highest Efficiency Multi-Junction Solar Cell for Terrestrial and Space Applications." European Photovoltaic Solar Energy Conference and Exhibition, September 2009

28. IEEE PV Specialists Conference, Silver Springs, MD, APL; chairman, Martin Wolf. The first PVSC to include a session on terrestrial PV.